UNIVERSITY OF SOUTHAMPTON

FACULTY OF SCIENCE, ENGINEERING AND MATHEMATICS

School of Chemistry

High Throughput Optical Materials

by

Mark James Hogben

Thesis for the degree of Doctor of Philosophy

August 2008

ABSTRACT

FACULTY OF SCIENCE, ENGINEERING AND MATHEMATICS

SCHOOL OF CHEMISTRY

Doctor of Philosophy

HIGH THROUGHPUT OPTICAL MATERIALS

By Mark James Hogben

The synthesis and characterisation of a variety of zeolites and aluminosilicates has been achieved using hydrothermal methods and solid state calcinations. The system using elemental aluminium, silica and sodium hydroxide solution as starting materials was explored using hydrothermal methods (200°C), and reactions conditions were optimised for the formation of analcime, sodalite, zeolite A and faujasite. All materials were characterised using powder x-ray diffraction.

The thermal conversion of zeolite A and sodium chloride into sodalite has been studied using combined TGA and DTA analysis and time resolved powder neutron diffraction heating up to 800°C. It was found that the thermal conversion occurred at 550°C and no intermediate phases were observed during this transition.

The synthesis and characterisation of a range of reversibly photochromic sodalites has been achieved via thermal processing of zeolite A with sodium sulphate and a variety of group I metal salts. All of the sodalites adopt the space group P-43n and were characterised by powder neutron diffraction and Rietveld refinement. Structural refinements show that substitutions at non-framework sites alter the framework bond distances of the sodalite and the observed optical property. Different colours of reversible photochromism have been observed and tailored by use of different salts in the synthesis, and trends between structure and optical property have been examined.

Synthesis of the anhydrous zeolite type phase $K_2Al_2Si_3O_{10}(KCl)$ with edingtonite topology has been achieved using a high temperature, high pressure reaction (600°C, 7000psi). Rietveld refinement of powder x-ray diffraction in the space group $P\text{-}42_1m$ was performed. The tetragonal unit cell was found to have refined lattice parameters of a = 9.7488 and c = 6.4879. Structural considerations have been examined as to the inaccessibility of the analogous rubidium phase.

Several different methods for formation of zeolite films have been investigated, and the properties of these films compared with view to thermal processing of the films, or forming the basis of a high throughput solid state array. Films were characterised using powder x-ray diffraction and scanning electron microscopy. Thermal processing of the zeolite films was performed to collapse the zeolite into a reversibly photochromic sodalite.

Chapter 1
Introduction

Section 1: Introduction

1.1 Introduction

Zeolite chemistry spans an exceptionally broad range of the materials industry. The diverse range of structures arising from naturally occurring and synthetic zeolites leads to a variety of potential applications. Zeolites are used as molecular sieves, catalysts and in the pigment industry amongst others. This versatility stems from the porous open framework structures characteristic of zeolites. Within these cavities small molecules and more exotic species may be encapsulated, allowing zeolites to be used for molecular sieving, heterogeneous catalysis and making novel pigments by trapping coloured species. These properties coupled with the low cost of starting materials, for example silica or aluminium, high chemical and thermal stability of zeolites and low toxicity make them ideal for research into novel pigments.

Research into the synthesis and structural characterisation of zeolites can give a better understanding of how structure can be related to properties of interest, such as colour or catalytic activity. The search for novel zeolite structures or synthetic routes to naturally occurring zeolites is ongoing, due to the demand for increased performance in the areas mentioned. Zeolites are framework structures built from simple building blocks based on aluminium and silicon oxide tetrahedra. In order to discuss aluminosilicates and how these structures arise an understanding of more simple chemistry is required and this discussion begins with silicate chemistry.

1.2 Silicates

Silicate chemistry is based around the SiO_4^{4-} tetrahedral unit. This SiO_4 unit can exist as discrete units, but is commonly found linked by corner sharing of oxygen atoms to build up an extended structure. Between one and four corners can be shared in this way, giving this most simple of building blocks a large variation in overall possible structures. For example, by corner sharing of one or two oxygen atoms of each tetrahedron 1 dimensional chains or 2 dimensional rings or sheet structures can be formed. Further corner sharing of all four apical oxygen atoms allows a 3 dimensional framework to be produced. These extended structures make up the family known as tectosilicates. The three most common forms of silicate formed in this way are quartz, cristobalite and tridymite. Silicates of this kind are abundant in nature and comprise about 95% of the earth's crust[1].

1.3 Aluminosilicates

By replacing up to half the silicon atoms in a silicate structure with aluminium aluminosilicates can be formed. As the aluminium tetrahedra contain Al^{3+} instead of Si^{4+} the new stoichiometry of aluminosilicates becomes $[(Al_xSi_{1-x})O_2]_n^{nx-}$. This means that the framework of aluminosilicates is negatively charged, and charge balancing cations must be present in non-framework sites to balance the charge. These are most commonly group 1 or 2 metal cations. It is this property of aluminosilicates that leads to many useful applications. Like pure silicates, naturally occurring aluminosilicates can adopt a wide variety of structure types, from simple chains to rings and extended 3 dimensional structures. Aluminosilicates are categorised into 3 main groups, namely feldspars, feldspathoids and zeolites.

1.3.1 Feldspars

Feldspars are the most common aluminosilicates found in nature. The group makes up approximately 60% of all igneous rocks found on earth[2]. Feldspar structures are further categorised into two groups: the orthoclase feldspars and the plagioclase feldspars. Orthoclase feldspars have the end members of orthoclase, [$KAlSi_3O_8$], and celsian, [$BaAl_2Si_2O_8$], and contain a solid solution between the end groups. Plagioclase feldspars have the end members of albite, [$NaAlSi_3O_8$], and anorthite, [$CaAl_2Si_2O_8$], and contain a solid solution of $Na_{1-x}Ca_xAl_{1+x}Si_{2-x}O_8$, where $0 \leq x \leq 1$.

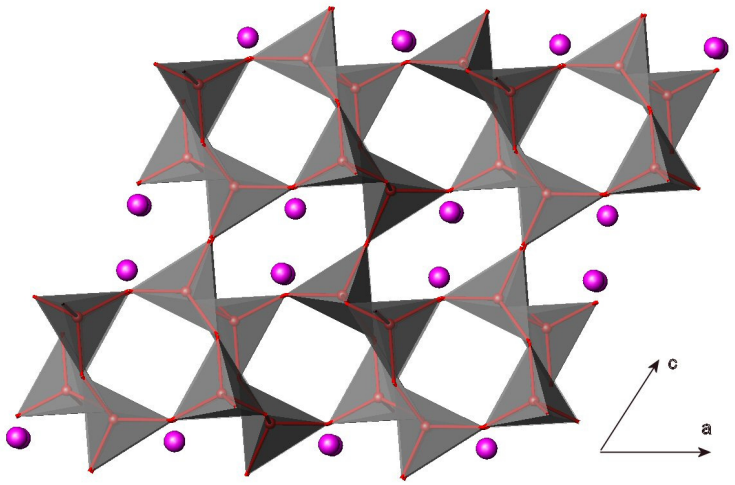

Figure 1.1 The structure of orthoclase: $KAlSi_3O_8$ with Al/Si corner sharing tetrahedra in grey and K^+ ions in pink.

Feldspars are characterised by a network of corner sharing aluminium and silicon tetrahedra, AlO_4 and SiO_4. Charge balancing, metal cations are trapped in the cavities formed by the continuous framework. Feldspars tend to have smaller cavities and channels than the other groups of aluminosilicate, and have therefore been less studied for applications involving entrapment of large species or ions. The density of an aluminosilicate can be described in terms of tetrahedral unit density, defined as the number of tetrahedra per 1000 $Å^3$. For feldpars this falls between approximately 25 and 30 units.

1.3.2 Feldspathoids

Feldspathoids have more open structures than feldspars, with tetrahedral unit densities between 20 and 25. Their larger cavities and channels allow them to contain larger and more metal cations, and even anions. Sodalite and nepheline are both examples of feldspathoids. Sodalite[3], $[Na_8[AlSiO_4]_6Cl_2]$, is a simple cubic feldspathoid, although now the name has become synonymous with the family of structures containing the same framework[4] with various anions and cations housed within. Examples of these Sodalites include *Lapis Lazuli*, a naturally occurring blue mineral whose synthetic analogue is ultramarine, and hackmanite, which are both discussed in more detail later.

Nepheline[5], $[NaAlSiO_4]$, is a feldspathoid containing distorted 6 member rings in the *ab* plane. This creates channels running along the *c* axis.

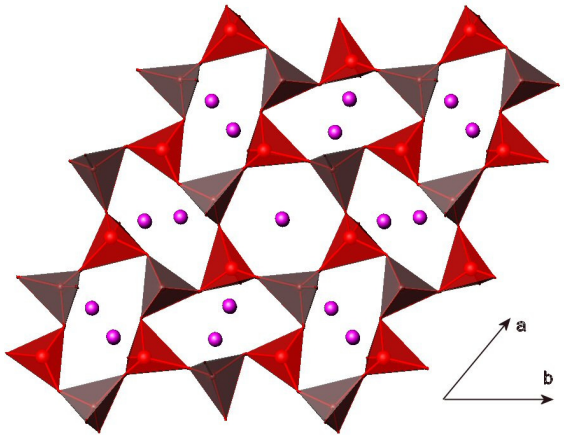

Figure 1.2 The structure of nepheline, $NaAlSiO_4$, with SiO_4 tetrahedra in grey, AlO_4 tetrahedra in red and Na^+ ions in pink.

Some structural analogues of feldspathoids display water absorption or ion exchange properties. These then fall into the class of zeolites, as these properties are indicative of that group of aluminosilicates.

1.3.3 Zeolites

Zeolites are microporous framework aluminosilicates, and can contain much larger cavities than either feldspars or feldspathoids, with typical tetrahedral unit densities of between 10 and 20. They too, are based on the tetrahedral building blocks of $[SiO_4]^{4-}$ and $[AlO_4]^{5-}$. A pure "tectosilicate" with a stoichiometry of SiO_2 would be uncharged, but for every aluminium atom present in the framework cations such as group 1 and 2 metals are needed to balance the charge. These cations sit on non-framework sites in the zeolite structure. As with feldspathoids, zeolites can also contain anions or larger molecular species, most commonly water. This substitution of aluminium into a silicate structure means that the framework composition of a zeolite is $[Si_{1-x}Al_xO_2]^{x-}$.

The first reported example of a zeolite was natural Stilbite, which was discovered in 1756 by Cronsted[6]. The group of materials was named from two Greek words meaning "boiling" and "stone" because of the steam observed to be produced upon heating a sample of the natural mineral. The first synthetic zeolites were produced much later. The first reliable syntheses of many zeolites were performed by Barrer in the twentieth century[7]. Barrer synthetically reproduced naturally occurring zeolites and later went on to introduce many novel synthetic zeolites. Some of Barrer's synthetic routes are still used today, or are modified for the mass production of zeolite systems.

Zeolite structures can be very complex and difficult to visualise, due to the very large and sometimes very complicated unit cells involved. Thus, unit cells can be simplified or broken down into smaller units to aid description of the structure. These units are referred to as secondary building units or SBUs.

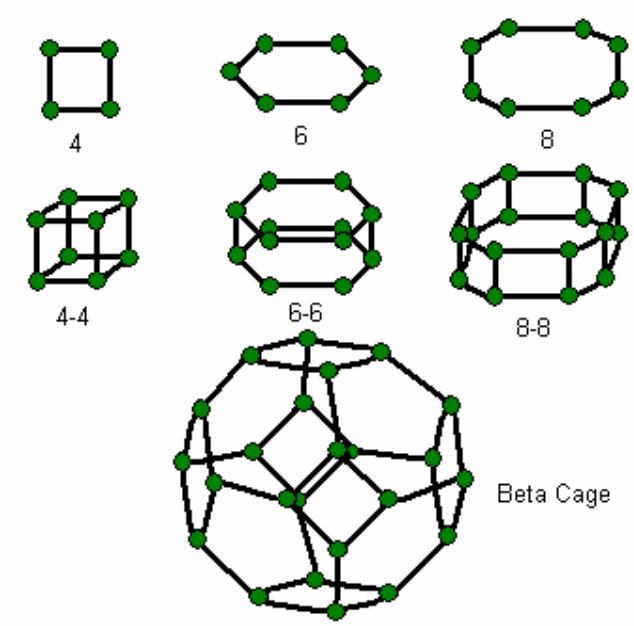

Figure 1.3 Examples of secondary building units of zeolites with green circles representing aluminium or silicon tetrahedra. Black lines represent oxygen bridges

These simple units can be combined to give a vast variation in theoretical zeolite structure types. Of the around 800 theoretical structure types possibly formed using these building units the International Zeolite Association[8] (IZA) currently recognises over 120 synthesised and characterised structures. Each framework type is then assigned a unique 3 letter code to distinguish it from other structures, for example SOD is chosen to represent the sodalite framework type. This system makes it much easier for the user to quickly identify structures.

The formation of zeolites is governed by Lowenstein's Rule[9]. This states whenever two TO_4 tetrahedra are linked by an oxygen bridge only one of these tetrahedra may be centred on an aluminium atom, or in essence that an **Al-O-Al** linkage is forbidden. The other centre must be occupied by silicon or another small ion of electrovalence four or more, e.g. phosphorus. If two aluminum centred tetrahedra are adjacently linked by an oxygen bridge, then one of them must be coordinated to at least 5 oxygen atoms. In this way *Lowenstein's Rule* governs which zeolite structures are theoretically possible. This means that the highest theoretical Al:Si ratio possible for a zeolite is

1:1. Some zeolites display this ratio, for example zeolite A and faujasite, as does sodalite. Zeolite A of the Linde Type A (LTA) structure type exhibits this 1:1 ratio of aluminium to silicon and was first synthesised by Reed and Breck[10]. The figure below shows how the structure is built up from secondary building blocks of 4-4 cubes and sodalite type cages, otherwise known as β-cages.

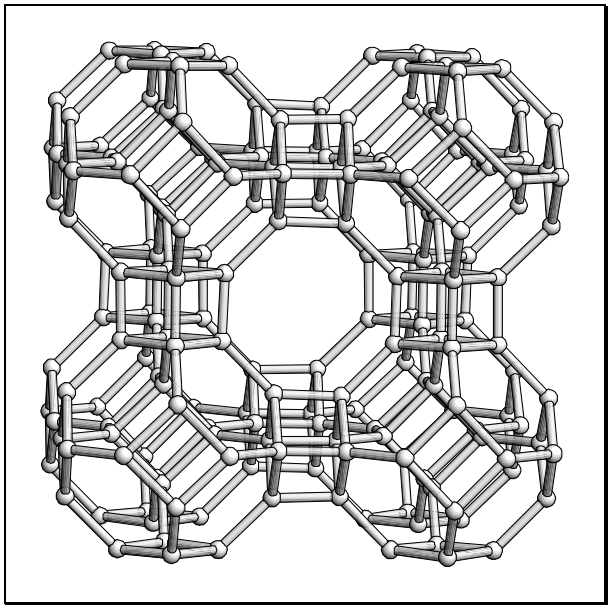

Figure 1.4 A simplified ball and stick based structure of zeolite A

Aluminium and silicon tetrahedra, TO_4, are represented here by balls connected by sticks to form the open framework. This is a common way of representing zeolites as it provides a less cluttered view, allowing the cavities to be seen much more easily.

Compared with the less open structures of feldspars and feldspathoids, zeolites are a lot less dense and possess much larger internal surface areas. This is generally about 300-700 $m^2\ g^{-1}$ with approximately 98%[11] of this housed within the cavities and channels of the framework. It is this large surface area that gives rise to the large array of potential zeolite applications, from molecular sieves to catalysis to pigments. On non-framework sites in the cavities between the TO_4 tetrahedra are the charge balancing cations. This gives rise to the general formula of a zeolite:

$$M^{n+}_{x/n}[Al_xSi_{(1-x)}O_4].yH_2O$$

Where M is a charge balancing cation, most usually a group 1 or 2 metal and n is the charge on this cation. The absorbed water content, y, will vary between different systems depending on the size of the pores and the nature of the charge balancing cations.

For the majority of zeolite systems x will not be greater than 0.5 to preserve Lowenstein's Rule, and this is the case for most zeolites formed hydrothermally by simple solution based syntheses. Other routes, for example high temperature solid state synthesis, can give rise to structures that fall outside of *Lowenstein's Rule*. For example the aluminate sodalites, $M_8(AlO_2)_{12}X_2$[12,13,14], formed from high temperature reactions between alumina and metal salts, where M is a group 2 metal cation and X is a divalent anion such as SO_4^{2-}, O^{2-}, S^{2-}, Se^{2-}. These framework structures only contain aluminium tetrahedra, and thus do not observe Lowenstein's Rule.

1.4 Sodalites

Sodalite[3], $[Na_8[AlSiO_4]_6Cl_2]$, is a simple cubic feldspathoid, although now the name has become synonymous with the family of structures containing the same framework[4] with various anions and cations housed within. The name sodalite is derived from the high sodium content present in the mineral. The first structural determination of sodalite was performed by Pauling in 1930[15], using a sample of the natural mineral. It was not until the late seventies that Henderson and Taylor[4] proposed the term sodalite be used to describe the whole family of minerals possessing the same framework structure.

Pauling's single crystal structural determination showed sodalite to have a cubic lattice parameter of 8.870 Å and a space group of *P*-43*n*. The aluminium, silicon and chlorine atoms are located on fixed sites in the structure and Lowenstein's rule is obeyed. Silicon to oxygen bond distances in the framework were shown to be approximately 1.65 Å and aluminium to oxygen bond distances approximately 1.73 Å. These distances are in agreement with the ionic radii of the two atom types, which would yield a longer Al-O separation than the Si-O length.

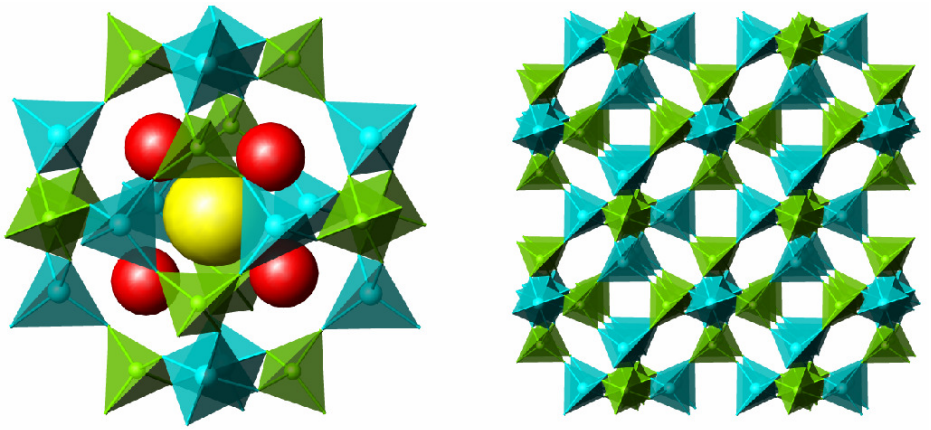

Figure 1.5 A cage and the extended structure of a sodalite framework

The extended structure of sodalite is made up of beta cages, which are larger units built from aluminum and silicon centred tetrahedra. Six-fold rings of $(Al,Si)O_4$ tetrahedra are packed parallel to the (111) plane and four-fold rings of $(Al,Si)O_4$ tetrahedra are packed parallel to the (100) plane. This results in a cubo-octohedral cavity being formed, also known as a beta cage, which then replicates to form the entire extended network.

Within the cages the Al-O-Si framework bond angle is fairly flexible and can vary in the range 120 - 160°[16]. This angle is dependent on the lattice parameter. The Al-O-Si bond is bent forcing the four and six membered rings to pucker as the oxygen atom is forced out of the Al-O-Si plane. Adjacent oxygen atoms alternate between pointing in and out of the cage, which results in varied coordination of the metal ions within the framework. More open frameworks with little or no puckering give a metal coordination number of 7, as the metal ion is able to coordinate strongly with six framework oxygen atoms as well as the anion at the centre of the beta cage. Less open frameworks with significant puckering lead to a coordination of 4, as the metal ion is only strongly coordinated to three framework oxygen atoms and the central anion.

The basic beta cage of sodalite forms part of the fundamental building blocks for a number of more complex zeolite structures. The structure type of sodalite can also be seen in many non zeolite framework type structures. For example sodalite is isotopic with the frameworks of beryllosilicate $[Be_6Si_6O_{24}]^{12-}$, borate $[B_{12}O_{24}]^{12-}$ and aluminate

$[Al_{12}O_{24}]^{12-}$. Other framework atoms are also apparent, with both gallium and germanium replacing silicon and aluminium respectively in the sodalite structure, and even the gallium germanium analogue being known.

The flexibility of the sodalite framework means that a large number of different anions and cations can be incorporated into the many varied framework types. Considering the general formula of a sodalite to be $C_8(T1_6T2_6O_{24})A_2$, examples of *C* include: Li^+, Na^+, K^+, Fe^{2+}, Zn^{2+}, Mn^{2+}, Ca^{2+}; *T1*: Al^{3+}, Ga^{3+}, Be^{2+}; *T2*: Si^{4+}, Ge^{4+}, Al^{3+}; and *A*: F^-, Cl^-, Br^-, I^-, OH^-, S^{2-}, SO_4^{2-}, although this list is by no means exhaustive.

1.5 Other Framework Materials

Although not technically zeolites, which contain only aluminium and silicon centred TO_4 tetrahedra by definition, other zeolite-like framework materials can be formed by substitution of other elements into the framework. The most commonly found elements in such structures are phosphorous, gallium and germanium, with other possible framework atoms including boron and beryllium. These frameworks can be categorised in much the same way as their parent zeolite structures.

By replacing the silicon in a zeolite structure with phosphorous a new family of aluminophosphates can be formed. This was first discovered by Union Carbide in 1982[17,18]. For the most part these structures have a Al:P ratio of 1:1 and consist of alternating AlO_4 and PO_4 tetrahedra. Unlike their corresponding zeolites, these frameworks are charge neutral and do not require the charge balancing non-framework cations found in aluminosilicates.

In a similar fashion gallium and germanium can be substituted into a zeolite framework to replace aluminium and silicon respectively. In this way gallium silicates, aluminogermanates, and even gallium germanates can be formed.

1.6 Zeolite Thin Films

Thin films or membranes of various zeolites have been synthesised on a number of different substrates, such as metals, glasses and mica. The desirable thickness of the layer is dependent on the specific application, which makes for a wide varied research area. For instance, ZSM-5 membranes are particularly useful in separating a mixture of hydrocarbons[19]. As well as being used for separations of mixtures of gases or liquids zeolite films can be employed in gas sensors[20,21], where a porous nanosized layer is preferable making for high sensitivity. These films can be produced by post synthetic attachment, or by carefully controlled crystallisation on a surface.

For other applications, for example depositing zeolite onto a substrate for subsequent reaction, or for forming the basis of a high throughput solid state or sol-gel type array, a thicker layer is preferable for ease of observation and characterisation. Thus, the method of layer formation must be carefully adjusted for the required application.

1.6.1 Film Formation by Direct Crystallisation

Zeolites can be crystallised directly onto the substrate using simple hydrothermal reactions[22]. The substrate is placed inside the reaction vessel with the normal reactants for synthesis of the particular zeolite. The substrate then acts as a nucleation site for crystal growth, resulting in film formation.

The thickness of the film can be controlled to some extent by the reaction conditions employed. The work by Cetin *et. al.*[22] suggests that thinner films can be produced by using lower temperatures for an extended period of time. Temperatures as low as 45ºC can be used to successfully produce films of about one micron. This method is very useful for the mass production of many zeolite covered substrates, but other methods of film formation need to be utilised if a thinner film is desired.

1.6.2 Organic Linkers to Film Formation

Organic linkers can be employed to couple zeolite crystallites to a substrate such as mica or glass. The deprotonated silanol groups act as binding sites for the organic linkers, which have functionalities that can react to produce a single chain linking the zeolite to the substrate. Work by Yoon *et. al.*[23,24] shows that this method of film formation can lead to a uniformly oriented film of crystallites with good coverage of the substrate.

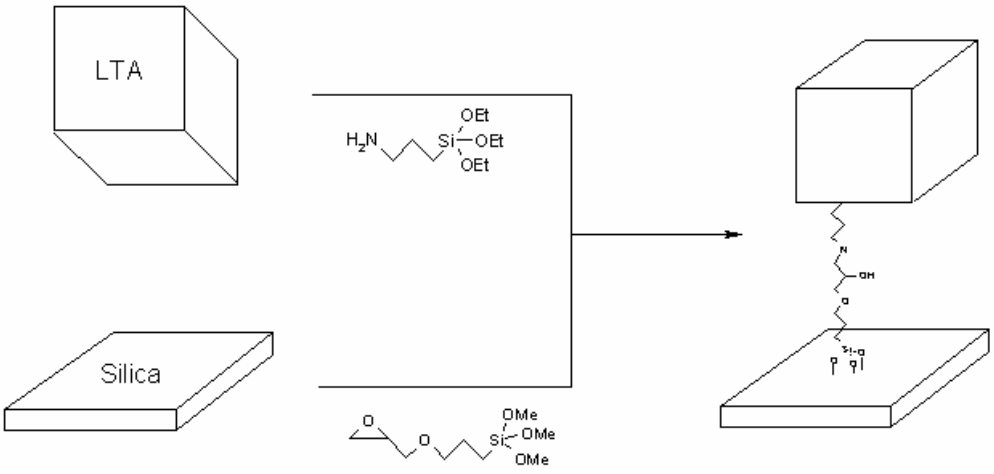

Figure 1.6 Organic linkers producing zeolite films

This example shows the formation of a chemical linkage by a ring opening of an epoxide by a primary amine, but other organic linkers could be easily employed, for instance a carboxylic acid and an alcohol to produce an ester linkage. This method of film formation is very useful for producing particularly thin films, as only one layer of crystallites will ever be deposited onto the substrate. Some drawbacks of this method are that it is a three step process, which is very time consuming and often expensive. To assure that the only linkages are between zeolite and substrate the two must be treated individually with one of the linkers and the combined in the third step.

Reactants such as epoxides can be air or moisture sensitive so reactions have to be undertaken in an inert atmosphere. This can lead to problems with finding a suitable reaction vessel if a large area of substrate is desired. This organic linkage method could be unsuitable if further reaction of the zeolite is required at high temperatures, because the heat may compromise the stability of the linkage and result in film degradation.

1.6.3 Film Self Assembly

Thin films of zeolites can be produced from a solution of amphiphiles and colloidal zeolite particles[25]. Molecules with a polar head group and a large hydrocarbon chain can be adsorbed to the suspended zeolite particles, which then aggregate on the surface of a substrate such as a silicon wafer. The hydrophobic tail groups pack together to minimise any interactions with the water, and form a bilayer at the silicon water interface. The aggregation of the colloidal zeolite particles at this bilayer forms the thin film of zeolite on the substrate.

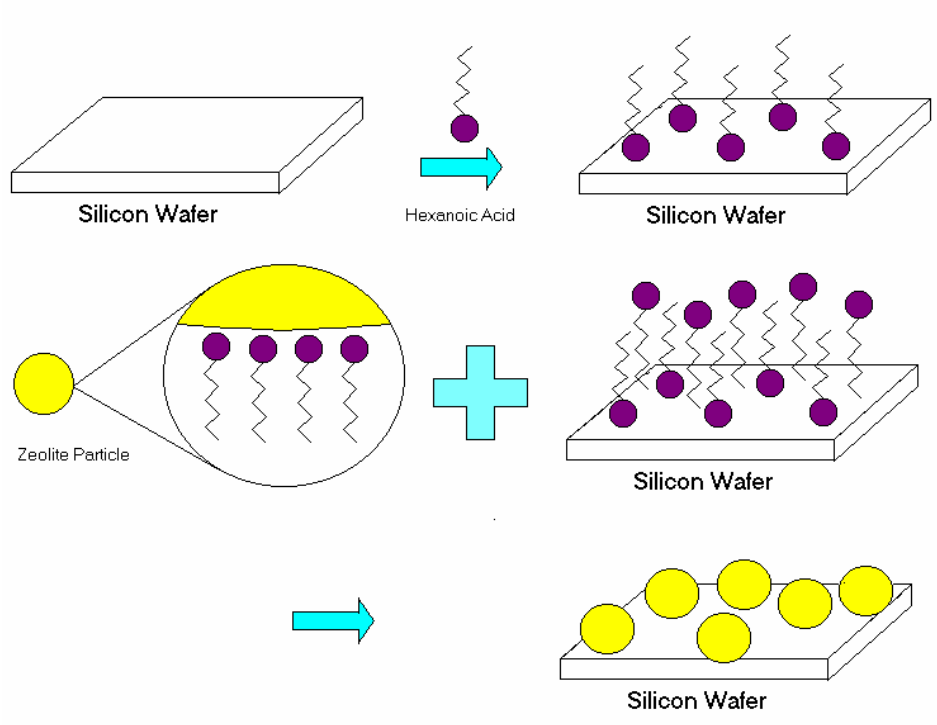

Figure 1.7 Zeolite film self assembly using hexanoic acid

The pH of the solution is thought to be of importance for the formation of such films[25]. Coagulation of the zeolite particles and deposition only occurs in acidic conditions, so an acid (HCl) must be added. This is because at high pH the hexanoic acid molecules will be deprotonated and will not be able to adsorb to the surface as easily as at lower pH. The concentration of the surfactant is also of key importance, as they need to aggregate in the correct fashion to allow adsorption to the substrate.

This method of film formation has some advantages over the other methods described here. The method is relatively inexpensive when compared to other methods of film formation and should lead to a uniform film thickness. Zeolite layers can be deposited quickly and easily using this method.

1.7 Optically Active Materials

1.7.1 Ultramarines

Ultramarine occurs naturally as "lapis lazuli" and is an important commercial pigment because of its desirable deep blue colour. The natural material was even used by the ancient Egyptians as decoration. Ultramarine was first produced industrially in the early nineteenth century[26], and the method of production is very simple, but environmental concerns mean it is desirable to come up with new methods of synthesis that limit sulphur emissions. One route for ultramarine synthesis uses zeolites as precursors, as first outlined by Kumins *et. al.* in 1953[27]. Sulphur chromophores, or colour producing species, can be introduced into the cavities of these porous structures to produce the intense colouration seen in ultramarine blue. Using zeolites as precursors to ultramarine can lead to either the sulphur being taken into the pores of the zeolite, or a collapse into the sodalite structure, which also produces pigments.

The intense colouration of ultramarine blue arises from the S_3^- chromophore with a formal oxidation state of minus one-third per sulphur atom[28]. Other polysulphide species are responsible for other colours, for example the S_2^- chromophore gives a yellow colour, and is present to a lesser extent in the sodalite ultramarines.

More recently, synthetic routes to ultramarines have been developed to reduce sulphur emissions, which are a problem because ultramarine is manufactured industrially on a large scale. A direct hydrothermal synthesis from zeolites and polysulphides can be used for this purpose[29]. Ultramarine can be synthesised in this way by impregnating zeolites with a solution of polysulphides and then a short calcination under milder conditions than the analogous solid state route. This synthesis produces fewer volatile sulphur emissions.

1.7.2 Tenebrescence

Also known as reversible photochromism, tenebrescent materials exhibit a distinct colour change when irradiated with UV light for a short period of time. This property would obviously be very useful for applications where a discreet marking of a product or property was required, for example stolen goods could easily be identified under a UV lamp if they were tagged with a tenebrescent pigment.

One group of materials that display the phenomenon of tenebrescence are the sodalites, an example of which is the chloride containing sodalite: $Na_8[AlSiO_4]_6Cl_2$. A naturally occurring example of sodalite is hackmanite, which has the structure: $Na_8[AlSiO_4]_6(Cl_{x-2}, S_{x/2}\square_{x/2})$ and can be seen to tenebresce upon UV exposure. This was first seen in the 1954[30] when a natural sample was repeatedly exposed to UV radiation. The crystal structure of hackmanite was not known until much later[31]. The sodalite framework is made up of alternating SiO_4 and AlO_4 tetrahedra forming 4 and 6 membered rings. These rings link to form the repeating beta cage unit found in many other zeolites.

Hackmanites are characteristically white and change to a colour such as pink or blue upon exposure to a UV light source. The sample will remain coloured if it is kept in a dark room and will slowly bleach when exposed to a white light source, for example natural sunlight.

It is thought that the mechanism of tenebrescence in hackmanites relies on F-centres. An F-centre is characterised by a trapped unpaired electron. The movement of this electron to an available energy level creates the colour, as the difference in energy of the electron after moving to another energy level corresponds to a wavelength in the visible region. Varying this difference in energy will give rise to different colour changes upon tenebrescence.

Cl	Na	Cl	Na	Cl
Na	Cl	Na	Cl	Na
Cl	Na	e^-	Na	Cl
Na	Cl	Na	Cl	Na
Cl	Na	Cl	Na	Cl

Figure 1.8 Schematic of an F centre

1.7.3 Triboluminescence

Triboluminescence, also known as mechanoluminescence, is the stress activated emission of light from a material. Applying direct mechanical pressure to a triboluminescent material will cause it to produce light, which can be in the visible region with an afterglow of hours. An application of such materials could be to identify stress fractures on an aeroplane coated with a paint containing the mechanoluminescent material.

Many natural materials exhibit this phenomenon, which can be intense enough to be seen with the naked eye in a dark room. Materials such as glasses, salt and sugars can be observed to emit light upon stress fracturing[32,33,34]. The most intense of the natural samples are sugars, and mechanoluminescence can clearly be observed by breaking some varieties of sweets in a darkened room, which give off a blue light.

More recently in the 1990's inorganic materials have been produced that exhibit triboluminescence. Materials such as $Sr_3Al_2O_6$: Eu, Dy[35] and $Sr_4Al_{14}O_{25}$: Eu, Dy[34] have been reported as having an emission intensity of up to 50 times greater than the sugars, and have a characteristically long afterglow of many hours.

It is thought that the doping of the phase with a lanthanide is responsible for this deformation luminescence, for example, in the case of the europium Eu^{2+} centres are the active species. The actual mechanism of the luminescence is thus far poorly understood, as the products of reactions are often mixed phase, making identification of the active phase difficult. It is theorised that deformation or fracture of the materials excites carriers from filled traps. Electron and holes then combine at the Eu centres to give the luminescence:

$$D + T^* \rightarrow D + T + C$$
$$L + C \rightarrow L^* \rightarrow L + hv$$

Fig. 1.9 Triboluminescence mechanism With D being the deformation, T a filled trap, C the carriers and L the luminescent centre.* [36]

These materials can also be "recharged" by exposure to UV radiation making them both scientifically interesting and very useful.

1.8 Scope of this Work

The scope of this work centred upon the synthesis, characterisation and development of aluminosilicate type framework materials with interesting optical properties. These properties included simple pigment or colour properties, or more advanced optical properties such as smart pigments. These types of pigment react to an external stimulus, such as an applied pressure, for example triboluminescent materials, or a particular wavelength of light, for example in the case of reversibly photochromic materials. The external medium will bring about a colour change in the materials, which could then be used decoratively or for a specific application such as security marking of property. After these pigments were structurally characterised an attempt was made to link the structure of the material to the optical property, and hence elucidate upon the mechanism of any observed colour change.

Some high throughput methods were employed in this work to speed up this discovery purpose. This involved two main high throughput approaches. The first method centred upon development of technologies allowing traditional organic solution chemistry array type synthesis and characterisation to be applied to synthesis in the solid state, using the deposition of films of zeolite on a substrate as a starting point for these investigations. The second approach, where appropriate, used technology to rapidly produce large numbers of materials in bulk using large scale equipment and apparatus, for example wide bore tube furnaces. This method was used when bulk amounts of the samples were specifically required for characterisation of the materials, in particular for neutron diffraction studies.

Initial work involved the synthesis of aluminosilcate precursors to framework materials capable of incorporating and stabilising chromophores which have the potential to be optically active in the manners outlined above. Development of these syntheses was tailored toward phase purity, allowing for efficient further reactions of the precursors, and yield allowing for subsequent bulk synthesis of the optically active materials.

The thermal conversion of these precursors into aluminosilicate frameworks capable of chromophore inclusion was studied in detail. This provided information about these transformations relevant to the effectiveness of incorporating chromophores into the framework. After these initial studies a single system was studied in greater detail. A library of a particular aluminosilicate framework, namely sodalite, containing various chromophores was synthesised and fully characterised. Variation of the composition of non framework sites in reversibly photochromic sodalite frameworks was studied to determine any relationship between structure and the observed optical property. Attempts were made to correlate changes in the optical properties of the materials with variation in the structure, and hence provide information about the mechanism of reversible photochromism.

1.9 References

[1] N. N. Greenwood and A. Earnshaw, *'Chemistry of the Elements'*, 1984 Pergamon Press, 399

[2] W. L. Brown (ed.), *'Feldspar and Feldspathoids'*, 1984 (NATO ASI Series No. C137), D. Riedel, Dordrecht

[3] L. Pauling, *Z. Kristallogr.*, 1930, **74,** 213

[4] C. M. B. Henderson and D.Taylor, *Spectrochim. Acta.,* 1979, **35A**, 929

[5] C. M. B. Henderson and D. Taylor, *Miner. Mag.,* 1988*,* **52,** 708

[6] A.F. Cronstedt, *Akad. Handl. Stockholb.*, 1756, **17**, 120

[7] R. M. Barrer, *Hydrothermal Chemistry of Zeolite*, Academic Press, London 1982, 72

[8] W.M. Meier, D.H. Olson and Ch. Baerlocher, *'Atlas of Zeolite Framework Types'*, 5th Edition, Amsterdam : Elsevier (2001)

[9] W. Löwenstein, *Am. Miner.*, 1954, **39**, 92

[10] T.B. Reed, D.W. Breck, *ibid.*, 1956, **78**, 5972

[11] J.M. Newsam, *'Solid State Chemistry: Compounds'*, Chapter 7, A.K Cheetham and P.Day (eds.), Oxford University Press (1992)

[12] R. Kondo, *Yogyo Kyokai Shi.,* 1965*,* **71,** 1

[13] M.E. Brenchley and M.T. Weller, *Angew. Chem. Int. Ed. Engl.,* 1993*,* **32** 1663

[14] G. Engelhardt, H. Koller, P. Sieger, W. Depmeier and A. Samosan, *Solid State Nucl. Magn. Reson.,* 1992*,* **1,** 127

[15] L. Pauling, *Z. Kristallogr.*,1930, **74**, 213

[16] Beagley and J.O. Titiloye, *Struct. Chem.*, 1992, **3(6),** 429

[17] S.T. Wilson, B.M. Lok, C.A. Messina, T.R. Cannan and E.M. Flanigen, J. *Am. Chem. Soc.*, 1982, **104,** 1146

[18] S.T. Wilson, B.M. Lok, C.A. Messina, and E.M. Flanigen, *Proc. 6th Int. Conf. On Zeolites*, 1984 Ed. D. Olson and A. Bisio Butterworths 97-109

[19] E. R. Geus, M. J. den Exter, H. van Bekkum, *J. Chem. Soc. Faraday Trans.,* 1992, **88**, 3101

[20] S. Mintova, T. Bein, *Micropor. Mesopor. Mater.*, 2001, **50(2-3)**, 159

[21] S. Mintova, S. Mo, T. Bein, *Chem. Mater.*, 2001, **13(3)**, 901

[22] T. Cetin, M. Tatlier, A. Erdem-Senatalar, U. Demirler, M. Urgen, *Micropor. Mesopor. Mater*., 2001, **47**, 1

[23] A. Kulak, Y. Lee, Y. S. Park, K. B. Yoon, *Angew. Chem. Int. Ed.,* 2000, **39**, 950

[24] A. Kulak, Y. Lee, Y. S. Park, Y. S. Chun, K. Ha, K. B. Yoon, *J. Am. Chem. Soc.,* 2000, **122**, 9308

[25] G. Cho, I. Moon, Y. Shul, K. Jung, J. Lee, B. M. Fung, *Chem. Lett.,* 1998, 355

[26] J. B. Guimet, *Bull de l'encouragement pour l'industrie nationale,* 1828, C. G. Gmelin, *Schweigger's polyt. Journal,* 1828, **54**, 360

[27] C. A. Kumins, A. E. Gessler, *Ind. Engng. Chem.,* 1953, **43**, 3

[28] J. R. Morton, in *Proc. Coll. Ampere,* ed. P. Averbruch, North Holland, Amsterdam, 1969, **15**, 299

[29] S. Kowalak, M. Pawlowska, M. Miluska, M. Strozyk, J. Kania, W. Przystajko, *Colloids and Surfaces A,* 1995, **101**,179

[30] D. B. Medved, *Am. Mineral.,* 1954, **39**, 615

[31] R. C. Peterson, *Can. Mineral.,* 1983, **21**, 549

[32] Y. Enomoto, H. Hashimoto, K. Kikuchi, *Philos. Mag.,* 1996, **74**, 1299

[33] B. T. Brady, G. A. Rowell, *Nature,* 1986, **321**, 488

[34] Y. Kawaguchi, *Phys. Rev. B,* 1995, **52**, 9224

[35] M. Akiyama, C. Xu, K. Nonaka, T. Watanabe, *App. Phys. Lett.,* 1998, **73**, 3046

[36] Y. Lin, Z. Tang, Z. Zhang, C. Wen Nan, *App. Phys. Lett.,* 2002, **81**, 996

Chapter 2
Experimental Techniques

2.1 Introduction

Samples described in this thesis have been synthesised either by standard high temperature solid state methods in air or flowing gas, or by standard or modified high pressure hydrothermal reactions.

Various techniques have been used to fully characterise the products described in this thesis. Primarily, powder x-ray diffraction (PXD) was used allowing fast phase identification by way of 30 minute scans over a small 2θ range of 5 – 70°. Information about phases present, impurities and unit cell parameters could be acquired in this way. Samples of interest were then subjected to longer scans (12-16 hours) over a larger 2θ range, typically 5 - 120°. This higher quality data was used to perform structural refinements using the Rietveld method[1,2],giving information about atom positions and bond lengths.

Where appropriate, powder neutron diffraction (PND) was used to further characterise products, and to conduct variable temperature diffraction studies to monitor reactions in progress. PND allowed a more accurate determination of the position of lighter atoms, such as oxygen, and was able to distinguish between atoms of similar atomic weight, such as aluminium and silicon. This is important to many of the aluminosilicates contained in this thesis.

Thermogravimetric analysis (TGA) was used as a precursor to thermal diffraction experiments, and gave information about thermal stability of a product, reaction temperatures of a reaction mixtures and amount of adsorbed water in a sample. Scanning electron microscopy (SEM) was used to study the morphology of samples, particularly of thin films of materials. Energy dispersive x-ray spectroscopy (EDX) was used as a basic method of studying elemental composition of samples.

2.2 Synthetic Methods to Solid State Products

2.2.1 High Temperature Solid State Reactions

Many zeolites can be used as precursors for the formation of other aluminosilicate frameworks, such as the collapse of zeolite A into sodalite type frameworks studied in detail in this work. High temperature solid state calcination methods were used to produce these materials. Samples were ground and intimately mixed using a pestle and mortar or a mechanical ball mill to ensure a greater contact surface area between starting materials. These were then heated to high temperatures to provide the thermal energy required for the reaction to take place. Where a reductive media were required, tube furnaces were used to allow a flowing gas mixture of 5% hydrogen in nitrogen over the sample.

2.2.2 Hydrothermal Methods

Two main hydrothermal methods were used as synthetic routes. The first, for relatively low pressure work, utilised Parr® General Purpose Acid Digestion bombs. These bombs comprise a Teflon inner, housing the reaction mixture, and a stainless steel casing to contain the pressure generated upon heating. Starting materials and solvent were loaded into these bombs and sealed, before being transferred to an autoclave oven for heating. The reaction pressure corresponds to the vapour pressure of the solvent used at the chosen temperature. For this work water was used as the solvent, and the reaction vessels are rated to a maximum of 240 °C for aqueous work. Bomb sizes of 28ml, 45ml and 125ml were used as appropriate for the reaction.

For some systems higher temperatures and pressures were required, hence a second hydrothermal method was employed. In these instances an in-house, high pressure hydrothermal rig was used to achieve the desired reaction conditions.

The high pressure hydrothermal rig uses reaction vessels capable of working at temperatures up to 800°C and pressures up to 3 kBar. Typically, reaction mixtures were sealed into gold capsules prior to heating. Gold tubing was pre-treated by cleaning in dilute acid, and then heated at 600°C for about 16 hours. This softened the gold to facilitate arc-welding into a sealed capsule around the reactants. The capsule was then transferred to a bomb, followed by addition of a steel spacer rod, which reduces the amount of water under high pressure. Finally, the remainder of the bomb was filled with distilled water.

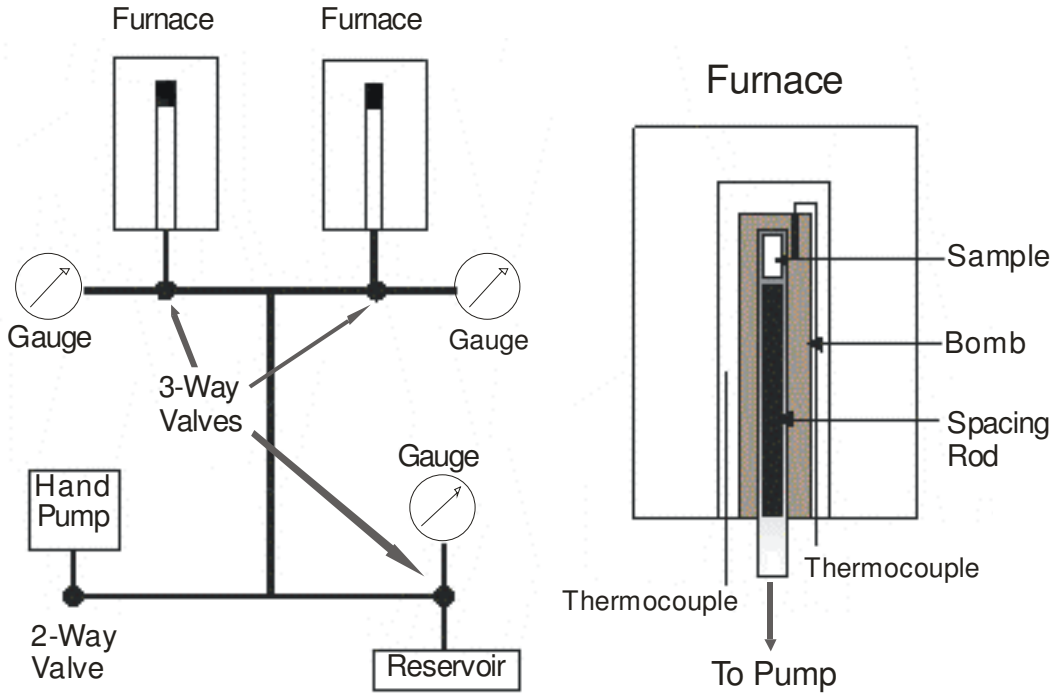

Figure 2.1 Schematic of the high pressure hydrothermal rig

The assembled bomb was then mounted and secured onto the pump system, and sealed by pressurising a machined hardened steel cone onto the pressure line. A thermocouple was attached to the bomb and a vertically mounted tube furnace was pulled down over the reaction vessel. This extra thermocouple gave a more accurate temperature reading of the reaction than the separate furnace thermocouple. This whole assembly was housed in a steel cabinet with sliding door for safety reasons. Whilst heating the system was opened to a safety reservoir maintained at 1 kBar, which was then closed as the reaction reached the desired temperature. After this the hand pump was used to pressurise the reaction as appropriate, and the bomb was closed for the duration of the reaction. The reservoir was then opened again while the apparatus cooled and the gold capsule was retrieved and opened.

This high pressure rig serves to mimic natural geological conditions to access synthesis of natural minerals and other phases that could not otherwise be formed under lower temperatures and pressures. A much wider range of synthetic conditions gives rise to a broader range of potential products and interesting structural chemistry.

2.3 Powder X-ray Diffraction (PXD)

X-ray diffraction is a structurally probing technique, which is used to give information about the relative positions of atoms in a structure. X-ray photons incident on the structure will be scattered. This scattering can be incoherent – which gives a change in the wavelength (and hence energy), or coherent – where the wavelength and energy of the outgoing x-ray photons remains the same as the incident ones. An important point to note is that x-rays interact with the electron cloud and not the nucleus. X-rays can be used in two ways to this effect. Firstly, for phase identification of known phases, achieved by searching a database of previously identified patterns. Secondly, for performing structural refinements on previously unknown phases.

2.3.1 Basic Diffraction Theory

A structure can be thought of as a series of planes of atoms, spaced at regular intervals. This regularly repeating perpendicular distance between sets of planes is known as the d spacing. Each of these families of planes in a structure has a unique set of integers to describe it, which are known as Miller indices. In a three dimensional structure three of these indices are required to completely describe the family of planes, and are conventionally labelled h, k and l. They are derived from a reciprocal relationship from the lattice parameters a, b and c.

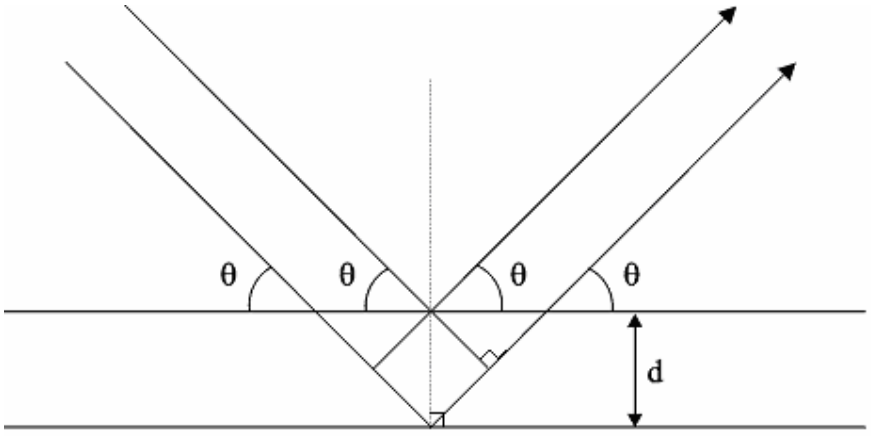

Figure 2.2 Schematic of scattering from parallel planes of point scatterers.

Considering the case of two parallel incident x-ray beams onto a target of separated planes, where θ is the angle of incidence, λ the wavelength of the x-rays and d the distance between the planes, constructive interference will occur if the path difference between the two x-rays is equal to an integer number of wavelengths. This is described by Bragg's Law[3]:

$$n\lambda = 2d\sin\theta$$

Where θ is known as the Bragg angle.

For all angles of θ where Bragg's Law is not satisfied, destructive interference will occur. This means a series of cones of diffraction arise from a sample of randomly oriented crystallites from angles of θ that satisfy Bragg's Law for all of the planes in a structure. The intensity of an observed reflection has many contributing factors. As x-rays interact with electron density as oppose to the nuclei, intensities of reflections will decrease for smaller atoms, making then difficult or even impossible to observe. Thermal vibrations of atoms within a structure can also lead to a decrease in observed intensity. Intensities can be seen to increase if multiple diffraction maxima contribute to a single observed peak. Another important consideration, particularly for very elongated tetragonal unit cells, is preferred orientation, whereby the crystallites in a powder sample prefer to pack in a direction along the long axis of the unit cell. This gives rise to an increase in intensity of certain peaks.

Systematic absences of observed peaks may arise from the symmetry elements of a structure, for example glide planes or screw axes[4,5].

For an orthorhombic unit cell with lattice parameters $a \neq b \neq c$ and angles of $\alpha = \beta = \gamma = 90°$ the relationship between d spacing and lattice parameters can be described as:

$$\frac{1}{d^2_{hkl}} = \frac{h^2}{a^2} + \frac{k^2}{b^2} + \frac{l^2}{c^2}$$

For a tetragonal unit cell with lattice parameters $a = b \neq c$ and $\alpha = \beta = \gamma = 90°$, this becomes:

$$\frac{1}{d^2_{hkl}} = \frac{h^2 + k^2}{a^2} + \frac{l^2}{c^2}$$

Thirdly, for a cubic system where $a = b = c$ and $\alpha = \beta = \gamma = 90°$ this expression can be easily simplified:

$$d = \frac{a}{(h^2 + k^2 + l^2)^{1/2}}$$

Similar expressions can be derived for other unit cell types, but these are not relevant to the work in this thesis.

2.4 D5000 Diffractometer

For the purpose of phase identification a thirty to sixty minute powder pattern was collected for all samples on the Siemens D5000 diffractometer. These "fingerprints" can be referenced against the Joint Committee on Powder Diffraction Standards (JCPDS) Powder Diffraction File (PDF) database[6]. This is a database of known powder diffraction patterns, which can be searched and matched to the collected data to identify all phases present in the sample.

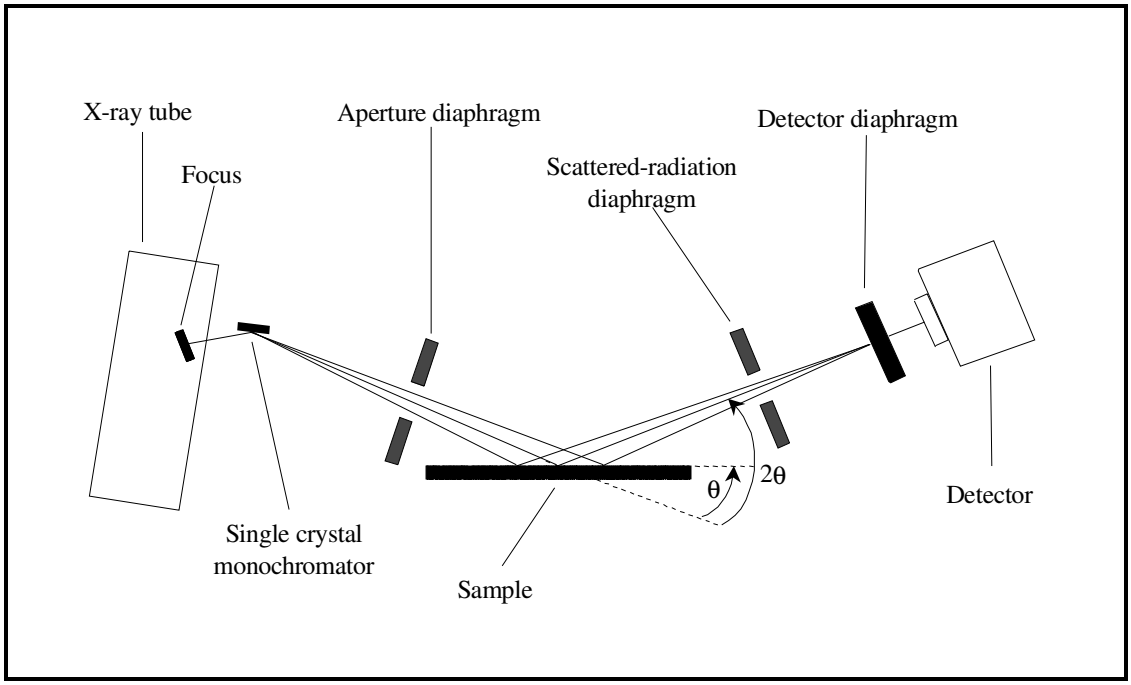

Figure 2.3 Schematic of the Siemems D5000 diffractometer

The D5000 Diffractometer produces x-rays by accelerating electrons over a potential of 40keV onto a copper metal target. These high energy incident electrons remove core electrons from the copper target. Higher energy electrons from the outer shells of the copper drop down to fill these core holes and release a photon, the energy of which corresponds to the difference in energy between the two levels.

There are many levels which the electron could drop from or to, so different energy x-rays are produced at the target. This is not suitable for a diffraction experiment, so one wavelength is selected by a single crystal monochromator. In the case of the D5000 this is copper $K_{\alpha 1}$, which has a wavelength of 1.5406Å. This is particularly suitable because it is similar to the inter atomic distances in a structure. The copper $K_{\alpha 1}$ radiation then passes through an aperture diaphragm, which collimates the x-ray beam, before it is directed onto the sample. Samples are mounted in recessed plastic or aluminium sample holders. Both sample stage and detector are scanned over a selected θ range, with the angular velocity of the detector always twice that of the sample. This ensures that for any angle θ, the diffracted x-rays are collected at 2θ. The detector on the D5000 is a conventional scintillation counter, consisting of a crystal that fluoresces when exposed to x-ray radiation and a photomultiplier tube that measures light from the crystal.

2.5 D8 with GADDS Diffractometer

In a conventional single crystal diffraction experiment there is only one orientation of a family of diffraction planes within the crystal, i.e. all the planes in a particular family are parallel to each other. This produces a pattern of diffraction "spots" in inverse space as the x-rays diffract to a point. In a powder sample there are many crystallites, which are randomly oriented throughout the bulk sample. This gives rise to a cone of diffraction corresponding to each d spacing.

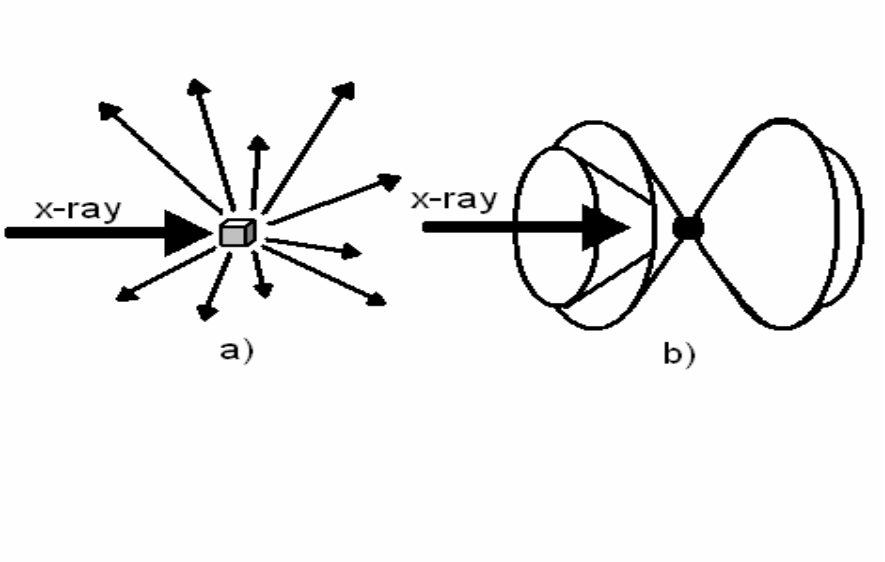

Figure 2.4 Showing diffraction from (a) a single crystal and (b) a powder sample

Conventional detectors only observe a small cross section of this diffraction cone within the plane formed by the source, sample and detector (sometimes referred to as the diffractometer plane), but all other information is lost. For example a scintillation detector scans through 2θ in the diffractometer plane, meaning that a long scan time is necessary. A linear position sensitive detector (PSD) will collect data over a larger 2θ range, leading to faster data collection than a scanning scintillation detector, but is still confined to the diffractometer plane. This means that data collection is still relatively slow.

Very fast collection of diffraction data can be accomplished by employing an area detector, such as the General Area Detector Diffraction System (GADDS). The Bruker D8 Discover with GADDS can collect over a range of 2θ simultaneously, and also sample part of the diffraction cone perpendicular to the diffractometer plane (Fig 2.4). This allows a much greater number of data points to be sampled at the same time, making the collection of powder patterns much faster.

2.6 Powder Neutron Diffraction (PND)

The first neutron diffraction experiments in 1936[7] were preceded by de Broglie's work[8] on wave particle duality. This states that the wavelength of any object in motion can be directly related to its momentum.

$$\lambda = \frac{h}{mv}$$

Where λ is the wavelength, m the object mass, v the velocity of the object and h Planck's constant. For heavy objects this wavelength becomes negligible, but for very light objects, such as neutrons, the wavelength is significant. If at 273 K the root mean square of a Boltzmann distribution of neutron velocities is 2200 ms^{-1}, wavelength is approximately 1.55 Å. As previously discussed in relation to the x-ray experiment, this magnitude of wavelength is particularly well suited to a diffraction experiment, as it is similar to the interatomic distances in a solid structure, and gives good spacings.

Although neutron diffraction experiments hold an added cost and level of complexity over x-ray diffraction experiments, the technique provides invaluable data that cannot be provided by x-rays. The most important physical difference between the two techniques is whereas x-rays are diffracted by the electron density surrounding nuclei, neutrons interact with nuclei themselves. This means that the scattering power of neutrons from a sample is not dependent on atomic number, but on the potential scattering and resonant scattering of a nucleus. As this scattering power can be very different for atoms of a similar atomic weight, a PND experiment can often distinguish between elements close to each other in the periodic table, for example aluminium and silicon. This also means that very light atoms can be observed in the presence of heavier ones, which is not the case for PXD.

Another benefit of using neutrons is that there is no angular dependence on scattering, which allows observation of high angle diffraction maxima. This is information usually lost to a PXD experiment. Conversely a PND experiment has an intrinsically low incident flux as compared to PXD, making experiment times much longer. This can be partially alleviated by being close to the source, using very large detector banks or using large amounts of sample in the experiment.

2.7 Time of Flight (TOF) Powder Neutron Diffraction

There are two main methods used to generate neutrons for diffraction experiments. The first uses a reactor source, such as found at the Institut Laue-Langevin in Grenoble, France. The neutrons are generated by fission in a nuclear reactor, very similar to those present in nuclear power stations, although the reactors are modified for the production of neutrons as opposed to heat. In such experiments neutrons of a single wavelength are selected by a single crystal monochromator, which gives a data output similar to that of a conventional PXD experiment. The second method of generating neutrons, and the one used for this work, is to generate pulsed neutrons from a spallation source, such as ISIS at the Rutherford Appleton Laboratory (RAL). In this method the neutrons are generated by firing high energy particles, in this case protons, at a heavy metal target.

An ion source produces H^- ions which are then injected in 70 MeV H^- ion pulses, via a linear accelerator, into an 800 MeV synchrotron. These H^- ions are stripped of electrons to create a proton beam, which is then accelerated in the synchrotron and directed onto a heavy metal target in the target station, by way of a series of magnets. The collision of these high energy protons with the metal target, usually depleted uranium or tantalum, produces high energy neutrons. Some energy is then removed from these neutrons before they reach the experimental beam lines by moderators. These moderators contain hydrogenated materials, for example water or methane, which slow the incident neutrons by collision due to the relatively large neutron scattering cross section of hydrogen. The neutron pulses then arrive at the beam lines with a suitable wavelength for diffraction experiments.

Using this method of producing pulsed neutrons gives a range of neutron velocities and wavelengths at the experiment and the experimental set-up is different to that of a conventional PXD experiment. For PXD the incident wavelength is fixed by a monochromator, d and the angle of detection θ are the variables, using a scanning detector. For TOF PND the incident wavelength is inherently variable and θ is fixed by using large stationary detector banks. The d spacing can be directly related to the time of flight of a neutron for any known θ by a combination of de Broglie's relationship and Bragg's Law:

$$\lambda = \frac{h}{p_n}$$

$$= \frac{h}{m_n v_n}$$

$$= 2d\sin\theta$$

where *h* is Planck's constant and p_n, m_n and v_n, are the momentum, velocity and mass of a neutron respectively.

Considering a neutron flight path between the three points of moderator, sample and detector where L_1 is the distance between moderator and sample, and L_2 the distance between sample and detector, with corresponding flight times of t_1 and t_2.

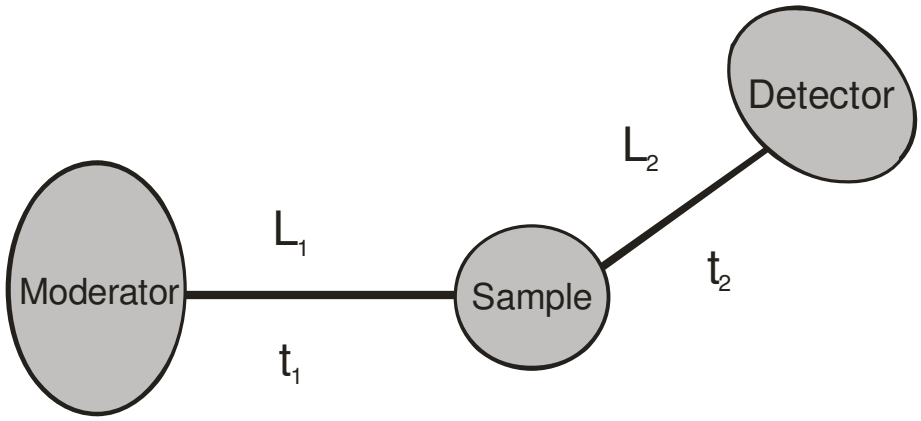

Figure 2.5 Schematic of the neutron flight path from moderator to detector

Then we have:

$$\frac{h}{m_n}.\left[\frac{t_1 + t_2}{L_1 + L_2}\right] = 2d\sin\theta$$

So with total time and path length equal to t and L where:

$$L_1 + L_2 = L \text{ and } t_1 + t_2 = t$$

We get:

$$t = 2dL\left(\frac{m_n}{h}\right)\sin\theta$$

In this way the time of flight of a neutron can be directly related to the d spacing, as all other terms are constant. This is facilitated by the fixed detector arrangement, allowing θ to be known.

2.8 PND Instrumentation – POLARIS

Two diffractometers housed at ISIS were used for the PND studies in this work. The first, POLARIS, is a high flux medium resolution powder diffractometer. POLARIS uses 295 K gadolinium poisoned water moderators to give a 'tight' neutron pulse time structure over a wide range of wavelengths. The main backscattered neutrons are detected by 58 ^{3}He gas filled detectors at fixed angles of $135\ ^{\circ} \leq 2\theta \leq 160\ ^{\circ}$ giving a resolution $\Delta d/d$ of ~5×10^{-3} and a d-spacing range of 0.2-3.2 Å.

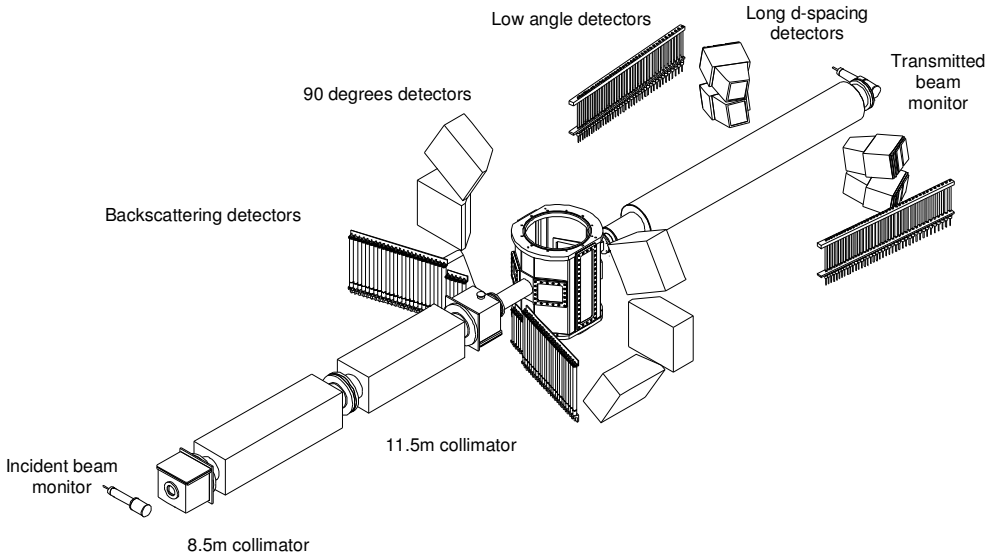

Figure 2.6 Schematic of the POLARIS diffractometer at ISIS[9]

Samples are loaded into Vanadium cans, chosen for low coherent scattering of neutrons, which is then mounted on a sample stage in beam line. POLARIS has a variety of sample environments available, including furnaces and cryostats for variable temperature work and a custom built 20 can sample auto-changer. This can be easily programmed collect data for samples in series eliminating the time taken to change and evacuate sample cans. In this way POLARIS is very suitable for relatively fast collection of a large number of data sets, where very high resolution is not a priority.

2.9 PND Instrumentation - GEM

The second diffractometer used in this work was the general materials instrument GEM, a high intensity, high resolution instrument housed at ISIS. GEM is designed to study disordered materials and crystalline powders and is versatile as a general materials neutron diffractometer. GEM is situated 17M from the target, giving a high incident flux of neutrons and achieves good resolution by using huge banks of detectors.

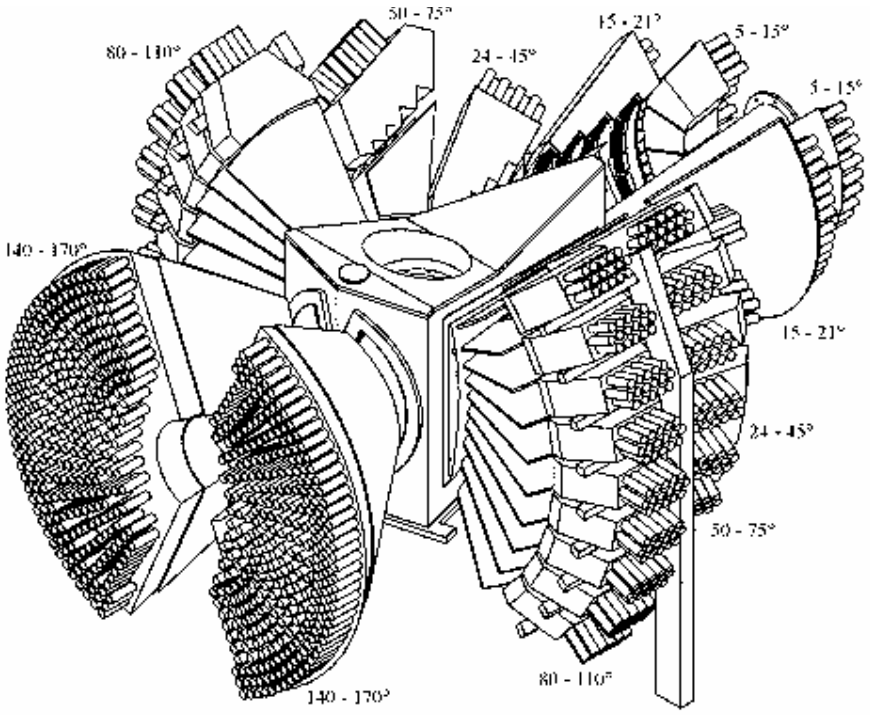

Figure 2.7 The detector banks on GEM at ISIS[10]

The 7 banks of around 9000 zinc sulphide scintillator detectors cover a very large angular range of 1.1° to169.3°, leading to a very large amount of data assimilation.

The high flux and resolution on GEM makes it ideal for monitoring reactions in progression, and phase changes can be observed in this way by collecting small "packets" of data as a reaction mixture is heated. Data is monitored and viewed using the Ariel[11] software.

2.10 Cell Parameters and Rietveld Refinements

The unit cell of a lattice is conventionally the smallest volume repeating unit in the structure that shows the full symmetry of the lattice, from which the whole long range structure could be reproduced by a translation of the unit cell along each of the three axes. The three dimensions of this unit cell can be labelled a, b and c, with the angles between them represented as α, β and γ. For example a cubic system has a = b = c and $\alpha = \beta = \gamma = 90°$.

These lattice parameters can be derived by using a program such as CELREF[12], which can calculate the lattice parameters from an initial structural model and a powder diffraction pattern. Peaks in the pattern are picked manually and the lattice parameter is varied by CELREF using an iterative method to fit the peak positions to the data. This then gives new lattice parameters, which better fit the measured data set.

For a more detailed structural analysis, such as determining bond lengths or atom positions within a unit cell, the GSAS[13] program was used. GSAS uses the Rietveld method[1,2], which compares the data set with a predetermined theoretical model, and minimises the difference between the two using an iterative least squares process.

In 1967 H. M. Rietveld[1,2] developed the method for structural refinements of powder diffraction patterns that GSAS is based on. The iterative method works towards lowering the difference between the observed intensity and a calculated intensity from a starting model. In GSAS this is achieved by flagging certain variables, for example peak shape parameters, the zero point, atomic co-ordinates or background parameters. These are then changed in the theoretical model to produce a better fit with the actual data. A starting model must be provided, making this a true refinement rather than a solution technique.

Early work by Rietveld was based around constant wavelength PND data, which has a near perfect Gaussian peak shape, making it easier to model than PXD data. Later, as

more complex peak shape functions were introduced the method was extended to encompass both types of diffraction pattern.

A typical structural refinement begins with the inputting of a starting model, a structure thought to be similar to the unknown phase. A good model is essential for a successful refinement. Once this is in place variables are refined to allow the model to change to better fit the experimental data. Firstly, scale factor and background parameters are refined. Refinement of these parameters involves only coefficients of ordinary or orthogonal polynomials so the problem is linear and convergence will be trivial. Next, zero point correction, sample displacement and lattice parameters are introduced to the refinement, allowing accurate determination of the position of Bragg reflections. Thirdly, atom positions and isotropic temperature factors on atoms are allowed to refine, fitting the intensities of peaks. Finally, peak shape parameters are refined and further background parameters are added to account for any asymmetry or sample broadening effects. This method is the same for both PND and PXD data, although different instrument parameter files are used in the refinement, to provide closer starting conditions which allows for easier refinement of the data.

During the refinement GSAS uses a least squares method to minimise the function M, which is related to the difference between the model and the experimental data.

$$M = \sum_i w_i (y_i^{obs} - y_i^{calc})^2$$

Where w_i is a weighting factor given by $1/y_i^{obs}$, y_i^{obs} is the observed intensity at each data point and y_i^{calc} is the calculated intensity at each data point.

For an x-ray pattern, all y_i^{calc} are determined from the $|F_K|^2$ values calculated from the starting model by summing of the calculated contributions from neighbouring Bragg reflections (k) and a background b_I :

$$y_i^{calc} = s\sum_k L_k |F_k|^2 \phi(2\theta_i - 2\theta_k) P_k A + y_{bi}$$

where s is the scale factor, L_k contains Lorentz polarisation and multiplicity factors, ϕ is a reflection profile function, F_k is the structure factor for the kth Bragg reflection, P_k is the preferred orientation function, A is an absorption factor and y_{bi} is the background intensity at ith step.

P_k, the preferred orientation function can be derived from

$$P_k = \left[G_2 + (1 - G_2)\exp(-G_1\alpha_k^2)\right]$$

Where G_1 and G_2 are program refinable parameters and α_k is the angle between the symmetry axis and the axis of preferred orientation.

y_{bi} , the background intensity, is modelled by a function that is a cosine Fourier series with a leading constant term[13].

$$y_{bi} = B_l + \sum_{j=2}^{N} B_j \cos[P*(j-l)]$$

For PXD experiments P is the position of the step in 2θ. For PND TOF experiments the times are scaled by 180/TMAX, where TMAX is the maximum allowed by the incident spectrum. Values of B_l and B_j are determined by least squares during the refinement.

The observed peak shape of a powder pattern is mainly instrument dependent. For the D5000 diffractometer the peak profile is described by:

$$\eta L + (1-\eta)G$$

Where

$$\eta = N_A + N_B(2\theta)$$

L is the Lorentzian contribution and G the Gaussian contribution to peak shape. η is a mixing parameter derived from N_A and N_B, which are both refinable.

The individual contributions to peak shape arise from:

$$L = \frac{2}{\pi H_k} 1 \Big/ \left[1 + 4 \frac{(2\theta_i - 2\theta_k)^2}{H_k^2} \right]$$

and

$$G = \frac{(4 \ln 2)^{½}}{H_k \sqrt{\pi}} \exp\left(-4 \ln 2 \left(2\theta_i - 2\theta_k \right)^2 / H_k^2 \right)$$

where $2\theta_k$ is the calculated position for the kth Bragg peak corrected for the counter zero-point and H_k is the full-width-at-half-maximum (FWHM) of the kth Bragg reflection.), $H_{k,}$ varies with the scattering angle $2\theta_k$[14] where:

$$H_k^2 = U \tan^2 \theta + V \tan \theta + W$$

U, V and W are sample and instrument dependent refinable parameters and are used to account for peak broadening arising from the particle size.

For a particular refinement the least squares parameters fall into two sets. The first set defines the peak shape and position and includes variables such as the unit cell parameters, zero point correction, and the asymmetry factor. The second set defines the contents of the unit cell and includes the profile scale factor and the atomic variables, atom coordinates and temperature factors. As well as a visual plot of the data, three reliability factors are used to give a mathematical representation of the fit between observed data and the calculated model, namely $R_{profile}$, $R_{expected}$, $R_{weighted\ profile}$. These are defined by:

$$R_{profile} = R_p = 100 \left[\frac{\sum_i \left| y_i^{obs} - y_i^{calc} \right|}{\sum_i y_i^{obs}} \right]$$

and

$$R_{\exp ected} = R_{\exp} = 100\left[\frac{(N-P+C)}{\sum_i \omega_i (y_i^{obs})^2}\right]^{1/2}$$

Where R_{exp} is defined from the statistics of the refinement, N is the number of observations, P is the number of parameters refining and C the number of constraints added.

$R_{weighted\ profile}$ (R_{wp}) is the most significant of these R factors described by:

$$R_{wp} = 100\left[\frac{\sum_i \omega_i \left[y_i^{obs} - y_i^{calc}\right]^2}{\sum_i \omega_i \left[y_i^{obs}\right]^2}\right]^{1/2}$$

This is the best reflection of the fit.

Finally chi-squared, the parameter being minimised during the refinement is defined as:

$$\chi^2 = \left[\frac{R_{weightedprofile}}{R_{\exp}}\right]^2$$

Chi-squared is used as a measure of how well the calculated model fits the actual observed data in conjunction with a visual analysis of the difference between the patterns. $R_{weighted\ profile}$ should approach R_{exp} for a good fit. For a perfect fit, chi-squared would be equal to 1, and this would manifest as a flat line when viewing a difference plot of the two data sets.

2.11 Thermogravimetric Analysis (TGA)

Thermal analysis of samples in this work was performed using a Polymer Laboratories STA-1500 simultaneous thermal analysis system. This instrument is capable of performing thermogravimetric analysis (TGA) and differential thermal analysis (DTA) simultaneously.

TGA measures the mass of a pre-weighed sample as a function of temperature. The ramp rate is set by the user between 1 and 50 °C per minute up to a maximum of 1500°C and the experiment can be conducted in air or other gases, such as oxygen, hydrogen in nitrogen or argon. This technique is particularly useful for studying transitions that involve a change in mass, for example, a dehydration or decomposition of a sample.

To study these transitions in more depth, or more importantly to identify transitions such as phase changes that do not result in a change of mass, DTA can be used in conjunction with TGA. In a DTA experiment the sample is heated along with a thermally stable standard, usually alumina. The temperatures of both are recorded, the rate of change of which will be identical if no thermal event, such as a phase change is happening to the sample. In the case of a thermal event the rate of change of the sample temperature will be different to the standard. For exothermic transitions a greater rate of heating will be observed, and for endothermic transitions a lower rate. Data can also be collected as the sample cools to see if any observed thermal events are reversible.

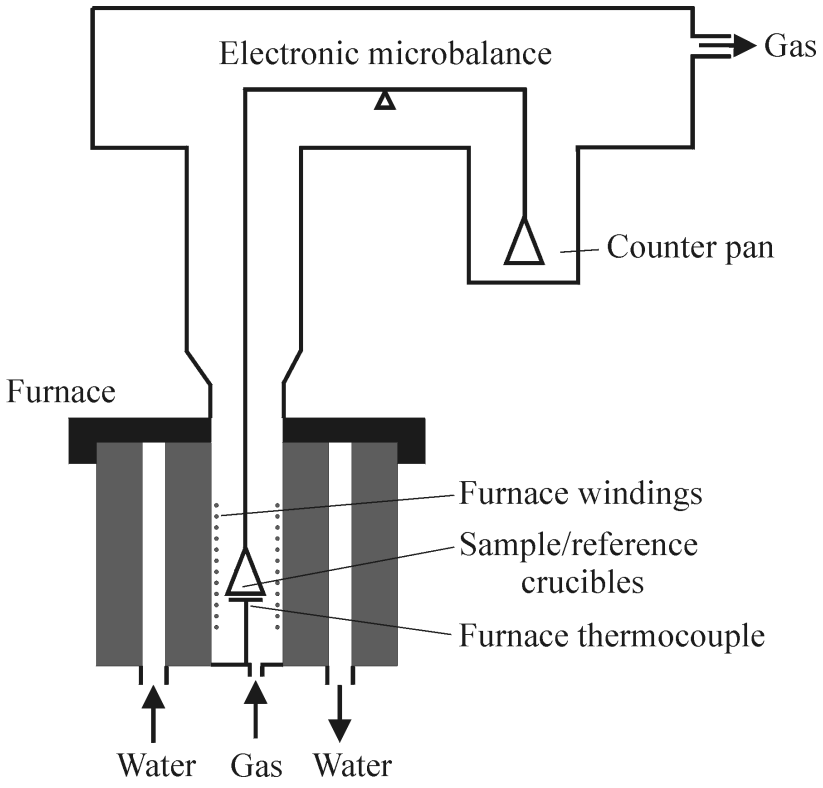

Figure 2.8 Schematic of the STA-1500 instrument

2.12 Scanning Electron Microscopy (SEM)

Scanning electron microscopy (SEM) is a powerful analytical tool, used here to image and study the morphology of a sample. Energy dispersive x-ray spectroscopy (EDX) can also be performed on the instrument, giving basic information about the elemental composition of a sample.

Acceleration of electron over a potential gives a stream of monochromatic electron according to:

$$\lambda = \left[\frac{1.5}{(V + 10^{-6} V^2)} \right]^{1/2} \text{nm}$$

where V is the accelerating voltage.

There are two ways that these incident electrons can interact with the sample; either elastically or inelastically. Elastically scattered electrons leave with the same energy as the incident electron. Inelastically scattered electrons will leave with a different energy after interacting with the sample, and various interactions provide different information about the sample.

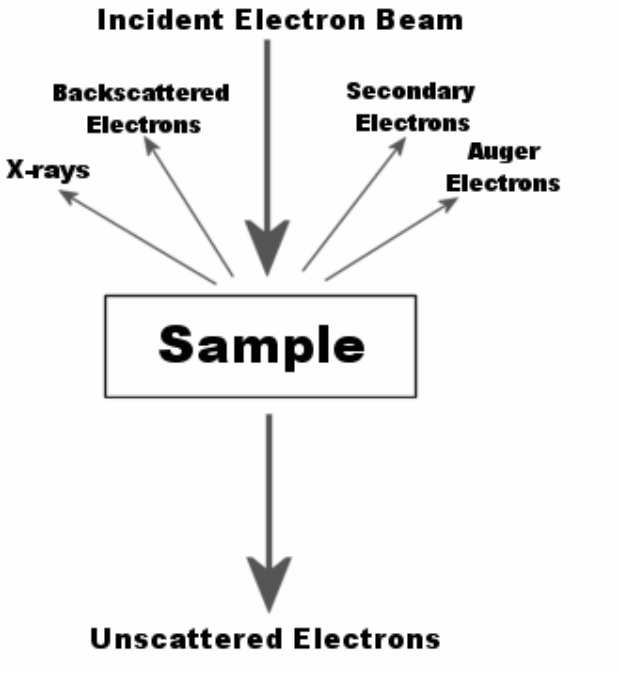

Figure 2.9 Possible scattering during SEM experiments

The secondary electrons leaving the sample have a relatively low energy below 50eV and can be used for imaging purposes. The backscattered electrons lose very little energy upon interaction with the sample and can be used for imaging or diffraction experiments. In some cases the incident electron beam will knock a core electron from the sample, which upon relaxation will emit either an x-ray photon or an Auger electron. These are both characteristic of the atom and can be used for EDX or Auger electron spectroscopy (AES).

For this work experiments SEM and EDX experiments were carried out using a Phillips XL30 ESEM instrument. Some samples were highly charged and required gold sputtering before imaging. Samples were mounted onto aluminium stubs using carbon tape.

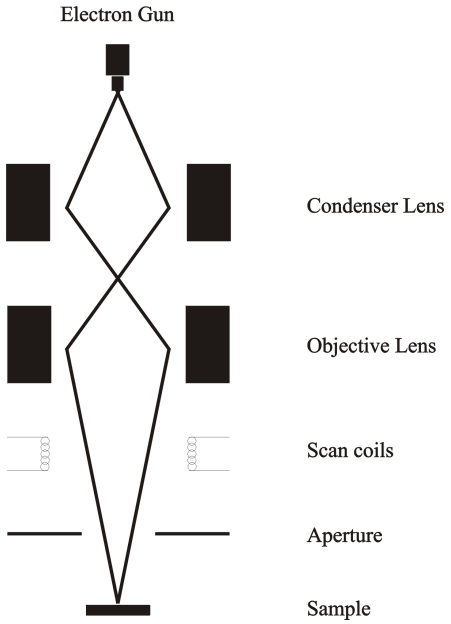

Figure 2.10 Schematic of the Phillips XL30 ESEM instrument

For a typical SEM experiment the electron beam is focussed through a series of electromagnetic lenses. The beam can then be scanned across the sample by a set of scan coils, and a detector counts the low energy secondary electrons. The images are transferred to a computer from which they can be manipulated.

For an EDX experiment the same instrument is used with the simple addition of an EDX detector and analyser. This characterises the atom specific x-rays emitted from the sample. This method is generally used for qualitative analysis of sample composition, as the errors can be very large for light atoms. In addition, emissions from different shells of different elements can overlap, which can be a problem for some samples.

2.13 References

[1] H. M. Rietveld, *Acta Cryst*., 1967, **22**, 151

[2] H. M. Rietveld, *J. Appl. Cryst*., 1969, **2**, 65

[3] W.L. Bragg, *Proc. Camb. Phil. Soc*., 1913, **17,** 43

[4] A.K. Cheetham and P. Day, *'Solid State Chemistry: Techniques'*, Oxford Science Publications, Clarendon Press, Oxford 1988

[5] T. Hahn, '*International Tables For Crystallography Vol. A'*, D. Reidel, Dordrecht, 1983

[6] International Centre for Diffraction Data, 12 Campus Boulevard, Newton Square, Pennsylvania 19073-3273, U.S.A, 1995

[7] D. P. Mitchell and P. N. Powers, *Phys. Rev.,* 1936*,* **50,** 486

[8] D. F. Shriver, P.W. Atkins and C.H. Langford, '*Inorganic Chemistry'*, Oxford University Press, 1990, 9

[9] S. Hall, R. I. Smith, W. I. F. David, A. C. Hannon, J. Mayers, R. Cywinski, *Physica B*, 1992, **180-181**, 1000

[10] W. G. Williams, R. M. Ibberson, P. Day, J. E. Enderby, *Physica B*, 1998, **241-243**, 1998, 234

[11] P. G. Radaelli, Ariel Version 3.3 PC, *Rutherford Appleton Laboratories,* 2000

[12] U. D. Aldermatt, I. D. Brown, *Acta. Cryst.,* 1987, **A34**, 125

[13] A.C. Larson and R.B. Von Dreele, Generalized Structure Analysis System, MS- H805, Los Alamos, NM 87545, 1990

[14] Caglioti G., Paoletti A., Ricci F.P, *Nucl. Instrum. Methods.* 1958, **35,** 223

Chapter 3
Zeolite Synthesis

Chapter 3: Zeolite Synthesis

3.1 Introduction – Synthetic Zeolites

There are many valid synthetic routes for the formation of aluminosilicate and zeolites. The most commonly used method for zeolite synthesis is hydrothermal reaction at low temperature. This is because many zeolites have fragile frameworks with low densities that are not thermally stable at high temperatures. For example, zeolite A can be easily crystallised in basic conditions at temperatures lower than 100 °C using basic starting materials[1-3], or can be templated with organic compounds to produce larger crystals[4]. Many zeolites and other framework materials also serve as precursors towards other frameworks, for example the conversion of natural kaolin into zeolite P[5]. Ion exchange reactions also are often used to change the non-framework ions in a structure.

Solid state synthesis of some aluminosilicates can be achieved by heating a mixture of ground oxides to temperatures of 600 - 1200 °C or by thermal restructuring of a framework precursor with the same stoichiometry, for example the collapse of zeolite A into the sodalite[6] structure which both possess an aluminium : silicon ratio of 1 : 1. This method is advantageous as it yields highly crystalline products making characterisation much simpler in many cases. The disadvantages of high temperature routes are that systems with low thermal stability frameworks or entrapped anions are inaccessible.

Hydrothermal or solution based synthesis methods provide much milder reaction conditions, allowing a broader range of potential products. The sodalite framework type is also accessible using hydrothermal techniques[7]. Synthesis generally involves heating of a basic solution of aluminium and silicon sources in a PTFE lined steel autoclave to temperatures of 50 - 250 °C. This method is beneficial as it allows the incorporation of anions with low thermal stability into a framework material and synthesis can often be directed using templating agents, such as large amines. Disadvantages of this method include reduced crystallinity as compared to solid state routes, and longer reaction times are often apparent. Hydrothermal synthesis of zeolites often leads to mixed or varied products, even with very similar reaction

conditions due to the large number of potential variables, including temperature, pH, volume, pressure, concentration of reagents, etc.

This chapter will explore some of the synthetic methods mentioned above in the preparation of some simple zeolites to be used for the work in this thesis.

3.2 Synthesis of Zeolite A

Various methods for the synthesis of Zeolite A were explored during the course of this work, in an attempt to produce phase pure samples of high crystallinity for use as precursors for the formation of other framework materials. Generally, hydrothermal methods were preferred, as at the elevated temperatures in solid state methods the framework will readily collapse into sodalite.

Firstly, a standard solution based method found on the International Zeolite Association (IZA) synthesis commission website was used[2]. This method involves adding a hot solution of sodium hydroxide and sodium aluminate to a hot solution of sodium metasilicate, used as the silicon source. 25g of sodium hydroxide (Fisher 97+%) was dissolved in 300ml of deionised water and 13.5g of sodium aluminate (Aldrich 99%) was added to the solution. Simultaneously 14.2g of sodium metasilicate (Fluka 97+%) was dissolved in 200ml of deionised water. Both solutions were heated to 90°C before the sodium aluminate/hydroxide solution was added slowly to the sodium metasilicate solution whilst hot. The reaction was then stirred for 4 hours at 90°C before the product was recovered by filtration and washed thoroughly with deionised water. The resultant white powder was then dried in an oven at 110 °C. The product was characterised using powder x-ray diffraction on a Siemens D5000 diffractometer and was shown to be phase pure Zeolite A by comparison with the JCPDS[8] powder diffraction database.

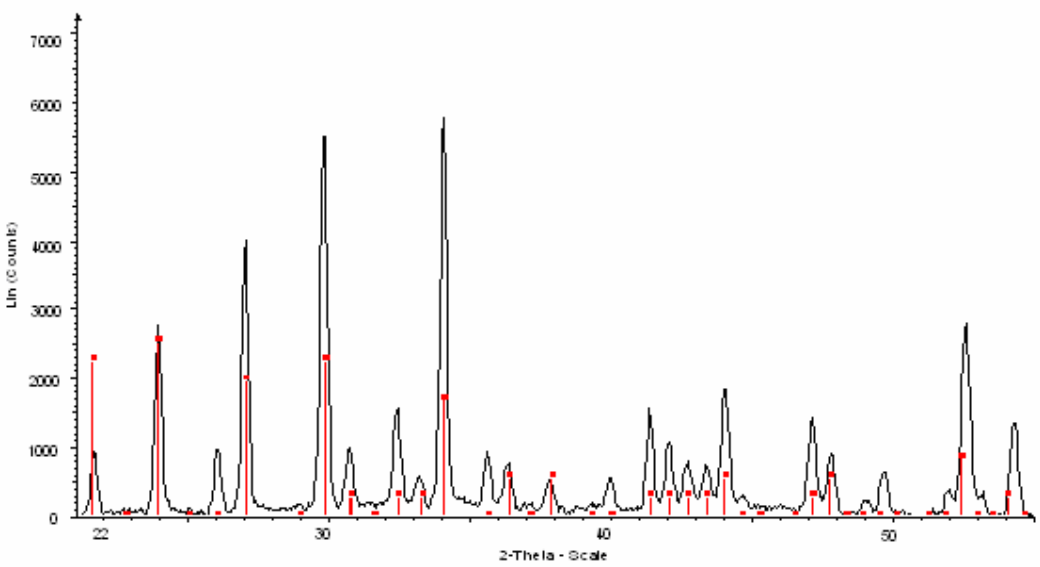

Fig 3.1 Powder diffraction pattern of LTA showing JCPDS data in red (01-089-8015)

EDX data showed an Al : Si ratio of approximately 1 : 1 and SEM imaging gave a particle size of between 2 and 5 microns.

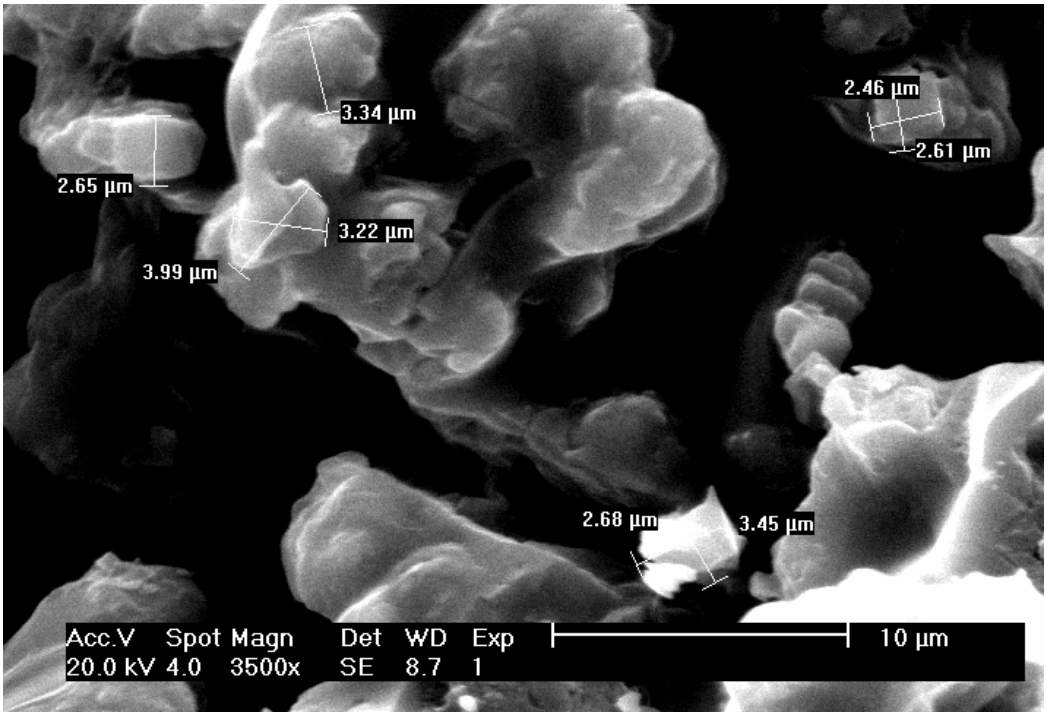

Fig 3.2 Showing the particle size of a typical LTA sample

3.3 Other Routes to Zeolite A

In an attempt to improve the crystallinity of the product, a hydrothermal method was used. 25g of sodium hydroxide (Fisher 97+%) was dissolved in 300ml of deionised water and 13.5g of sodium aluminate (Aldrich 99%) was added to the solution. Simultaneously 14.2g of sodium metasilicate (Fluka 97+%) was dissolved in 200ml of deionised water. 20ml portions of this solution were loaded into 45ml PTFE lined steel autoclaves (bombs). The bombs were loaded into an oven and heated to 110 °C for 18 hours, before being allowed to cool slowly to room temperature. The bombs were then opened and the white product was filtered and dried before characterisation. This method gave an improvement in crystallinity of the product, although there were often competing phases present in the form of sodalite and faujasite. Phase pure Zeolite A could be produced by subtle changes in the reaction time and temperature. The disadvantage to this synthetic route is that only roughly 1g of product is formed from each reaction vessel. The route is very labour intensive when attempting to produce large amounts of zeolite.

3.4 Sodalite Synthesis

Two main methods were explored as synthetic routes to sodalites, namely hydrothermal synthesis at elevated pressures, and high temperature solid state reactions, involving heating a mixture of powdered starting materials.

3.5 Hydrothermal Synthesis of Sodalites

A hydrothermal method was first explored for the formation of a hydroxysodalite, $[Na_8[AlSiO_4]_6(OH)_2]$, using silica and aluminium powder as the silicon and aluminium sources respectively.

0.225g of aluminium powder (Aldrich 99.9%) was dissolved in 25ml of 4M sodium hydroxide. 1.0g of SiO_2 (Aldrich 99.9%) was then added to the aluminium hydroxide solution. The reaction mixture was subsequently loaded into a 45ml capacity PTFE lined steel autoclave before being heated to 200 °C for 18 hours. The reaction vessel

was allowed to cool to room temperature before the product was recovered by filtration and washed thoroughly with deionised water.

The white powder was found to be a mixture of sodalite and faujasite phases by powder X-ray diffraction. It was found that by increasing the reaction time, or by using a more concentrated hydroxide solution phase pure crystalline hydroxysodalite could be synthesised using this hydrothermal method. This was achieved successfully using 0.225g of aluminium powder, 1.0g of SiO_2 and 25ml 4M sodium hydroxide solution heated to 200 °C for 36 hours. The amount of sodalite to be synthesised by this method is limited by the size of the reaction vessel and the reaction was also found to be very temperamental, with similar reaction mixtures and reaction times producing a mixture of phases.

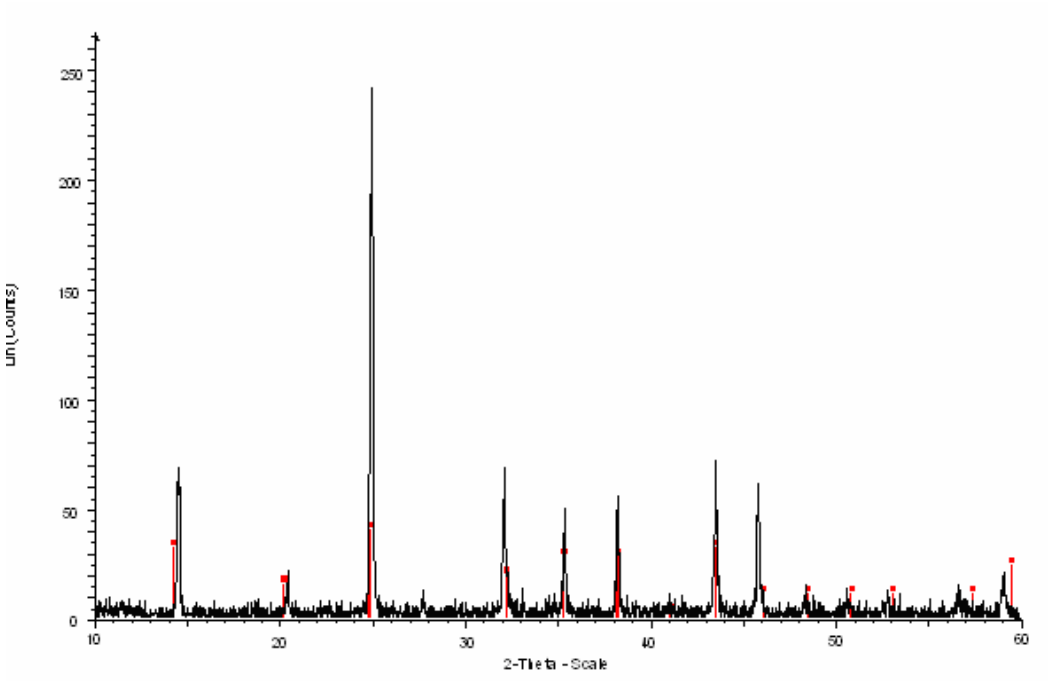

Fig. 3.3 Powder diffraction pattern of a synthetic sodalite with black lines showing experimental data and red lines showing JCPDS pattern (01-076-1639)

The hydrothermal method also allows encapsulation of soluble species in the beta cages of the sodalite, which can also be used to direct synthesis by templating the final product. For example, many polysulphide species can be used in this way. All of these factors make the hydrothermal synthesis of zeolites both versatile, as there exists a huge range of potential products, and very imprecise, as small errors can produce erratic results.

3.6 Solid State Sodalite Synthesis

The second synthetic route explored for sodalite formation was a high temperature solid state method involving the collapse of a more open framework structure. 1.0g of zeolite A was prepared using standard laboratory methods outlined above. This was ground and intimately mixed with an excess of sodium chloride (5g, Aldrich 99%) and this reaction mixture was heated to 650 °C in air for 18 hours. After cooling NaCl was removed by washing with deionised water and the final product was dried at 180 °C. The product was found to be single phase sodalite, $[Na_8[AlSiO_4]_6Cl_2]$ by powder X-ray diffraction.

As sodalite is the thermodynamic product in this system the reaction proceeds to completion very quickly and is a much more reliable method of forming sodalite than the corresponding hydrothermal synthesis. Many various anions and cations can be substituted into the $C_8(T1_6T2_6O_{24})A_2$ system in this way, simply by heating a zeolite with the corresponding metal salts. Most zeolites exhibiting a 1 : 1 Aluminium to silicon ratio will collapse into the thermally stable sodalite framework upon heating to high temperatures. Little is known is about the reaction mechanism or whether the framework collapses around the ions trapping them, or if diffusion into the beta cages occurs after framework formation, and this will be explored in more detail in subsequent chapters.

One advantage of using high temperature solid state synthesis is that oxidative or reductive flowing gases can be used to alter the oxidation state of the encapsulated species. This can be achieved by performing the experiment in a high temperature tube furnace connected to a pressurised gas cylinder. For example flowing oxygen will allow the formation of higher oxidation states not available in a normal experiment. Carefully tuning the oxidation state of trapped species can dramatically change the properties of the final product, for example in the ultramarine system can be the difference between a pink or deep blue colouration. These species are stabilised by the sodalite framework and would not exist discretely outside the beta cages.

3.7 Analcime Synthesis

Analcime, $Na(AlSi_2O_6)\ H_2O$, is a discrete aluminosilicate unit[9,10] with potential uses as a starting material for the formation of large open framework zeolite type structures. Analcime is readily ion exchanged, for example leucite, $K(AlSi_2O_6)$, can be easily formed from a mixture of analcime and a suitable potassium salt. Other analogues, such as the equivalent rubidium phase can also be produced in this way. This is a potentially useful method of incorporating different metals into the non framework sites of a zeolite. There exist a variety of synthetic routes to analcime including synthesis from aluminosilicate gels[11], glasses[12], mixtures of metal oxides and quartz[13] and hydrothermal methods[14].

It was noted whilst exploring the hydrothermal synthesis of sodalites (sec 3.5) that analcime was often observed as an impurity phase in these reactions. Experiments were undertaken to tailor the conditions of the Al / SiO_2 / NaOH system to produce analcime by hydrothermal methods using the method outlined in sec. 3.5 as a starting point. The first variable to be investigated was the reaction time, as it was speculated that analcime may be an intermediate in the formation of sodalite from elemental aluminium and silica.

0.225g of aluminium powder (Aldrich 99.9%) was dissolved in 25ml of 4M sodium hydroxide solution. 1.0g of SiO_2 (Aldrich 99.9%) was then added to the reaction mixture. The reaction mixture was subsequently loaded into a 45ml capacity PTFE

lined steel autoclave before being heated to 200 °C for times between 2 and 72 hours. The reaction vessel was allowed to cool to room temperature before the product was recovered by filtration and washed thoroughly with deionised water. The resulting white powders were characterised by powder x-ray diffraction in reference with the JCPDS database. Results are outlined in the table below.

Table 3.1 Effect of reaction time on product: 0.225g Al, 1.0g SiO_2, 4M NaOH, 200°C system

Al mass (g)	**SiO_2 mass (g)**	**(g) NaOH in 25ml water**	**Time (Hours)**	**Dominant Products**	**Impurities**
0.225	1	4	72	Sodalite	None
0.225	1	4	48	Sodalite	None
0.225	1	4	36	Sodalite	None
0.225	1	4	24	Sodalite	None
0.225	1	4	16	Sodalite	None
0.225	1	4	8	Sodalite	Analcime
0.225	1	4	4	Sodalite	Faujasite + analcime
0.225	1	4	2	Sodalite	Faujasite + Analcime

It was found for this set of reaction conditions that sodalite was the dominant phase regardless of reaction time, although very small amounts of analcime and faujasite were observed for some of the smaller reaction times. Reaction times much below 2 hours resulted in non crystalline products.

The effect of the silicon source on the reaction was also investigated. 0.225g of aluminium powder (Aldrich 99.9%) was dissolved in 25ml of 4M sodium hydroxide solution. 1.0g equivalent of the chosen silicon source (fumed silica, silica sol, ground glass and sand) was then added to the reaction mixture. The reaction mixture was

subsequently loaded into a 45ml capacity PTFE lined steel autoclave before being heated to 200 °C for 18 hours. The reaction vessel was allowed to cool to room temperature before the product was recovered by filtration and washed thoroughly with deionised water. Selected results of the PXD characterisation are shown below.

Table 3.2 Effect of silicon source on product: 0.225g Al, 1.0g SiO_2, 4M NaOH, 200°C system

Al mass (g)	**SiO_2 mass (g) / source**	**(g) NaOH in 25ml water**	**Temperature (°C)**	**Time (Hours)**	**Dominant Products**
0.225	1g fumed silica	4	200	16	Sodalite
0.225	Eq. 1g silica sol	4	200	16	Sodalite
0.225	1g ground glass	4	200	16	Sodalite + analcime + quartz
0.225	1g sand	4	200	16	Sodalite + analcime + quartz

The results show that the amount of analcime observed is increased by using ground glass or sand as the silicon source, although sodalite is still the main phase observed in these cases. Unreacted quartz is also observed, implying that the relatively large particle size of the starting material leads to a slower dissolution into the reaction. This translates to an effective lower concentration of silicon, which explains why analcime is observed as a low concentration of dissolved silicon would tend to favour formation of discrete units over extended aluminosilicate frameworks.

To this effect the concentration of the starting materials was investigated. As above, aluminium powder (Aldrich 99.9%) was dissolved in 25ml of 4M sodium hydroxide solution and SiO_2 (Aldrich 99.9%) was then added to the reaction mixture. The

reaction mixture was subsequently loaded into a 45ml capacity PTFE lined steel autoclave before being heated to 200 °C for times 18 hours. The reaction vessel was allowed to cool to room temperature before the product was recovered by filtration and washed thoroughly with deionised water. The resulting white powders were characterised by powder x-ray diffraction in reference with the JCPDS database. Selected results are outlined in the table below.

Table 3.3 Effect of concentration of starting materials: Al, SiO_2, 4M NaOH, 200°C system – dominant phases listed first

Al mass (g)	**SiO_2 mass (g)**	**(g) NaOH in 25ml water**	**Temperature (°C)**	**Time (Hours)**	**Dominant Products**
0.225	1	4	200	16	Sodalite
0.45	1	4	200	16	Sodalite + analcime + faujasite
0.90	1	4	200	16	Sodalite + analcime + faujasite
0.45	2	4	200	16	Sodalite + faujasite + analcime
0.9	4	4	200	16	Faujasite + sodalite

Most of these experiments yielded a mixture of phases, with sodalite, analcime and faujasite all present in the reaction product. It was observed that increasing the aluminium concentration relative to silicon resulted in greater amounts of analcime formed, shown by the analcime peaks becoming more pronounced in the powder pattern. This could be a concentration effect, or could more simply be explained by the greater concentration of dissolved aluminium lowering the pH of the reaction mixture and these milder conditions slowing the transformation into sodalite.

Increase of the silicon content above an Si : Al ratio of 1:1 generally resulted in residual unreacted silica in the end product, and thus such experiments were not investigated further, because silica is difficult to remove from the sample and would cause difficulties in data analysis.

Higher concentrations of both aluminium and silicon seemed to favour faujasite synthesis, although both sodalite and analcime are also found in these experiments to varying degrees. The higher concentrations of the starting materials promote framework formation over the discrete analcime units, and the reduced pH caused by dissolved aluminium slows the reaction from proceeding completely to sodalite. It was expected that by working at low concentrations and by reducing the pH of the initial reaction mixture that phase pure analcime could be synthesised.

Finally, aluminium powder (Aldrich 99.9%) was dissolved in 25ml of 2M sodium hydroxide solution and SiO_2 (Aldrich 99.9%) was then added to the reaction mixture. The reaction mixture was subsequently loaded into a 45ml capacity PTFE lined steel autoclave before being heated to 200 °C for times 18 hours. The reaction vessel was allowed to cool to room temperature before the product was recovered by filtration and washed thoroughly with deionised water. The resulting white powders were characterised by powder x-ray diffraction in reference with the JCPDS database. Selected results are outlined in the table below.

Table 3.4 Effect of concentration of starting materials: Al, SiO_2, 2M NaOH, 200°C system – dominant phases listed first

Al mass (g)	**SiO_2 mass (g)**	**(g) NaOH in 25ml water**	**Temperature (°C)**	**Time (Hours)**	**Dominant Products**
0.113	0.5	2	200	16	Analcime
0.225	1	2	200	16	Analcime
0.45	1	2	200	16	Analcime + faujasite + sodalite
0.9	1	2	200	16	Faujasite + analcime + sodalite

Phase pure analcime was successfully synthesised using lower concentrations of starting materials and milder conditions. It was found that above 0.225g of aluminium and 1.0g of silica impurity phases started to appear at this pH. At lower concentrations only analcime was observed. The 0.225g Al, 1.0g SiO_2, 2M NaOH system highlighted in the table above was hence considered the most efficient for formation of analcime. It was later noted that some small impurity phases could occur, which could be minimised by quenching the reaction by removing it from the oven and placing the reaction vessel in cold water. This synthetic route can produce analcime from solutions at a lower concentration of NaOH than other methods reported in the literature, and from the very basic starting materials of elemental aluminium and silica.

3.8 Faujasite Synthesis

The hydrothermal investigation of sodalite synthesis mentioned above (sec 3.5) elucidated that other aluminosilicates of interest to this work could also be produced in a similar manner, in particular faujasite and analcime phases, which were often observed as impurities in the sodalite work. Faujasite type frameworks can be readily symthesised from hydrothermal reactions and aluminosilicate gels[15,16]. An investigation into the reaction conditions was undertaken to determine if phase pure faujasite could be synthesised by these simple hydrothermal reactions using elemental aluminium and silica as the starting materials.

As sodalite is the most thermodynamically stable product in this system it was speculated that other phases would be more prominent when using less harsh reaction conditions, or by quenching the reaction in progress. In addition to sodalite, LTA frameworks are also known to be competing phases during hydrothermal syntheses of faujasites[17]. Synthesis was achieved by using a less basic solution, shorter reaction times and lower temperatures. Quenching could be performed by rapidly cooling the reaction vessel by removing it from the oven and placing it in cold water. It was found that mild conditions and high concentrations of starting material favoured synthesis of faujasite.

By varying the reaction conditions in this way a sodium aluminium silicate hydrate of the faujasite (FAU) framework type was successfully synthesised – $Na_{86}Al_{86}Si_{106}O_{384}:xH_2O$ which is a porous zeolite structure.

3.9 Conclusions

A variety of basic zeolites and aluminosilicates have been successfully synthesised in this chapter to be used as simple starting materials throughout the rest of this work, most importantly the phases sodalite, zeolite A, faujasite and analcime. Where appropriate, reaction conditions have been optimised towards high purity and yield to maximise efficiency and produce good quality bulk samples to be used in further reactions. An important point to note is that the work reported in this chapter is by no means exhaustive, and often very similar reaction mixtures yield very different end products. In some cases even the dimensions of the reaction vessel seem to affect the final outcome of the experiment, making consistency paramount when working in the area of zeolite synthesis.

The system using aluminium, silica and sodium hydroxide as starting materials has been fully explored. Using these three simple cheap reactants, conditions can be tailored to produce markedly different products, elucidating to the diverse and sometimes unpredictable nature of zeolite synthesis. It was found that long reaction times and harsh condition, for example high pH, favour sodalite synthesis, which is to be expected because this is the most thermodynamically stable of the potential products. By using a lower pH or decreasing reaction times the system could be tailored toward faujasite synthesis, possibly an intermediate in the sodalite reaction. Finally, by using lower concentrations of starting materials and lower pH and reaction times, the system tended toward analcime synthesis, with the lower concentrations favouring formation of discrete units over framework formation.

3.10 References

[1] R. W. Thompson, M. J. Huber, *J. Cryst. Gr.*, 1982, **56**, 711

[2] J. F. Charnell, *J. Cryst. Gr.*, 1971, **3**, 291

[3] D. W. Breck, *Zeolite Molecular Sieves*, John Wiley, New York, 1974, 270

[4] H. Neels, W. Schmitz, E. M. Berger, D. Lutz, *Krist. Tech.,* 1978, **13**, 1345

[5] L. V. C. Rees, S. Chandrasekhar, *Zeolites,* 1993, **13**, 535

[6] R. M. Barrer, *Hydrothermal Chemistry of Zeolites,* 1982, Academic Press, New York

[7] A. Stem, G. A. Ozin, G. Stucky, *J. Am. Chem Soc*., 1992, **114,** 5171

[8] International Centre for Diffraction Data, 12 Campus Boulevard, Newton Square, Pennsylvania 19073-3273, U.S.A, 1995

[9] W. H. Taylor, *Z. Kristallogr*., 1930, **74**, 1

[10] G. Ferraris, D. W. Jones, J. Yerkess, *Z. Kristallogr.,* 1972, **135**, 240

[11] R. M. Barrer, E. A. D. White, *J. Chem. Soc.,* 1952, **286,** 1561

[12] Saha, Prasensit, *Am. Mineral.,* 1959, **44,** 300

[13] D. S. Coombs, *Trans. Roy. Soc. N.Z.,* 1954, **82**, 65

[14] A. Dyer, A. M. Yusof, *Zeolites,* 1987, **13**, 191

[15] H. Lechert, H. Kocirek, *Zeolites,* 1991, **11**, 720

[16] H. Lechert, H. Kocirek, *Zeolites,* 1992, **13**, 1345

[17] G. H. Khul, *Zeolites,* 1987, **7**, 451

Chapter 4
Sodalite Reaction Kinetics

4.1 Introduction

Very little is understood about the mechanism of formation of sodalites from zeolites. It is widely known that the treatment of many aluminosilicates with various metal salts at high temperature will result in the formation of sodalite[1] type structures, but it remains unclear what factors affect this reaction. For example, the parent compound sodalite, $[Na_8[AlSiO_4]_6Cl_2]$, can be easily formed by heating zeolites such as faujasite or linde type A with sodium chloride[1,2], but the role of the salt in the reaction mechanism is unknown. There are three distinct possibilities as how this collapse proceeds. The first being that at high temperature these mobile salt ions serve to template the beta cages, and the chosen zeolite collapses around these ions to form a sodalite. The second possibility is that the salt has a relatively redundant role in the reaction and that the zeolite collapses into sodalite structure before the mobile salt ions migrate into this new framework. A third possible mechanism exists, whereby the salt moves into the cavities of the zeolite, which then in turn collapses into the sodalite framework.

The use of time resolved diffraction experiments over a temperature range is an important tool for understanding the mechanisms and phase transitions in zeolite reactions. Thermal conversion of zeolites and clays can be studied *in situ* by time resolved x-ray diffraction experiments, which provides useful information about any transitional phases and hence the mechanism of thermal conversion[3,4,5]. Time resolved neutron thermodiffraction experiments have also been used in this way to study the chemistry of clays and zeolites at high temperatures[6,7,8]. Specialised reaction environments and software have been developed for collection and manipulation of data for these types of experiments[7,10].

The work conducted in this chapter aims to look closely at the reaction kinetics of sodalite formation from various zeolites and natural clays in high temperature solid state reactions. Various techniques such as TGA and thermodiffraction will be used to examine the reaction in detail *in situ* in an attempt to determine how these collapse reactions actually occur. Thermodiffraction experiments should provide information about crystalline phases being destroyed or produced as the reaction mixtures are

heated, and should give a good overall picture of the role of the various reactants in the collapse.

4.2 Combined TGA and DTA Analysis of Sodalite Formation

TGA and DTA experiments were conducted to determine the temperature of any transformations or weight losses of chosen zeolites upon heating with sodium chloride. It was expected that zeolites with a 1 : 1 aluminium to silicon ratio would ultimately collapse into the sodalite framework, which exhibits a very high thermal stability. The various zeolites were ground and intimately mixed with sodium chloride and a small amount of the sample was weighed before being heated to 1000 °C at a rate of 4 °Cmin^{-1} and collapsed into sodalite on the STA 1500 TGA instrument. Large exotherms in the DTA trace would show the reaction to form sodalite after an initial weight loss from water. Powder XRD of the reaction mixture was conducted after the heating process to define the products formed. Firstly, the collapse of zeolite A was explored.

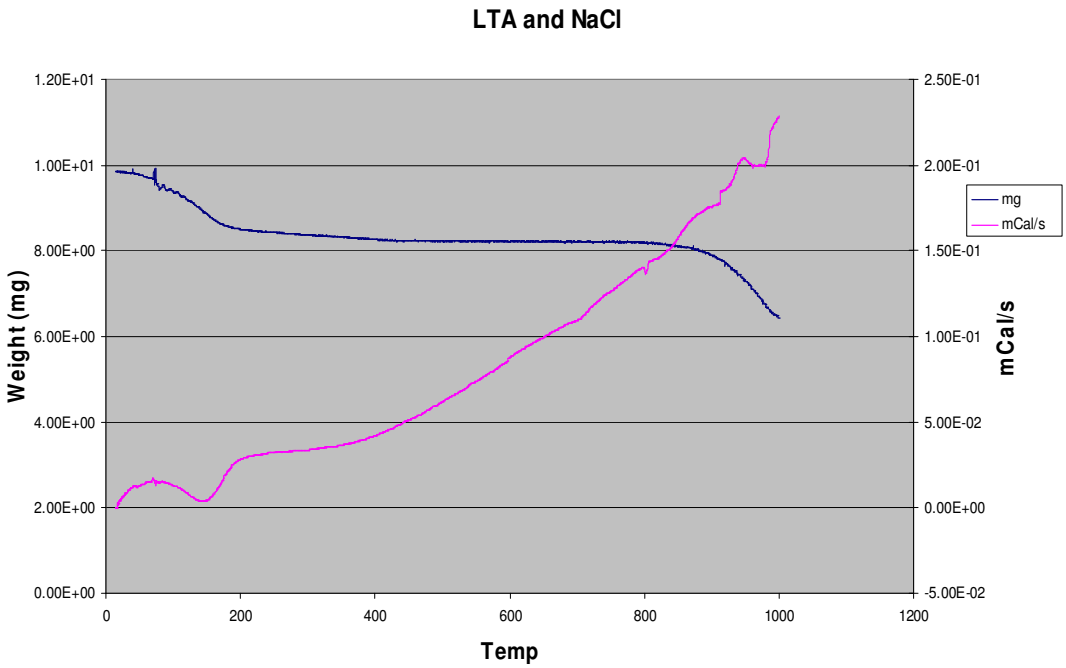

Fig 4.1 TGA and DTA traces of LTA and NaCl collapse to sodalite

The traces in the above example show loss of weight and exotherm between 100 and 200 ºC corresponding to the loss of trapped water from the framework of the zeolite. Subsequently a small exotherm at around 800 ºC is observed, possibly corresponding to any unreacted sodium chloride melting. The loss of weight observed after 800 ºC corresponds to a loss of NaCl vapour from the sample

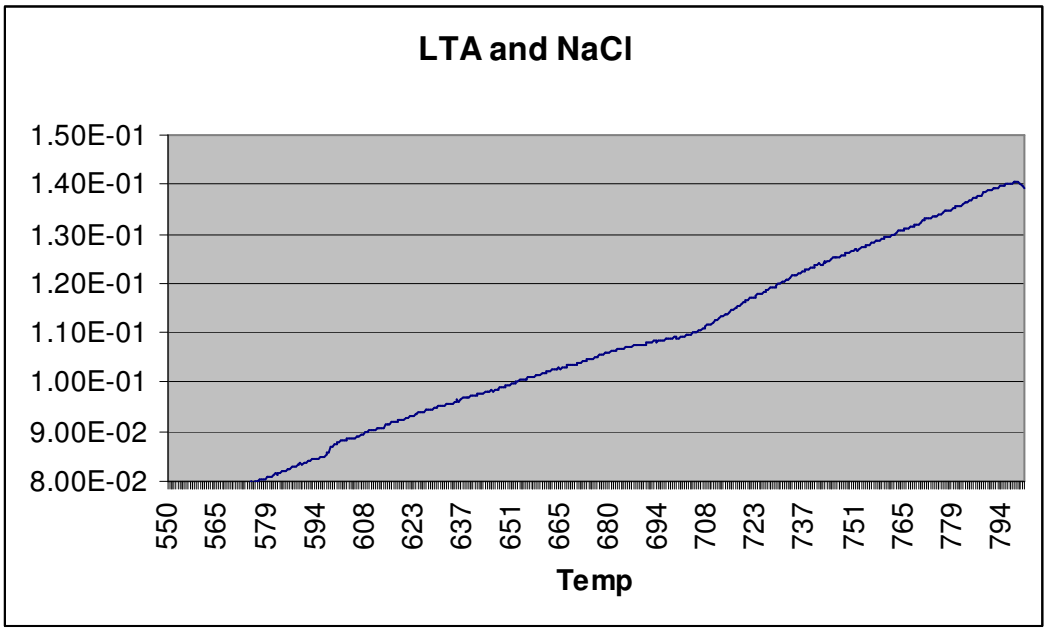

Fig 4.2 Showing an expanded view of the DTA trace for the LTA/NaCl collapse between 600 ºC and 800 ºC

From this expanded view of the temperature range in which the collapse was thought to occur, an interesting feature can be observed at around 700 ºC, which is less easily visible on the view of the entire set. Another small feature is visible at around 600 ºC in the trace. The presence of these two distinct features implies that the mechanism of collapse has two distinct stages, which supports the theory that the sodium chloride enters the cages of the zeolite before a subsequent collapse into the sodalite framework. Powder XRD of the post treated sample showed single phase sodalite as produced upon heating, confirming that collapse of the LTA framework to sodalite must be responsible for the small exotherm.

With this result in mind other zeolites with aluminium and silicon contents close to parity were heated with sodium chloride on the STA 1500 TGA instrument, namely zeolite X, zeolite MAP, and a naturally occurring clay, kaolin. The various zeolites were ground and intimately mixed with sodium chloride and a small amount of the sample was weighed before being heated to 1000 °C and collapsed into sodalite on the STA 1500 TGA instrument. All the experiments showed very similar results to the LTA example, although the exotherms were observed to varying degrees of clarity. The temperature of collapse of these frameworks into sodalite was generally between 550 °C and 750 °C It is clear from these results that aluminosilicates possessing a 1 : 1 aluminium to silicon ratio tend to from the sodalite framework upon heating to high temperatures with sodium chloride.

The water loss and subsequently reaction were most prominently observed in the zeolite MAP experiment.

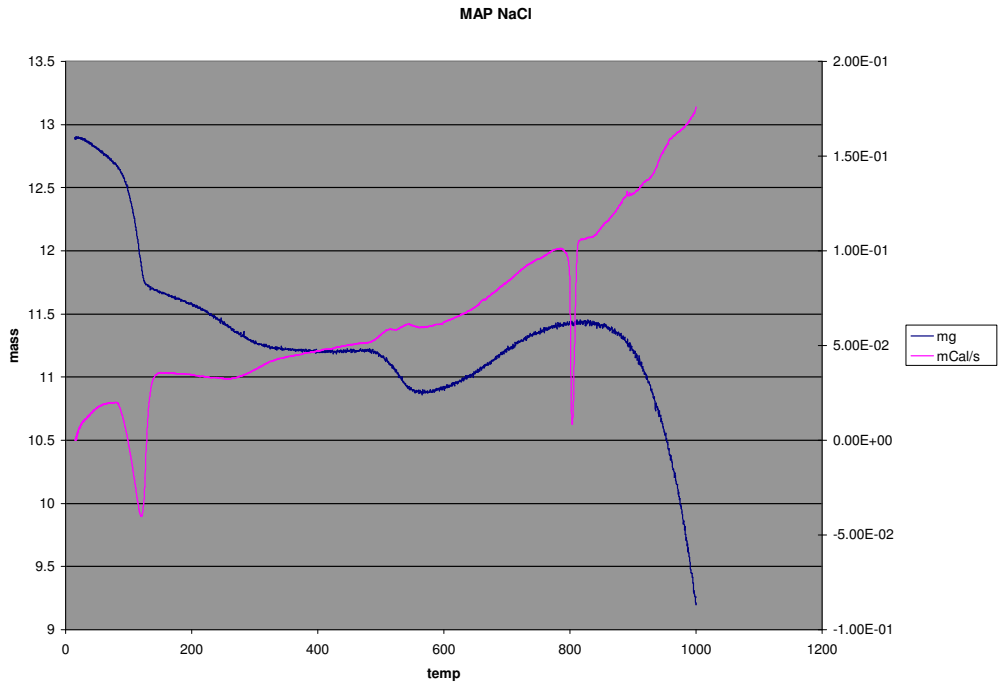

Fig. 4.2 TGA and DTA Traces of MAP and NaCl collapse into sodalite

As in the previous example, the loss of water can be clearly observed after 100 ºC. There are also clear features in the DTA trace at around 600 ºC, showing the rearrangement of the framework into sodalite. Subsequently an exotherm at around 800 ºC is observed, possibly corresponding to any unreacted sodium chloride melting. The loss of weight observed after 800 ºC corresponds to a loss of NaCl vapour from the sample. Powder XRD of the reaction mixture after heating confirmed a total transformation of the zeolite to the sodalite framework.

To observe in more detail the phases present around these exotherms and hence the mechanics of how these reactions proceed, detailed diffraction data of the reaction *in situ* was necessary. This would require fast data collection without compromising resolution, so that any transient phases present could be identified. X-ray sources were not appropriate for the volume of data required to observe these transformation properly.

With these results in mind variable temperature neutron diffraction studies could be undertaken to elucidate the mechanism of formation of the sodalite structure, without having to insert the sulphur chromophore to produce ultramarine. Diffraction patterns could be collected at temperatures around the 800ºC to show if the zeolite cages collapse around the salt, or if they move into the pores after sodalite formation. Using neutron diffraction for this experiment is more suitable than powder XRD as neutrons probe the bulk of the sample, as oppose to XRD, which only provides information about the surface of the sample.

4.3 Thermodiffraction Using Neutrons

All thermodiffraction experiments were conducted on the general materials neutron diffractometer, GEM[9], housed at ISIS at the Rutherford Appleton Laboratories in Oxfordshire. GEM was considered to be particularly useful for this type of experiment, as it maintains a relatively high resolution for a high flux instrument. The GEM sample chamber is situated only 17 metres from the target, making it a high incident flux instrument. This normally leads to a decrease in resolution when compared to diffractometers with longer path lengths. GEM combats this problem by

collecting vast amounts of data from 7 very large detector banks which almost completely encompass the sample environment. In this way, very little information is lost and useful diffraction data can be assimilated very quickly.

GEM was also the pilot instrument for the ARIEL[10] software, which was used to collect and view the thermodiffraction data for this work. ARIEL allows the user to view the diffraction data as it is being collected, and can be used to generate a 3 Dimensional picture of the reaction by plotting d-spacing against intensity and a third variable, such as time or temperature. Because of these factors GEM in combination with the ARIEL system were considered the ideal solution for thermodiffraction experiments on zeolites.

4.4 Thermodiffraction Experiments

Initial brief experiments were conducted to determine the minimum amount of time needed to be able to determine the phases present from the diffraction data. From these initial results it was decided that 10 microamp hours would provide an appropriate amount of information for each temperature or "packet" of data collected. This is equivalent to approximately 4 minutes of real time per data set. By collecting data every 5 degrees Kelvin for 10 microamp hours the entire experiment was conducted in roughly 6 hours. From the TGA experiments conducted earlier it was decided that data would be collected between 300 and 800ºC.

Another particular consideration for these experiments was the sample environment. Standard vanadium cans are used for neutron diffraction experiments as they display very little coherent scattering, however, upon high temperature treatment with sodium chloride elemental vanadium will readily form vanadium chloride. This would compromise the sample environment, so another more suitable reaction vessel was chosen. It was decided that the best compromise between low coherent scattering and stability with sodium chloride was to use a quartz reaction vessel, which only displayed a mild etching when heated with the salt. The background diffraction pattern of this glass sample holder was obtained and subtracted from the acquired data

sets. To be sure this was modelled correctly at all temperatures a blank quartz tube was heated to 800ºC to calibrate the instrument before further experimentation.

To start 1.0g of zeolite A was ground and intimately mixed in a pestle and mortar with an excess of sodium chloride. This mixture was heated at 800ºC for 6 hours before being cooled. Powder XRD of the products showed that all zeolite A had been successfully converted to sodalite. This same initial reaction mixture was then loaded into the quartz sample holder and heated to 800ºC in 5ºC steps for 10 micro amp hours for each step. The data was collected and later viewed using the ARIEL software.

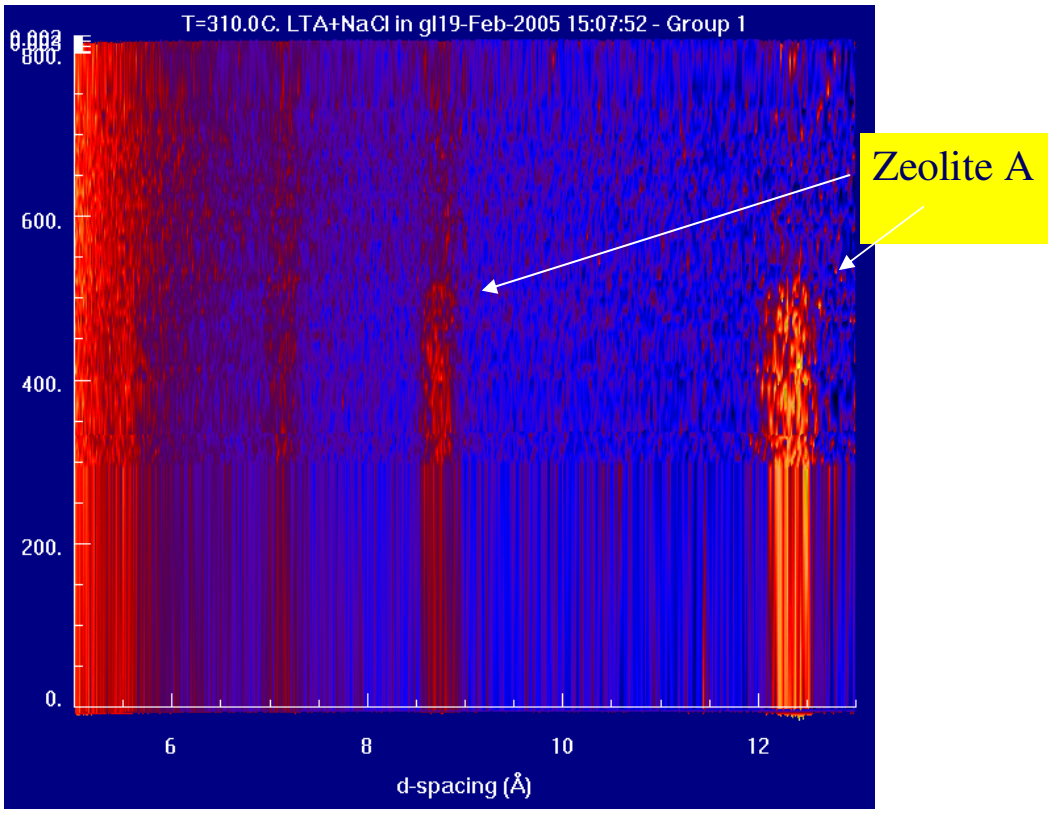

Fig 4.3 Low angle detector bank for LTA and NaCl reaction showing Zeolite A peaks plotted using ARIEL

The zeolite A could best be viewed on the low angle detector banks shown above because of the large d-spacings, and should be the only material present to have diffraction maxima in this region. The data was extrapolated by the software below 300ºC, explaining the smooth plot for temperatures below that value. It can be seen above that at around 550ºC the diffraction peaks corresponding to zeolite A start to reduce and disappear. This alone could signify the collapse into the sodalite framework, or potentially the formation of an intermediate material, perhaps nephelene or an amorphous intermediate, which then goes on to further react with the sodium chloride to form sodalite.

To view the diffraction maxima corresponding to sodium chloride a higher angle detector bank was used. Again the data was plotted as a function of temperature using ARIEL. In the thermodiffraction pattern below the first observation is the slight increase in d-spacing for the NaCl peaks as the reaction is heated. This is common, and is simply due to a thermal expansion of the structure. This effect is not noted for the zeolite as LTA is a relatively rigid framework and a small thermal expansion coefficient.

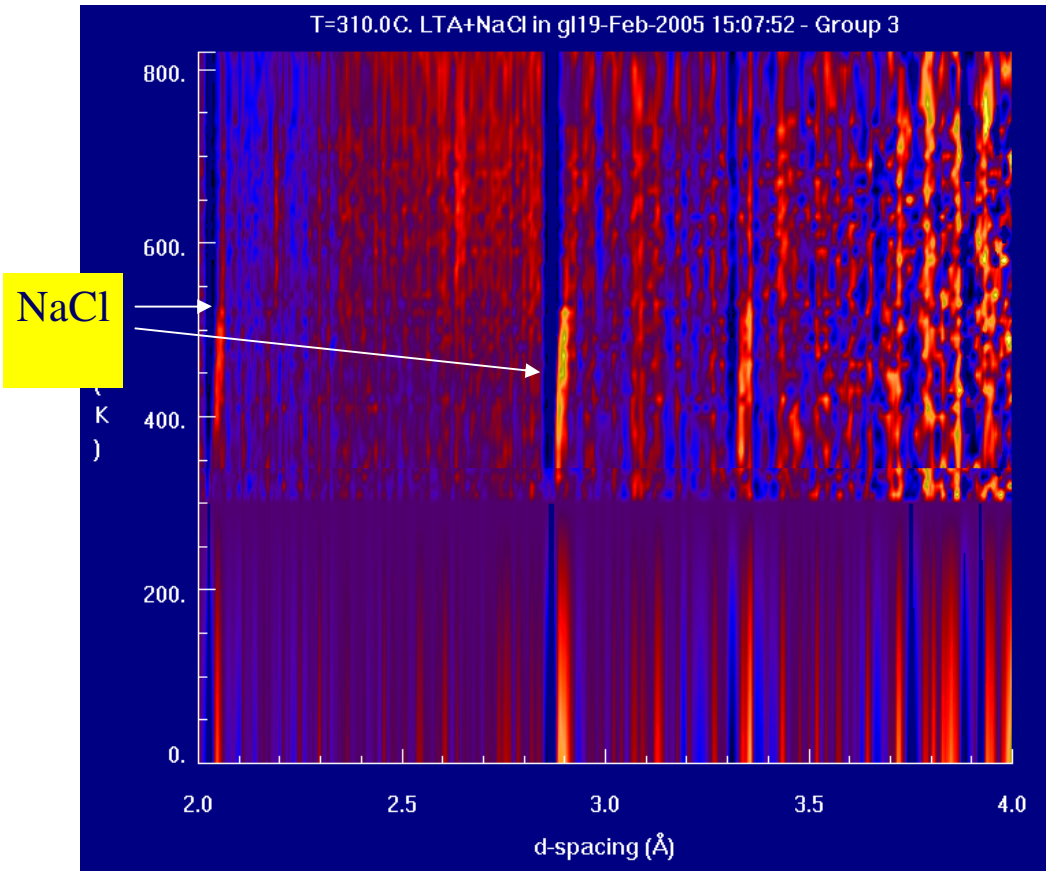

Fig 4.4 Medium angle detector bank for LTA and NaCl reaction showing sodium chloride peaks plotted using ARIEL

In figure 4.4, as with the zeolite, the sodium chloride diffraction maxima are seen to reduce and disappear after around 550ºC. This corresponds again to the transformation into the sodalite framework.

To observe the sodalite diffraction maxima the same data was manipulated using the ARIEL software, as it was difficult to observe using only the raw data. As with the sodium chloride, the sodalite was most easily observed using one of the higher angle detector banks of GEM.

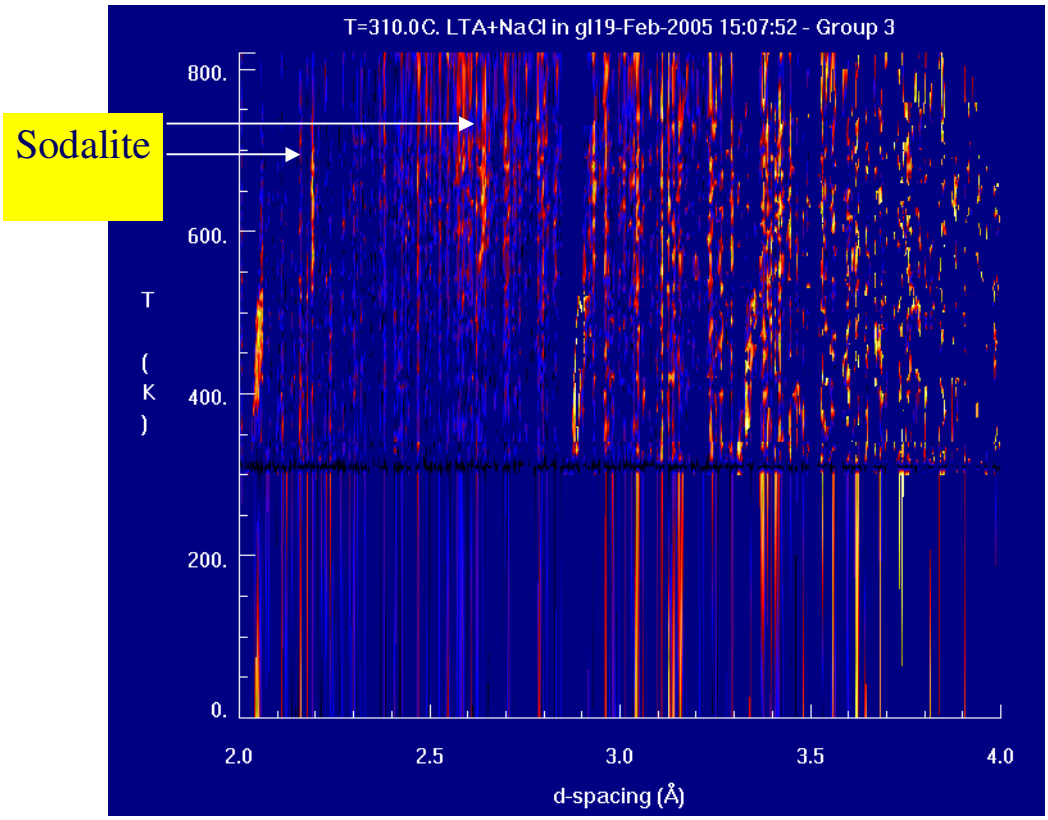

Fig 4.5 Medium angle detector bank for LTA and NaCl reaction showing sodalite peaks plotted using ARIEL

Data manipulation was performed by using a higher tolerance for the data set. Essentially the threshold in the software determining the presence of a peak was raised allowing the sodalite to be easily observed.

Figure 4.5 shows the manipulated data set. From this it can be seen that after 550ºC new diffraction peaks can be seen to grow, which are not observed below this temperature. These new peaks correspond to the sodalite framework, as referenced with JCPDS powder diffraction database. By comparison of this data set to figure 4.3 showing the low angle detector bank, it is notable that the sodalite peaks do not appear until temperatures greater than that of 550ºC, when the zeolite and sodium chloride peaks are seen to suppress.

From a combination of all these data sets it can be deduced that there are no intermediate crystalline phases apparent during the formation of sodalite from zeolite

A. As the zeolite and sodium chloride peaks cease with increase in temperature new sodalite peaks are seen to appear. This transition occurs at about 550ºC in this particular example. This is not the same transition temperature observed in the TGA data, but the rate of heating is much slower in the thermodiffraction experiment, thus being exposed to lower temperatures for longer time frames results in the same chemical transition. By looking at figures 4.4 and 4.5 it can be seen that the salt peaks continue to reduce after formation of the sodalite framework, and this could be rationalized by diffusion into the beta cages of the sodalite after it has been formed. A control experiment was run in the absence of sodium chloride, and the results of this experiments showed that the transformation into the sodalite framework did not occur if the salt was not present. In this instance the zeolite persisted up to much higher temperatures.

By examining the combined TGA/DTA data and the thermodiffraction data of the collapse of zeolite A with sodium chloride it can be deduced that the salt has a role in the collapse mechanism. Thermodiffraction experiments show that the collapse of the zeolite occurs over a very small temperature range. The presence of two exotherms in the DTA trace for the LTA/NaCl collapse reaction imply that there is some form of rearrangement immediately prior to the collapse, which can be rationalized by diffusion of the salt into the beta cages of the zeolite.

4.5 Conclusions

Factors affecting the collapse of various aluminosilicates in the sodalite framework have been explored. It was found that most zeolites possessing an aluminium to silicon ratio close to 1 : 1 will ultimately form the sodalite framework if heated for long enough at high temperature. It was deduced that sodalite is the thermodynamic sink of such systems.

The collapse of zeolite A into the sodalite framework was studied in more detail using thermodiffraction neutron experiments. These experiments were performed on the high flux, high resolution materials diffractometer GEM at ISIS. It was found that zeolite A collapsed easily into sodalite, facilitated by the presence of sodium chloride. These diffraction studies showed that there were no crystalline intermediates between the zeolite and the sodalite, and the transition was completed quickly over a short temperature range. It is apparent that some diffusion of sodium and chloride ions into the beta cages of the sodalite may occur after the framework has formed, which is possible due to the flexible nature of the framework.

4.6 References

[1] R. D. Kirk, *J. Electrochem. Soc.,* 1954, **109**, 461

[2] R. M. Barrer, *Hydrothermal Chemistry of Zeolites,* 1982, Academic Press, New York

[3] P. Norby, *J. Am. Chem. Soc.,* 1997, **119,** 5215

[4] A. Galteri, P. Norby, G. Artioli, J. Hanson, *Micro. Meso. Mat.,* 1997, **9,**189

[5] D. O'Hare, J. S. O. Evans, R. J. Francis, P. S. Halasyamani, P. Norby, J. Hanson, *Micro. Meso. Mat.,* 1998, **21,** 253

[6] R. Collins, A. N. Fitch, C. R. A. Catlow, *J. Mat. Chem.,* 1991, **1**, 965

[7] R. I. Walton, R. I. Smith, D. O'Hare, *Micro. Meso. Mat.,* 2001, **48**, 79

[8] M. Wiebcke, G. Engelhardt, J. Felsche, P. B. Kempa, P. Sieger, J. Schefer, P. Fischer, *J. Phys. Chem.,* 1992, **96**, 392

[9] W. G. Williams, R. M. Ibberson, P. Day, J. E. Enderby, *Physica B,* 1997, **241**, 234

[10] P. G. Radaelli, Ariel Version 3.3 PC, *Rutherford Appleton Laboratories.* 2000

Chapter 5
Hackmanite : Synthesis and Structure

5.1 Introduction

Hackmanite is a naturally occurring mineral of the sodalite framework type. Original studies of this mineral have shown that samples of the rock were deep pink in colour when freshly cleaved, though this colour faded to white over a period of minutes in natural sunlight[1]. It was also shown that freshly exposed sample of hackmanite retained this deep pink colouration when kept in the dark. Further investigation into the interesting optical properties of this mineral found that the pink colour could be induced by exposing the sample to ultraviolet radiation. In fact, this colour transition was found to be completely reversible and the sample could be repeated bleached and coloured using direct sunlight and UV radiation respectively[2]. It is documented that sulphur impurities[3,4] exist in natural hackmanite and it is now understood that these sulphur impurities in non framework sites of the structure are responsible for this reversible photochromism[5,6,7] or tenebrescence, making the hackmanite formula $Na_8[AlSiO_4]_6(Cl_{x-2}, S_{x/2}\square_{x/2})$ from the parent sodalite, $Na_8[AlSiO_4]_6Cl_2$.

Fig 5.1 Photographs of a natural sample of hackmanite before and after exposure to UV radiation at 254nm

Incorporation of sulphur impurities into the structure creates vacant non-framework anion sites in the structure. It is the movement of an electron to one of these defects or holes in the structure that creates a coloured material, with the difference in energy between the two states corresponding to the absorption of UV light. This trapped electron, also known as an F centre, absorbs visible light. This can result in the electron having enough energy to escape the trap, explaining why the samples will bleach back to a white state over time when exposed to sunlight.

The remarkable optical property of the hackmanite mineral gives it many potential applications, ranging from security marking of property to formation of smart, optically active pigments for decorative use in the arts industry. Hackmanites could potentially even find uses as protection from harmful UV radiation if the optical property could be tuned to a desired wavelength.

5.2 The History of Hackmanite

The first reported incidence of natural hackmanite was made by Giesecke in Greenland between 1806 and 1808. Later, in 1834 mineralogist Robert Allan[8] first observed the pink colouration of a natural sample of hackmanite reporting that: "Its colour is green unless freshly fractured, when it presents a brilliant pink tinge, but this on exposure to light goes off in a few hours", but reversible photochromism was not reported at this point. In 1925 Walker and Parsons[9] reported that fresh surfaces of hackmanite, this time collected from Bancroft, contained pink spots, which disappeared upon exposure to direct sunshine in seconds. Later still, in 1936 mineralogist O. Ivan Lee[2], looked more closely at the properties of natural hackmanite and observed reversible photochromism in a sample by exposing it to UV radiation. More recently, Pererson studied the structure of a natural hackmanite sample from Quebec, Canada[10].

5.3 Mechanism of Reversible Photochromism

All ionic crystalline materials contain defects within the structure. A defect manifests as an absence of an ion within the structure, and are favourable to a degree because of the accompanying increase in entropy or disorder. These types of defects are known as intrinsic defects and do not affect the overall stoichiometry of the structure. There are two types of defect to be discussed here, namely Schottky defects and Frenkel defects. Schottky defects are characterised by ions being absent from their lattice points, creating a vacancy or hole in the structure. These are found in pairs, as both the anion and cation are absent to maintain charge balance.

Frenkel defects are also characterised by the absence of an ion from a lattice site, however in the case of Frenkel defects the ion is moved to another site which is not usually occupied. Frenkel defects, like Schottky defects, create a vacancy or hole on a lattice site, and can be responsible for tenebrescence. Unpaired electrons trapped in these vacancies become colour centres, sometimes known as F centres. They are so named from the German word *fabre,* meaning colour, and were first proposed by de Boer in 1937 [11].

The mechanism of reversible photochromism, or tenebrescence was first proposed by Medved[12]. Medved's model involves the movement of electrons between dopants and vacant sites, labeled U, the F centres and both the valence and conduction bands. Tenebrescent materials usually have a large band gap, meaning the difference in energy between the valence band and the conduction band is too large to absorb light in the visible region. This makes the F centres an important transition state in the mechanism of tenebrescence.

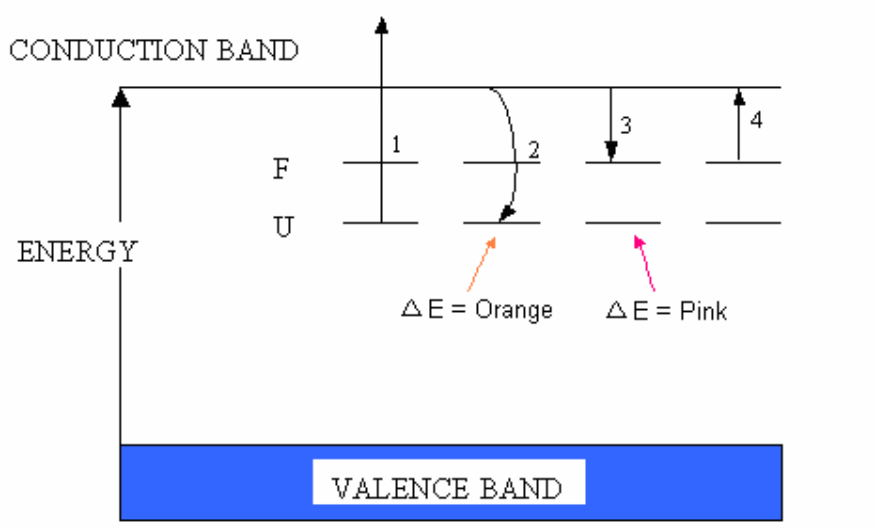

Fig. 5.2 Band picture of a tenebrescent hackmanite as proposed by Medved showing the mechanism of tenebrescence

When a hackmanite sample in the relaxed state is exposed to uv radiation electrons in the U levels are promoted to the conduction band (1). From the conduction band the electrons can take one of two paths. The first is to relax back to U levels, releasing energy as visible light(2). This is seen as an orange coloured fluorescence when

hackmanite is irradiated with UV radiation and results in a loss in energy from the system.

The second pathway is for the electrons to move from the conduction band to a vacancy or F centre(3) creating a colour centre. This arises because the electron can now absorb light of a wavelength in the visible region of the spectrum(3). This gives rise to the pink colouration observed after natural hackmanite samples are exposed to UV radiation. The absorption of sunlight or white light can then be used to bleach the sample by exciting the electron back into the conduction band (4).

5.4 Scope of this Work

The work presented in this chapter centred upon the synthesis and characterisation of various sodalites with a view to observing how changes in the structure and composition of the sample affect the optical property. Firstly a natural sample of hackmanite displaying reversible photochromism was studied in an attempt to link structural considerations of the sample with this remarkable optical property. With these results in mind, a large library of hackmanites with various compositions was synthesised. Primarily, a suitable synthetic route towards sodalite was identified, which allowed the introduction of a reduced form of sulphur into non framework sites in an attempt to reproduce the reversible photochromism observed from natural hackmanite samples. With the synthetic route in place a number of different variables were investigated to ascertain how, if at all, this affected the reversible photochromism.

This system lends itself to a variety of possible different substitutions into non framework sites. The inclusion of various cations was investigated, for example Li^+, Na^+, K^+ and Cs^+, which also altered the lattice parameters and bond lengths of the framework. Anion substitutions were also investigated specifically Cl^-, $Br^-$and I^- inclusion in the non framework sites.

5.5 Natural Hackmanite

A natural sample of hackmanite was obtained, which displayed reversible photochromism at 254nm and 365nm, which were the wavelengths available on the lamp used for the screening. The sample possessed fast colouration times of 5 seconds and 30 seconds at these two wavelengths respectively, with a bleaching time of about 30 minutes under exposure to a white light source. This sample was characterised fully by a variety of methods. Firstly the crystal structure of the sample was characterised, using single crystal x-ray diffraction.

Table 5.1 Showing the crystal structure of a natural hackmanite sample

Empirical formula	$Al_6Cl_2Na_8O_{24}Si_6$
Wavelength	0.71073 Å
Crystal system	cubic
Space group	$P\bar{4}3n$
Unit cell dimensions	a = 8.8778(2)Å α= 90°. b = 8.8778(2)Å β= 90°. c = 8.8778(2)Å γ = 90°.
Volume	699.71(3) $Å^3$
Z	1
Density (calculated)	2.300 mg/m^3
Crystal size	0.7 x 0.3 x 0.3 mm^3
R(int)	0.0390
Refinement method	Full-matrix least-squares on F^2
Final R indices [I>2sigma(I)]	R1 = 0.0175, wR2 = 0.0436
R indices (all data)	R1 = 0.0184, wR2 = 0.0442

Next SEM imaging of the crystal was performed along with EDX analysis. This would give an idea of the amount of sulphur present in the sample, thought to be important for reversible photochromism to occur.

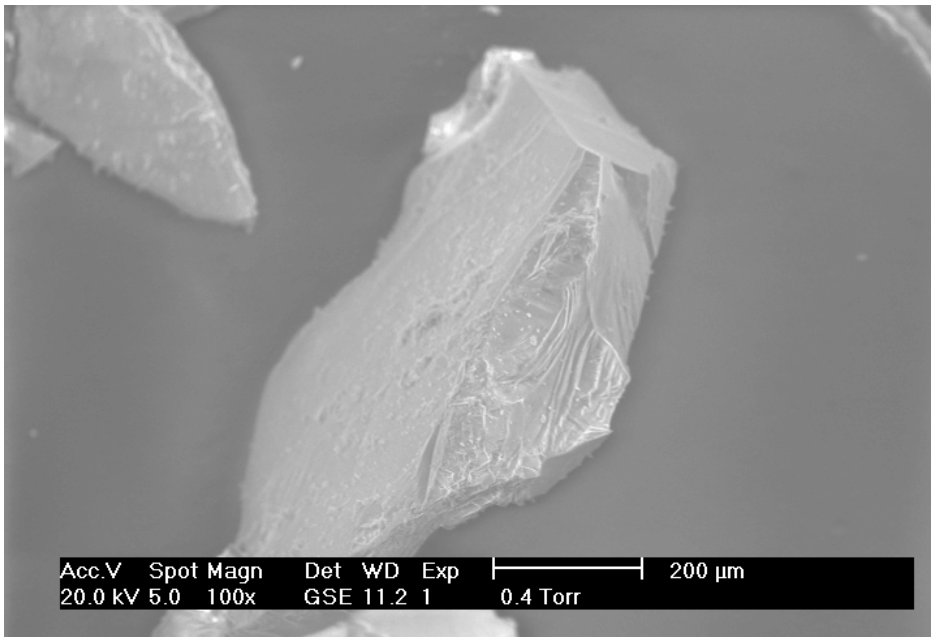

Figure 5.3 An SEM image of a single crystal of natural hackmanite with rough dimensions of 400x800nm

Table 5.2 The elemental composition of the natural hackmanite sample obtained by EDX analysis

Element	Atomic Percentage/ %
O	52.48
Na	16.19
Al	14.75
Si	12.8
S	0.29
Cl	3.48

The EDX data show that approximately 8% of the anion sites are occupied by sulphur with an empirical formula of $Na_{7.8}Al_{6.0}Si_{5.0}S_{0.10}Cl_{1.08}$. Although EDX data should not

be considered as quantitative due to the high errors involved, as the number of incident and backscattered electrons can fluctuate it does give an estimate of the amount of sulphur present in the sample. With these results in mind synthesis of a hackmanite could be attempted, with view to mimicking the reversible photochromism displayed by natural hackmanite samples by doping the anion sites with impurity levels of sulphur.

5.6 Sodalite Synthesis

A method was developed for the synthesis of a sodalite. It was hoped that sulphur species could be introduced into the beta cages of the sodalite after it had been formed. These sulphur species could then be reduced to give the required oxidation state of sulphur suitable for reversible photochromism.

0.225g of aluminium powder (Aldrich 99.9%) was dissolved in 25ml of 4M sodium hydroxide solution. 1.0g of SiO_2 (Aldrich 99.9%) was then added to the reaction mixture. The reaction mixture was loaded into a 45ml capacity PTFE lined steel autoclave before being heated to 200 °C for a period of 24 hours. The reaction vessel was allowed to cool to room temperature before the product was recovered by filtration and washed thoroughly with deionised water. The resulting white powder was then ground and intimately mixed with 1.0g of sodium chloride (Aldrich 99%) before being heated to 650 °C in a box furnace. The phase was thoroughly washed and characterised by powder x-ray diffraction and found to be phase pure sodalite, $Na_8(AlSiO_4)_6Cl_2$ in reference with the JCPDS database.

1.0g of elemental sulphur was dissolved in a solution of 20%wt ammonium sulphide in water. 1.0g of the synthetic sodalite was ground to a fine powder using a pestle and mortar and suspended in the sulphur rich solution. The reaction was stirred rapidly at 70 °C for about 4 hours until all water had evaporated leaving a dry yellow powder. The powder was then transferred to an alumina crucible and heated to 650 °C in a tube furnace under a flowing gas mixture of 5% hydrogen in nitrogen for a period of 18 hours, before being allowed to cool under the same flowing gas conditions. A pale green powder was produced which was then recovered and washed thoroughly with

deionised water before being dried at 90 °C. Powder x-ray diffraction showed the product to be a sodalite phase in reference with the JCPDS database.

The product displayed no tenebresence at either 254nm or 365nm, and there is no evidence of any sulphur species being encapsulated in the pores of the structure. Upon examination of powder XRD data the phase appears to be a sodalite type framework but does not contain a sulphur species suitable for tenebrescence.

5.7 Solid State Synthesis

A synthetic route was explored to produce a hackmanite with reversible photochromism from a high temperature solid state reaction[13]. The reaction involved the collapse of a zeolite with an aluminium to silicon ratio of 1 : 1 (Zeolites Linde type A or Faujasite for example) into sodalite. A sulphur source was incorporated at the collapse stage and was simultaneously reduced to the correct oxidation state by using a flowing gas mixture containing hydrogen as a reducing agent in a tube furnace.

A quantity of Zeolite A was prepared as discussed previously in Sec. 3.2.1g of this Zeolite A was then ground and intimately mixed with 0.3g of sodium chloride (Aldrich 99%) and 0.2g of sodium sulphate (INC 99%) using a pestle and mortar. This reaction mixture was then transferred to an alumina crucible, which was then placed inside a tube furnace. The tube furnace was then flushed with a mildly reducing gas mixture of 5% hydrogen in nitrogen for a period of 30 minutes. Next, the reaction was heated to 750 °C for 16 hours under flowing gas of 5% hydrogen in nitrogen.

The reaction was allowed to cool and the product was recovered. The resultant white powder was characterised by powder x-ray diffraction and found to be single phase sodalite by comparison with the JCPDS database. The sodalite was then screened for optical activity using a commercial ultraviolet light source, capable of switching between wavelengths of 254nm and 365nm. The sample was found to be optically active under exposure to 254nm radiation with a colouration time of 10 seconds. The bleaching time of the synthetic sample was around 30 minutes when placed under a white light source. The sample was found to be inactive upon exposure to 365nm UV radiation.

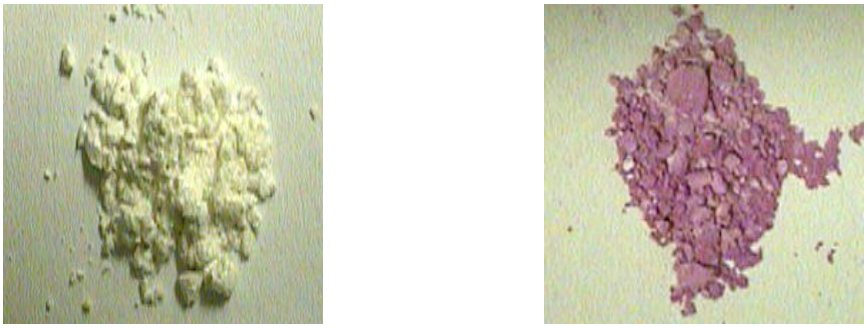

Fig 5.4 Photographs of a synthetic hackmanite sample taken before and after exposure to 254nm UV radiation, showing the distinct colour change

5.8 Elemental Analysis of a Synthetic Hackmanite

The synthetic hackmanite was imaged by SEM and EDX data was collected on the sample to discern if any sulphur had been incorporated into the beta cages of the sodalite framework.

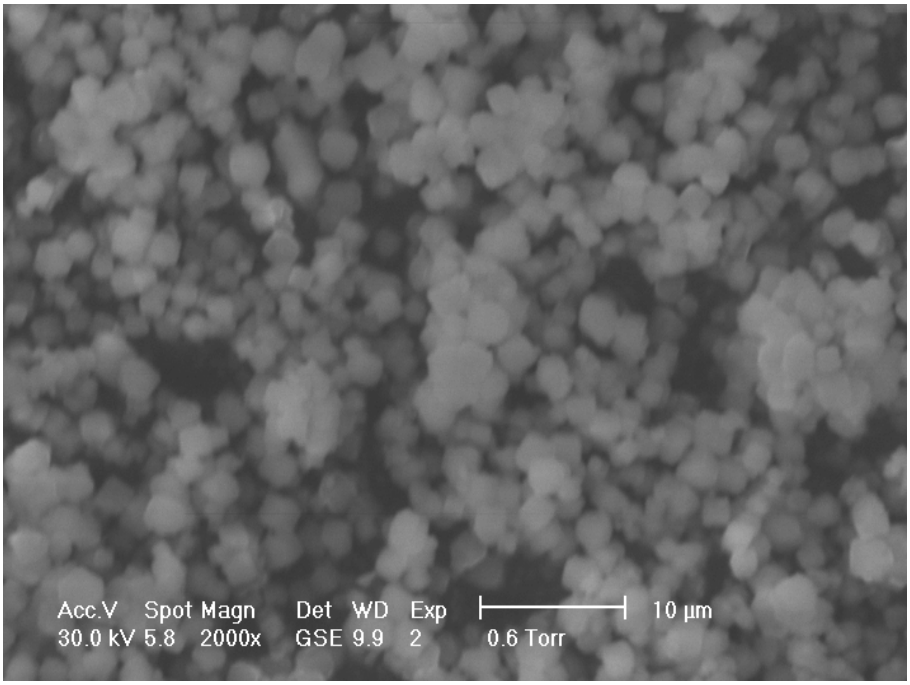

Fig 5.5 SEM Image of the sodalite showing cubic crystallites and a particle size of a few microns

Table 5.3 Atomic composition by percentage of a synthetic hackmanite sample shown to display reversible photochromism

Element	Atomic Percentage/ %
O	47.6
Na	18.2
Al	14.96
Si	14.27
S	0.57
Cl	4.4

The atomic percentages given in the above table for a synthetically produced hackmanite are similar to the atomic composition of the mineral sample given in table 5.2. One point of interest is the higher percentage composition of sulphur in the synthetic sample. Although EDX data should not be considered quantitative this increased sulphur content is of interest as sulphur is thought to be key in the photochromic mechanism. The natural sample is seen to tenebresce at 254 and 365 nm, whereas the synthetic sample only displays the phenomenon upon exposure to 254nm radiation. The natural sample also has a much more obvious colour change, with the activated state being a much deeper pink in colouration.

5.9 Structural Studies by Powder Neutron Diffraction

Considering the observed poor performance of the synthetic hackmanites compared to the natural sample, experiments were devised in an attempt to link this interesting optical property with the structure of the sodalite. A large number of sodalites were synthesised by grinding and intimately mixing 2g of zeolite A with various amounts of sodium chloride (Aldrich 99%) and sodium sulphate (INC 99%). These reaction mixtures were then transferred into alumina crucibles, which were then placed inside a large bore tube furnace capable of housing 10 of these reactions at once. The tube furnace was then flushed with a mildly reducing gas mixture of 5% hydrogen in nitrogen for a period of 30 minutes. Next, the reaction was heated to 750 °C for 16 hours under flowing gas of 5% hydrogen in nitrogen. The product was then allowed to cool under the same gas mixture before being recovered, washed thoroughly with distilled water and dried in a drying oven. By quantifying the effect that structure has on the observed photochromism, it was hoped that extrapolation of trends could lead to improved performance of the products.

The products were characterised by powder neutron diffraction on the POLARIS instrument, housed at ISIS in the Rutherford Appleton Laboratories. Neutrons, as opposed to x-rays, can distinguish between S^{2-} and Cl^{-}, which have identical electron configurations. This is because unlike with an x-ray diffraction experiment, the scattering power of atoms is not related to the number of electrons of the individual atoms or ions in the lattice.

POLARIS is a high flux medium resolution powder diffractometer. The close vicinity of the instrument to the target results in a high incident flux and means the instrument is ideal for a fast sample turnover. Early experiments indicated that refinable quality data suitable for the Reitveld method could be produced by collecting for roughly 100 microamp hours. In terms of time this relates to about 45 minutes in the sample chamber, compared to a standard collection of x-ray data for the Reitveld method of about 18 hours. This means that it would take longer to change the sample and produce a vacuum in the sample chamber than to collect the data set for each sample.

To solve this problem the POLARIS sample auto-changer was used, which allowed for many samples to be loaded into the sample environment together to minimise the time taken to change samples between collection of data sets, and hence optimized the use of beam time. In total, 20 vanadium sample holders can be mounted at one time on the sample changer

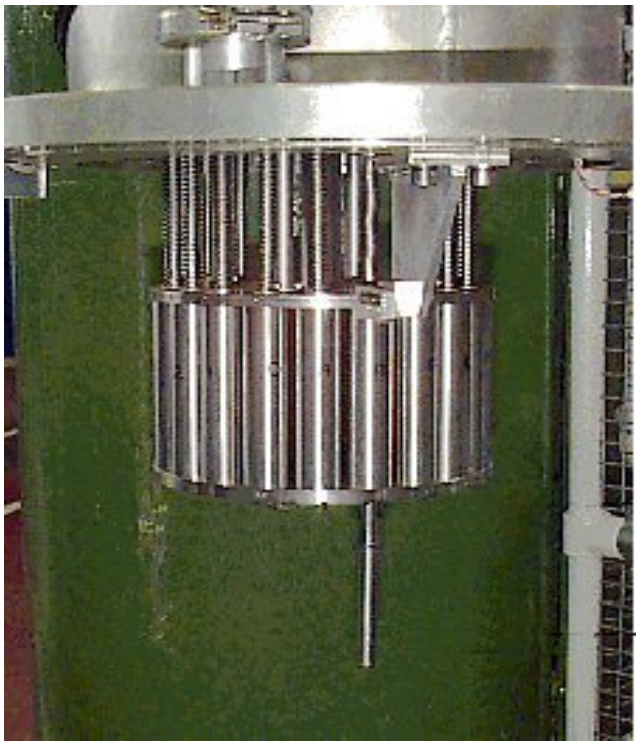

Fig 5.6 A photograph of the POLARIS sample changer showing a vanadium can in the down position

5.10 Reitveld Refinements of the Sodalite Library

Structural refinements of the sodalite compound library were performed using the Reitveld method. The sodalite phase, $Na_8[AlSiO_4]_6(Cl,S)_2$, was modeled in the space group P-43n, using single crystal data of a natural hackmanite sample as the starting model. The refinements were carried out using the GSAS program[14]. Initial stages of the refinement included all the instrument parameters (background, scale factor and peak shape parameters). The atomic parameters (atomic positions and temperature factors) of the sodalite phase were then slowly introduced for all atoms. Next the atomic parameters (atomic positions and temperature factors) of the sodalite phase were introduced to the refinement. The lattice parameter of the phase was also allowed to vary at this point, along with adding some additional background parameters.

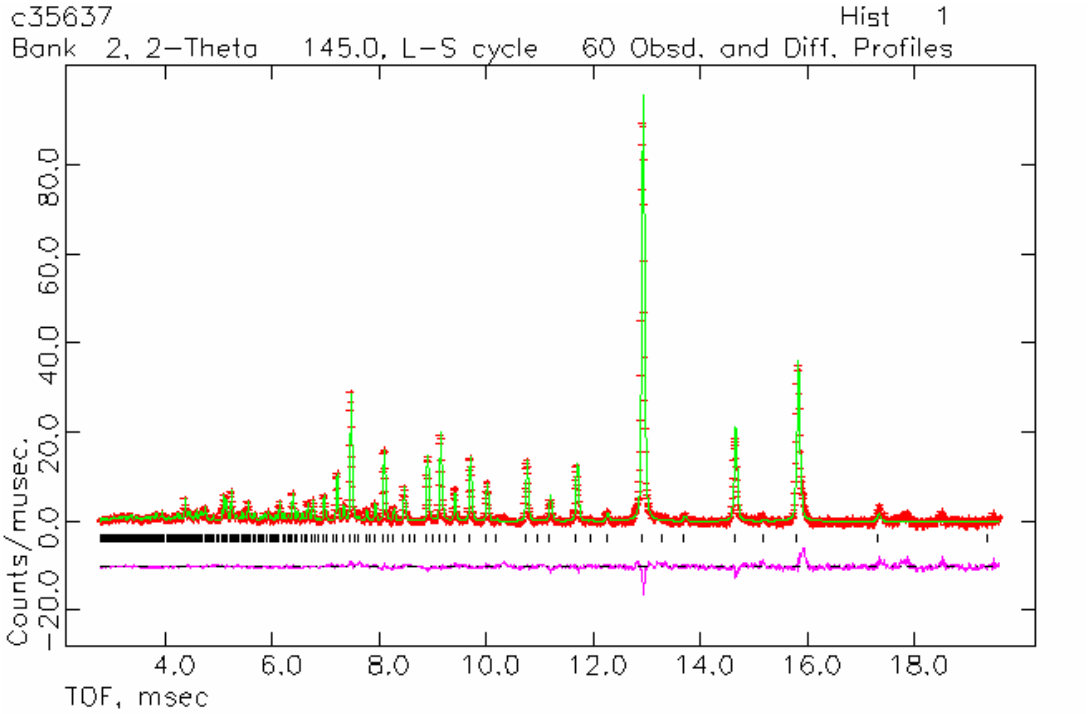

Fig 5.7 A picture showing the fit between the model and the data set for Reitveld refinement of a sodalite using the GSAS program with model shown in green, data in red and the difference plot in pink. (2.0g LTA, 0.0999g sodium sulphate, 0.137g sodium chloride.)

Similar structural refinements were performed for a number of sodalite phases containing varying amounts of chlorine and sulphur, the results of which are summarised below. As the samples were similar in composition, the output of one refinement was used as the starting point for the next and the structures were refined sequentially in this way. Data of interest from the refinements is summarised below, in particular lattice parameters and averaged Na-O bond distances.

Table 5.4 Showing the variation in lattice parameter and average Na-O bond distances of the sodalite system for varying amounts of sulphur and chlorine used in the reaction mixture

Zeolite A (g)	**Sodium Sulphate (g)**	**Sodium Chloride (g)**	**Lattice Parameter (Å)**	**Na-O distance (Å)**	**M-X distance (Å)**	**Salt/S molar ratio**
2.0	0.0119	0.137	8.8779(4)	2.3740(29)	2.737(6)	17.6
2.0	0.0119	0.206	8.88337(11)	2.3579(11)	2.7416(22)	26
2.0	0.0119	0.274	8.88637(12)	2.3559(12)	2.7450(23)	35.2
2.0	0.0665	0.137	8.88473(19)	2.3685(19)	2.730(4)	5.3
2.0	0.0665	0.206	8.88332(9)	2.3578(10)	2.7389(19)	7.9
2.0	0.0665	0.274	8.88346(9)	2.3533(9)	2.7443(17)	10.5
2.0	0.0665	0.342	8.88104(16)	2.3585(16)	2.7344(30)	13.3
2.0	0.083	0.137	8.88610(19)	2.3658(20)	2.733(4)	4.2
2.0	0.0999	0.0206	8.89152(24)	2.3712(27)	2.733(5)	0.7
2.0	0.0999	0.137	8.87896(13)	2.3533(13)	2.7403(24)	3.5
2.0	0.0999	0.137	8.88710(19)	2.3713(18)	2.735(4)	3.5
2.0	0.0999	0.206	8.88982(10)	2.3626(10)	2.7446(19)	5.3
2.0	0.0999	0.206	8.88475(11)	2.3588(11)	2.7371(20)	5.3
2.0	0.0999	0.342	8.88548(21)	2.3556(22)	2.739(4)	8.8
2.0	0.0999	0.342	8.88782(14)	2.3545(14)	2.7429(27)	8.8
2.0	0.116	0.137	8.88283(21)	2.3676(23)	2.732(4)	3
2.0	0.116	0.206	8.88769(10)	2.3586(11)	2.7402(20)	4.5
2.0	0.116	0.274	8.88487(10)	2.3437(11)	2.7438(20)	6
2.0	0.116	0.342	8.88104(17)	2.3557(17)	2.7351(32)	7.6
2.0	0	0.206	8.88247(28)	2.3671(23)	2.742(4)	0

Using the results of the Rietveld refinements any trends between the amount of chlorine and sulphur and the structure of the sodalites were explored. Firstly any relationship between chloride content and lattice parameter was examined using the series containing 0.0999g of sodium sulphate.

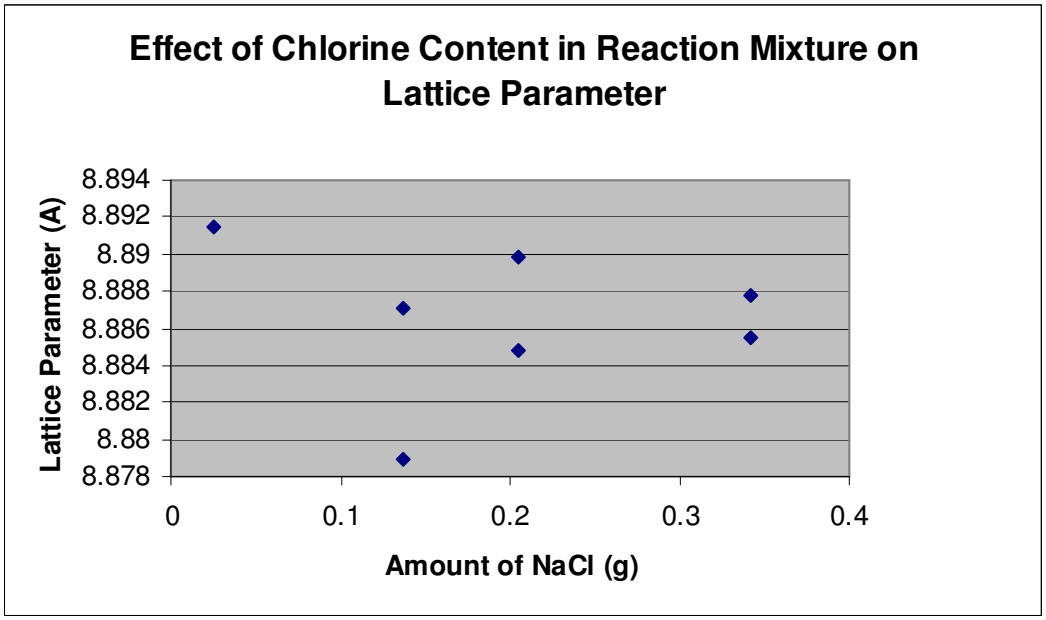

Fig 5.8 A graph showing the relationship between the amount of chloride present in the reaction mixture and the lattice parameter of the sodalite

As expected from this data set, the amount of sodium chloride used in the reaction has no marked effect on the lattice parameter. At higher levels of sodium chloride any excess salt that is left after thermal conversion is washed out with water. The lattice parameters for this data set are comparable to that found by Peterson[10] in a natural sample with a=8.887(2).

Any trend between the amount of sulphur present and the lattice parameter was also examined. Again, the results seemed to show no correlation between lattice parameter and sulphur content for the entire data set as shown in figure 5.9. Subsequently a single data set was examined, varying the sulphur content for a single weight of sodium chloride. The results of this are displayed in figure 5.10.

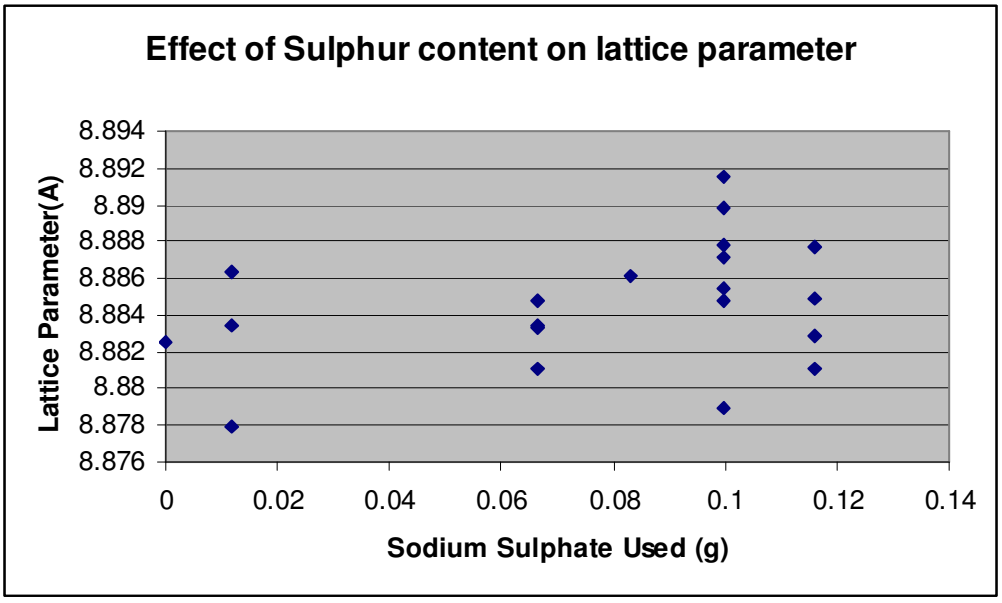

Fig 5.9 A graph showing the trend between amount of sulphur present in the reaction mixture and the lattice parameter

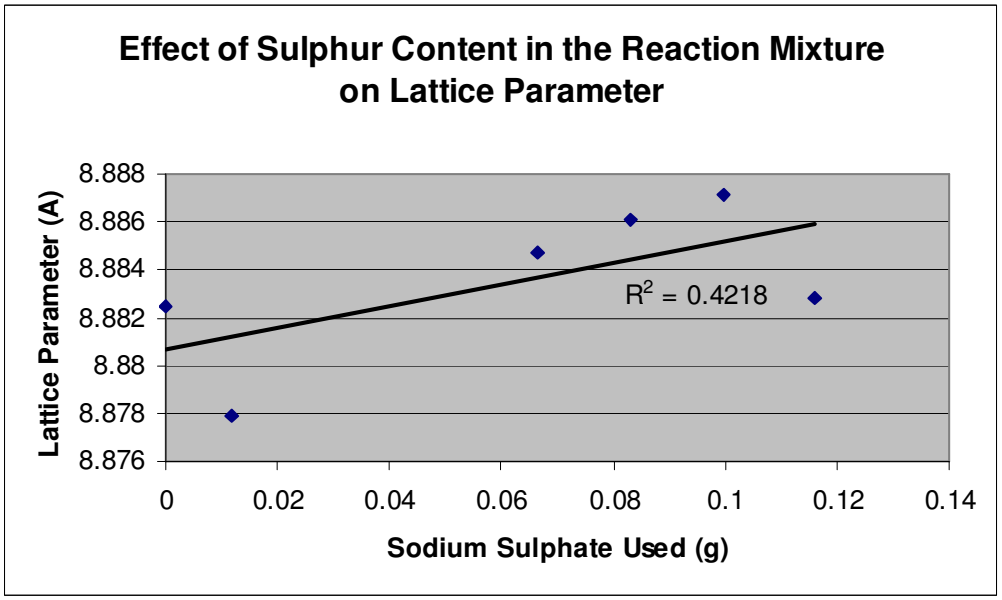

Fig 5.10 A graph showing the trend between amount of sulphur present in the reaction mixture and the lattice parameter for a fixed weight of 1.47g sodium chloride

The relationship between the amount of sulphur used and sodium to oxygen bond distances were also examined using the output from the structural refinements. This gives more information regarding what is happening inside the beta cages of the sodalite, which cannot be determined by studying changes in lattice parameter. Results of this are outlined below.

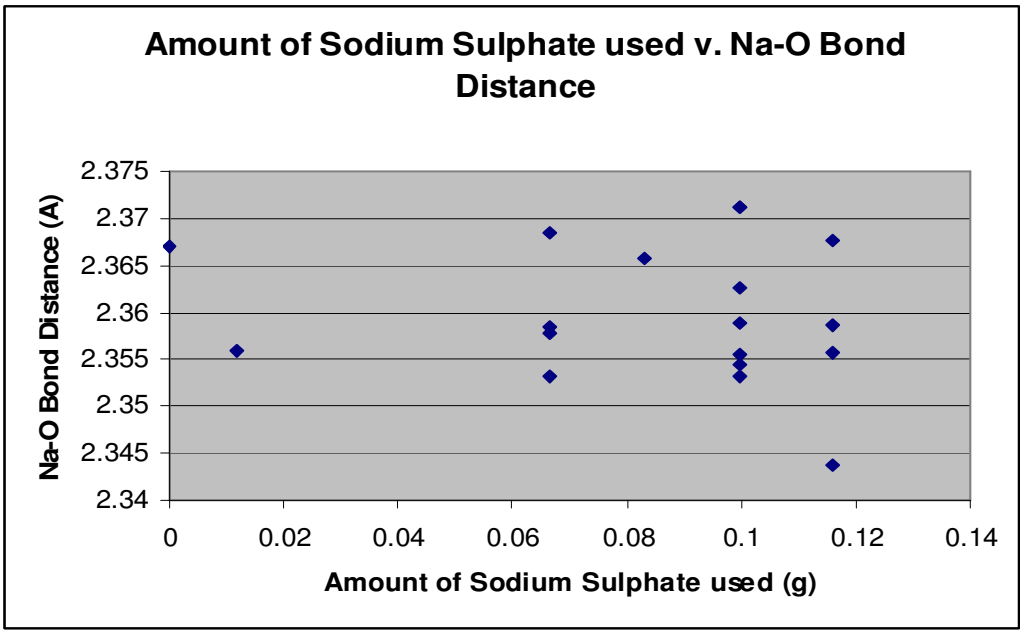

Fig 5.11 Showing the trend between amount of sulphur present in the reaction mixture and Na-O bond distances

It can be seen from figure 5.11 that the Na-O bond length does not dramatically change upon addition of sulphur to the phase. This, at first, seems counter intuitive as the sulphur species is much larger than the chlorine anion. When sulphur is substituted into the system it is incorporated at a chlorine site in the structure, and a corresponding vacant site is formed as $2Cl^-$ is replaced by S_2^{2-} and a hole. The incorporation of sulphur could force the aluminosilicate framework in the immediate environment around the sulphur species to expand to incorporate the larger anion. The important consideration is that all Na-O bond distances listed are average bond distances, and any changes around the sulphur species could be offset by changes at the vacant site.

This same trend can be seen from a plot of lattice parameter versus Na-O bond distances in the same data series shown below.

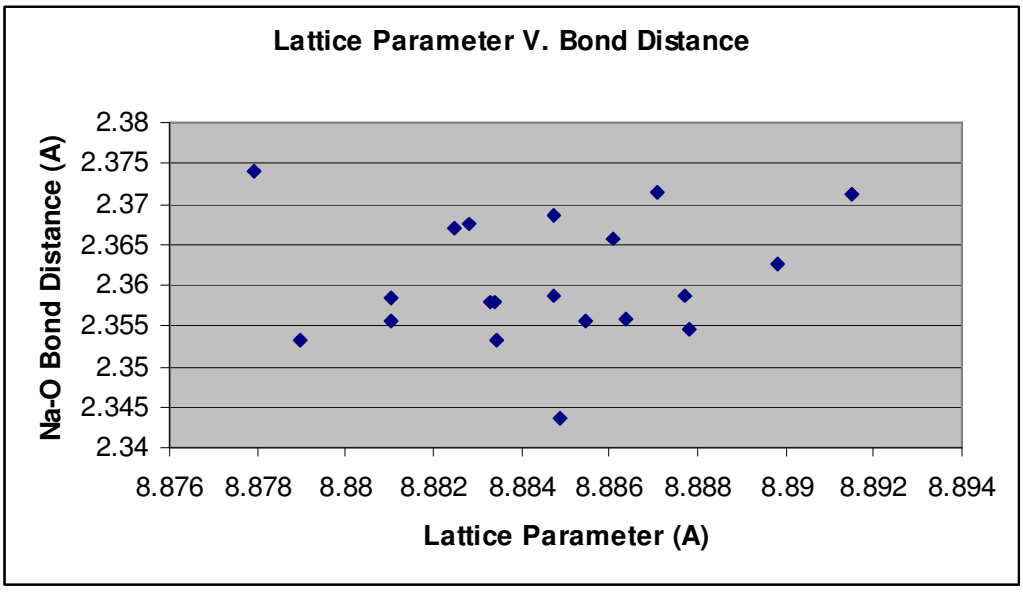

Fig 5.12 showing the trend between lattice parameter and Na-O bond distances

Again, there seems to be no correlation between the data sets, with the increase in Na-O bond distances having no effect on the overall lattice parameter.

The relationships between the amounts of sulphur and chlorine used in the reaction mixture and the M-X bond distance was also examined, the results of which are shown below.

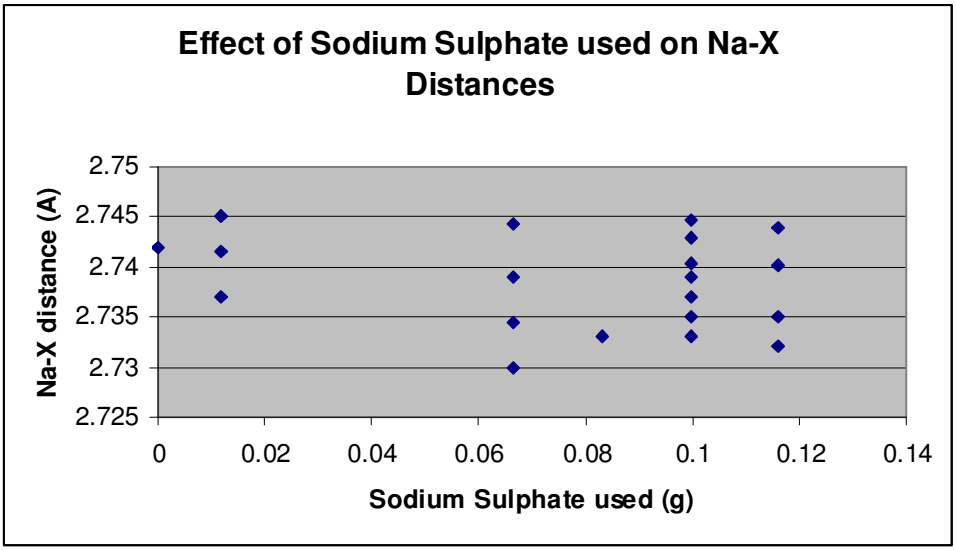

Fig 5.13 showing the trend between amount of sodium sulphate used and M-X distances

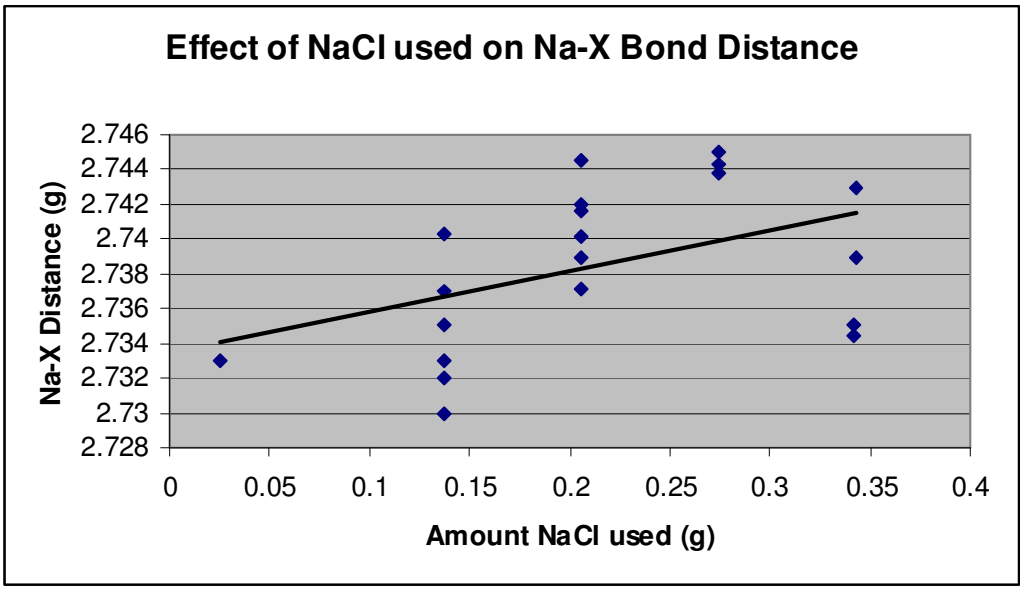

Fig 5.14 showing the trend between amount of sodium chloride used and M-X distances

From fig. 5.13 it can be seen that the amount of sulphur used in the reaction has no marked effect on the M-X bond distances. Fig 5.14 shows a general increase in M-X bond distances upon increased use of sodium chloride in the reaction mixture. This is to be expected, as inclusion of a large electronegative anion will force the beta cages

of the extended framework to expand, moving the sodium and chloride ions further apart.

All the phases were also screened for photochromic activity using an ultraviolet light source capable of switching between 254 and 365nm wavelengths. All the phases containing sodium and chlorine displayed activity at 254nm but not at 365nm. The phases changed from white to pink upon an exposure time of around 30 seconds. The phases then bleached back to the white state when left under white light over a period of about 30 minutes. This colour change was found to be completely reversible after multiple exposures to UV radiation and samples continued to display reversible photochromism after 100 separate exposures.

Fig 5.15 A photograph of a sodium chloride containing hackmanite partially exposed to 254 nm UV radiation showing a distinct colour change from white to pink

5.11 Bromide Substitutions

A large number of bromide containing sodalites were synthesised by grinding and intimately mixing 2g of zeolite A with various amounts of sodium bromide (Aldrich 99%) and sodium sulphate (INC 99%). These reaction mixtures were then transferred into alumina crucibles, which were then placed inside a large bore tube furnace capable of housing 10 of these reactions at once. The tube furnace was then flushed with a mildly reducing gas mixture of 5% hydrogen in nitrogen for a period of 30 minutes. Next, the reaction was heated to 750 °C for 16 hours under flowing gas of 5% hydrogen in nitrogen. The product was then allowed to cool under the same gas mixture before being recovered, washed thoroughly with distilled water and dried in a drying oven.

Structural refinements of the sodalite compound library were performed using the Reitveld method on neutron diffraction data collected on Polaris. The sodalite phase, $Na_8[AlSiO_4]_6(Br_{x-2}, S_{x/2}\square_{x/2})$, was modeled in the space group P-43n using the GSAS program[14].

Table 5.5 Showing the variation in lattice parameter and average Na-O bond distance of the sodalite system for varying amounts of sulphur and bromine in the reaction mixture

Zeolite A (g)	**Sodium Sulphate (g)**	**Sodium Bromide (g)**	**Lattice Parameter (Å)**	**Na-O distance (Å)**	**M-X distance (Å)**	**Salt/S molar ratio**
2.0	0.0665	0.241	8.9377(4)	2.3862(27)	2.845(6)	5
2.0	0.0665	0.362	8.94334(12)	2.3573(10)	2.8950(21)	7.5
2.0	0.0665	0.362	8.9401(4)	2.3816(20)	2.865(4)	7.5
2.0	0.0665	0.486	8.94226(11)	2.3554(10)	2.8977(19)	10.1
2.0	0.0665	0.603	8.93425(11)	2.3539(10)	2.8913(20)	12.5
2.0	0.0665	0.603	8.94332(19)	2.3622(13)	2.8955(27)	12.5
2.0	0.083	0.241	8.93945(21)	2.3585(20)	2.889(4)	4
2.0	0.083	0.362	8.94639(12)	2.3563(11)	2.9033(21)	6
2.0	0.083	0.486	8.94371(11)	2.3533(10)	2.9049(20)	8
2.0	0.083	0.603	8.94050(10)	2.3538(9)	2.8980(18)	10
2.0	0.0999	0.603	8.93633(12)	2.3563(11)	2.8911(22)	8.3
2.0	0.116	0.241	8.93906(21)	2.3674(18)	2.876(4)	2.9
2.0	0.116	0.362	8.93950(11)	2.3531(10)	2.8999(19)	4.3
2.0	0.116	0.486	8.93990(13)	2.3533(11)	2.8998(23)	5.8
2.0	0.116	0.603	8.94126(11)	2.3548(10)	2.8981(19)	7.2

All the phases were also screened for photochromic activity using an ultraviolet light source capable of switching between 254 and 365nm wavelengths. All the phases containing sodium and bromine displayed activity at 254nm but not at 365nm. The phases changed from white to purple upon an exposure time of around 30 seconds. The phases then bleached back to the white state when left under white light over a period of about 30 minutes. This colour change was found to be completely reversible after multiple exposures to UV radiation and samples continued to display reversible photochromism after 100 separate exposures.

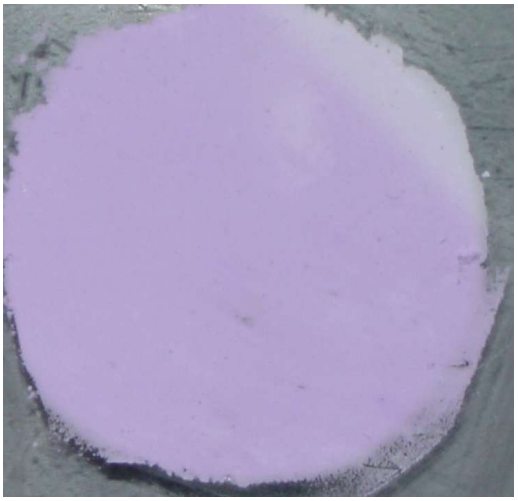

Fig 5.16 A photograph of a sodium bromide containing hackmanite exposed to 254 nm UV radiation showing a distinct colour change from white to purple

As with the example of increased sulphur inclusion discussed in section 4.7 the effect of bromide inclusion on the structure was examined, particularly the relationship between increased bromide content and the lattice parameter and Na-O bond lengths of the structure.

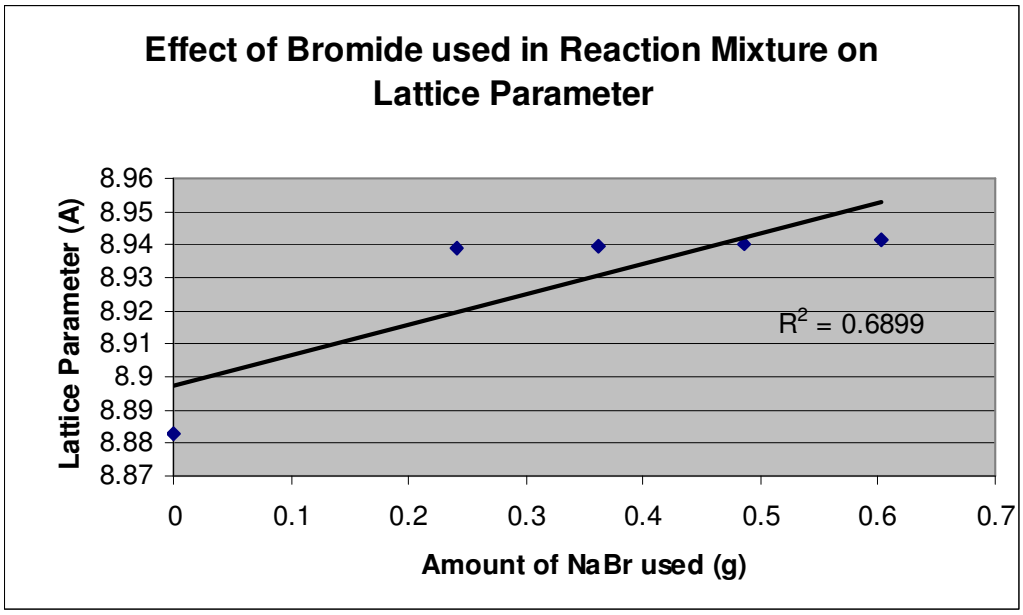

Fig 5.17 A graph showing the trend between amount of bromide present in the reaction mixture and the lattice parameter of the sodalite phase for a fixed weight of 0.116g sodium sulphate in the reaction mixture

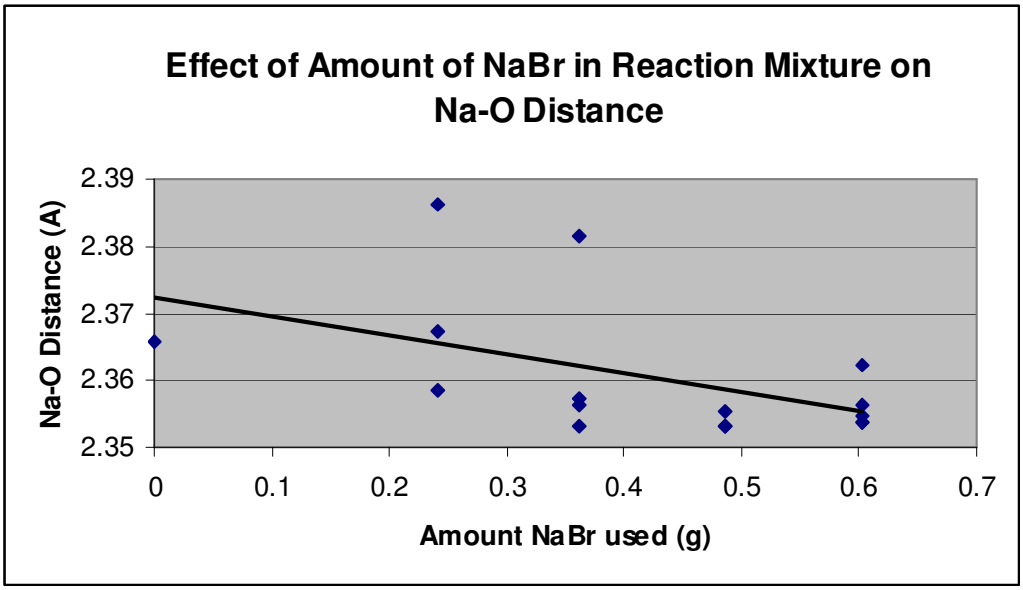

Fig 5.18 Showing the trend between the amount of bromide present in the reaction mixture and Na-O bond distances

The expanded environment around the larger anion site is responsible for a marked reduction in the average Na-O bond distances and a general increase in lattice parameter. This effect is most prominently observed when comparing a chloride containing sodalite with the bromide substituted data set. There is a dramatic increase in lattice parameter (compared to that found by Peterson[10] in a natural sample with a=8.887(2).) and corresponding decrease in Na-O bond distance upon the inclusion of the larger bromide anion. There are two main points of consideration for this example. Firstly the bromide anion is less electronegative than the chloride, which results in a weakening of the halide sodium interaction. This in turn makes the Na-O interaction more significant, drawing the framework oxygen closer to the sodium. Secondly, the bromide has a larger ionic radius than the chlorine, resulting in steric interactions forcing the sodium closer to the framework oxygen. These factors combined produce a net reduction in average Na-O bond distances for this data set.

Another observation from Fig 5.18 is that the two anomalous data points at 2.3862Å and 2.3816Å have the largest errors of all the data, and impurities in these systems may be responsible for their apparent removal from the trend.

The M-X distances were also examined for increased use of sodium bromide.

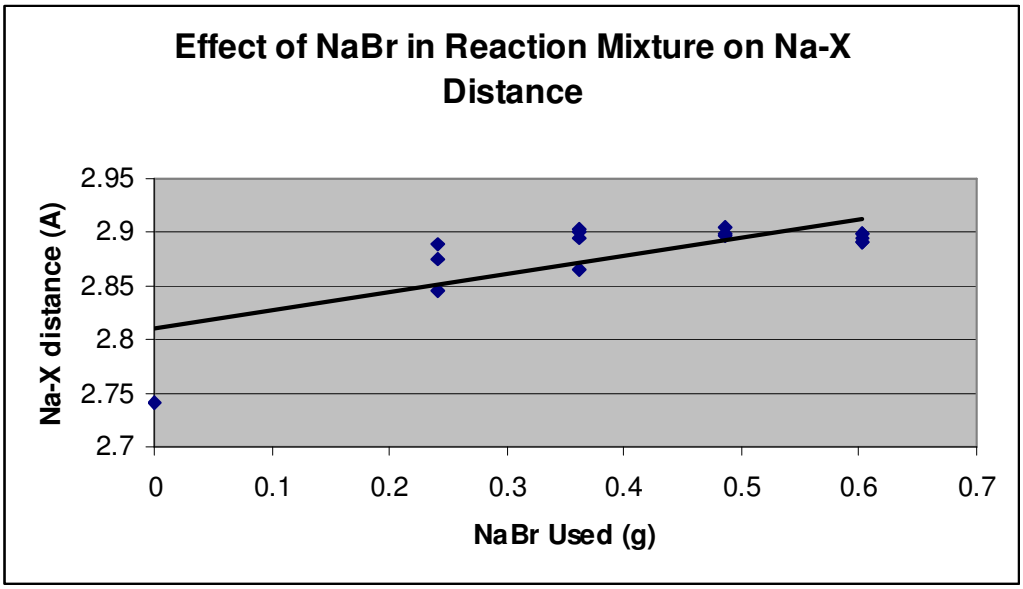

Fig 5.19 Showing the trend between the amount of bromide present in the reaction mixture and Na-X bond distances

The results display a similar trend to the example of NaCl content, with an increase in the amount of NaBr used in the reaction mixture corresponding to an increase in the M-X bond distance. The data for amount of NaBr used have a greater Na-X bond distance than the corresponding NaCl data set. This is rationalized by the much larger ionic radius of bromide, forcing the beta cages of the structure to expand even further to accommodate them. This increase in Na-X bond distance implies a change in environment at the chloride site and also the site of any holes or defects in the structure. This could lead to a change in the energy level of any f-centres present, and could explain the change in the colour of tenebresence from the chloride sodalites to the bromide sodalites.

5.12 Iodide Substitutions

A large number of iodide containing sodalites were synthesised by grinding and intimately mixing 2g of zeolite A with various amounts of sodium iodide (Aldrich 99%) and sodium sulphate (INC 99%). These reaction mixtures were then transferred into alumina crucibles, which were then placed inside a large bore tube furnace capable of housing 10 of these reactions at once. The tube furnace was then flushed with a mildly reducing gas mixture of 5% hydrogen in nitrogen for a period of 30 minutes. Next, the reaction was heated to 750 °C for 16 hours under flowing gas of 5% hydrogen in nitrogen. The product was then allowed to cool under the same gas mixture before being recovered, washed thoroughly with distilled water and dried in a drying oven.

Structural refinements of the sodalite compound library were performed using the Reitveld method on neutron diffraction data collected on Polaris. The sodalite phase, $Na_8[AlSiO_4]_6(I_{x-2}, S_{x/2}\square_{x/2})$, was modeled in the space group P-43n using the GSAS program[6].

Table 5.6 Showing the variation in lattice parameter and average Na-O bond distance of the sodalite system for varying amounts of sulphur and iodine in the reaction mixture

Zeolite A (g)	**Sodium Sulphate (g)**	**Sodium Iodide (g)**	**Lattice Parameter (Å)**	**Na-O distance (Å)**	**M-X distance (Å)**	**Salt/S molar ratio**
2.0	0.05	1.407	9.01645(24)	2.3735(13)	3.1336(34)	26.6
2.0	0.05	2.110	9.01432(24)	2.3706(12)	3.1323(33)	40
2.0	0.05	2.814	9.01913(21)	2.3718(11)	3.1405(31)	53.3
2.0	0.05	3.517	9.01697(19)	2.3720(11)	3.1313(28)	62.8
2.0	0.0665	0.352	9.0220(5)	2.3800(33)	3.069(8)	5
2.0	0.0665	0.528	9.0169(4)	2.3772(25)	3.073(6)	7.5
2.0	0.0665	0.703	9.02311(13)	2.3694(9)	3.1241(24)	10
2.0	0.0665	0.879	9.02605(11)	2.3712(9)	3.1307(24)	12.5
2.0	0.083	2.110	8.9476(6)	2.381(6)	2.871(11)	24.1
2.0	0.0999	2.814	9.0149(5)	2.3691(28)	3.171(9)	26.7
2.0	0.0999	3.517	9.0103(6)	2.3671(29)	3.167(9)	33.3
2.0	0.116	0.352	9.01337(25)	2.3682(18)	3.095(4)	2.9
2.0	0.116	0.528	9.01260(13)	2.3667(10)	3.1086(24)	4.3
2.0	0.116	0.703	9.02063(11)	2.3655(8)	3.1213(21)	5.7
2.0	0.116	0.879	9.01834(10)	2.3644(8)	3.1247(19)	7.2

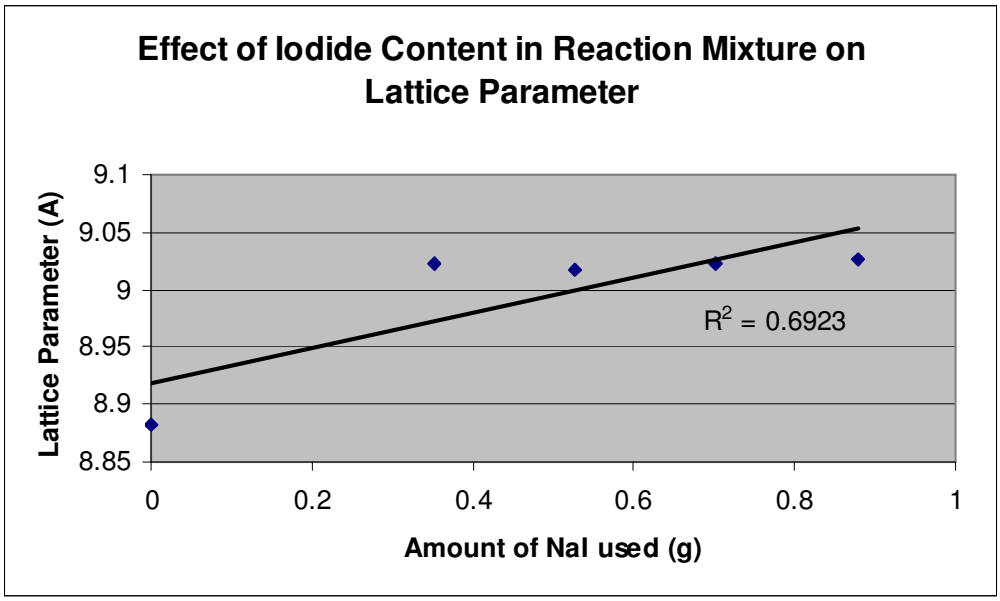

Fig 5.20 A graph showing the trend between amount of iodide present in the reaction mixture and the lattice parameter of the sodalite phase for a fixed weight of 0.0665g of sodium sulphate in the reaction mixture

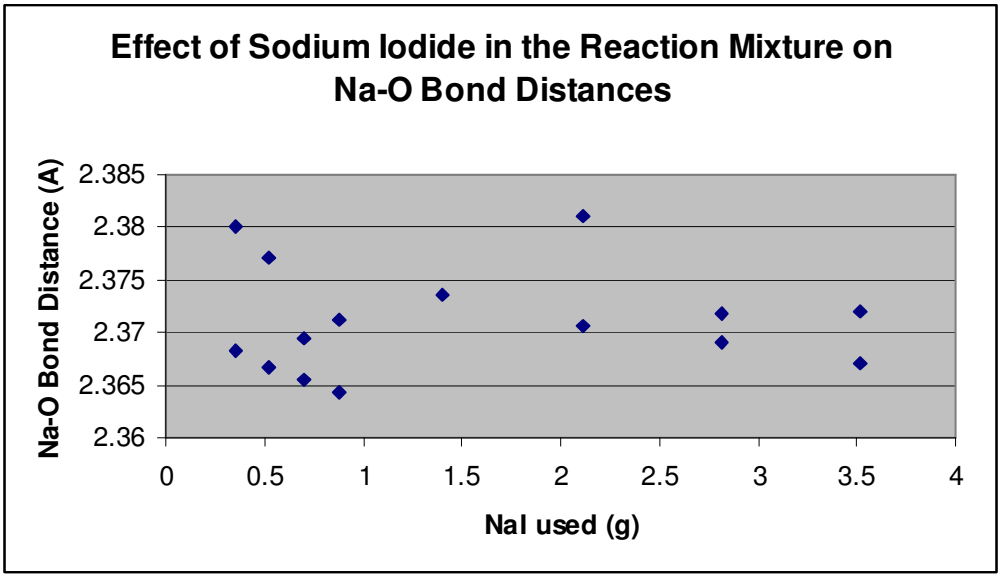

Fig 5.21 A graph showing the effect of increased amount of iodide in the reaction mixture on Na-O bond distances. The blue points show decreasing bond lengths for addition of Iodide. The pink points show increased impurities for higher amounts of iodide used.

The trend observed here is less clear than for the bromide example above, although there seems to be a reduction in Na-O bond distances upon addition of more iodide to the reaction mixture. This trend can be rationalized in a similar way to the example of bromide inclusion as both the reduced electronegativity and increased ionic radius of the iodide anion as compared to chloride result in a shortening of the Na-O bond distance.

The effect of iodide used in the reaction mixture on Na-X bond distances was also examined.

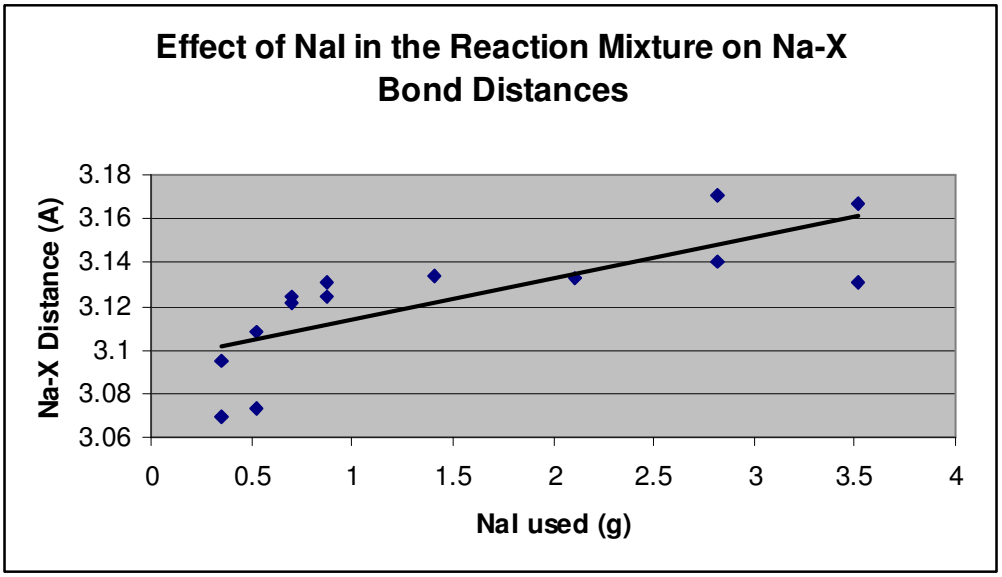

Fig 5.22 Showing the trend between the amount of iodide present in the reaction mixture and Na-X bond distances

As with both the previous examples of chloride and bromide, an increased presence of iodide in the reaction mixture leads to an increase in Na-X bond distances. Again, the data for amount of NaI used have a greater Na-X bond distance than either the corresponding NaCl or NaBr data set. As the ionic radius of iodide is even larger, it has a greater impact on the framework, forcing the beta cages to expand further than with chloride or bromide. These iodide containing sodalite are blue upon tenebresence at 254nm, and this colour change could be due to the change in environment, and hence energy level, of any f-centres located at defects on the iodide sites.

All the phases were also screened for photochromic activity using an ultraviolet light source capable of switching between 254 and 365nm wavelengths. All the phases containing sodium and iodide displayed activity at 254nm but not at 365nm. The phases changed from white to blue upon an exposure time of around 30 seconds. The phases then bleached back to the white state when left under white light over a period of about 30 minutes. This colour change was found to be completely reversible after multiple exposures to UV radiation and samples continued to display reversible photochromism after 100 separate exposures.

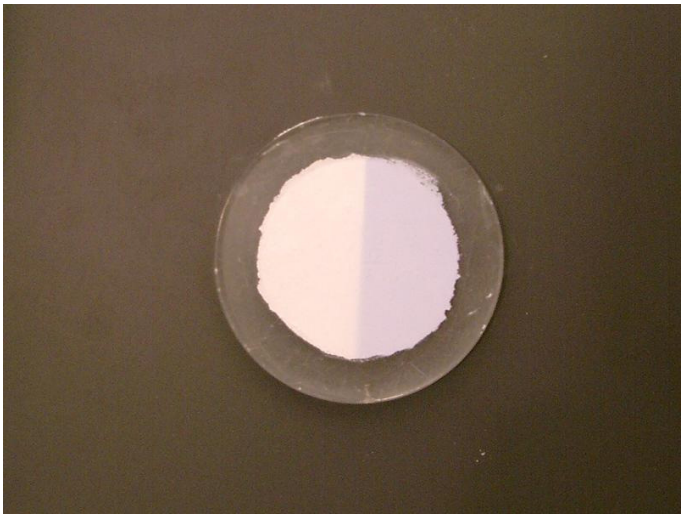

Fig 5.23 A photograph of a sodium iodide containing hackmanite exposed to 254 nm UV radiation showing a distinct colour change from white to blue

5.13 Structural Considerations

The increase in lattice parameter for these sodalite systems upon inclusion of greater amounts of halide, in particular the larger bromine and iodine, is to be expected. The decrease in Na-O bond lengths is explained by the decreased electronegativity down the halide group, combined with an increase in ionic radius both forcing the framework oxygen closer to the sodium. Ionic radii for non framework anions and cations relevant to this work are summarised in the table below.

Table 5.7 Ionic Radii of relevant ions

Ion	Charge	Coordination	Ionic Radius (A)
Cl	-1	VI	1.81
Br	-1	VI	1.96
I	-1	VI	2.20
Li	1	VI	0.76
Na	1	VI	1.02
K	1	VI	1.38
Rb	1	VI	1.52
Cs	1	VI	1.67
S	-2	VI	1.84

Perhaps more surprising than the structural changes for greater levels of halide inclusion was the effect of these structural changes on the observed optical property of the materials. There seemed to be no correlation between the optical property and the amount of sulphur or halide present in the structure, for example adding more sulphur or chlorine to the non framework had limited if any effect on the colouration of the sodalite upon tenebrescence or the colouration time or bleaching time of the sample. This implies that the mechanism of tenebrescence also relies upon other factors, for example the number of defects or vacant sites within the framework.

Interestingly, it was found that variation of the particular halide used had a dramatic effect on the observed tenebresence. By using different halides the colour change observed could be tailored to some degree. Larger halide inclusion tended toward a decrease in wavelength of the observed colour. Physically this manifests as a pink colour change for chlorine inclusion, a purple colouration for bromide inclusion and a blue colour change for iodine inclusion.

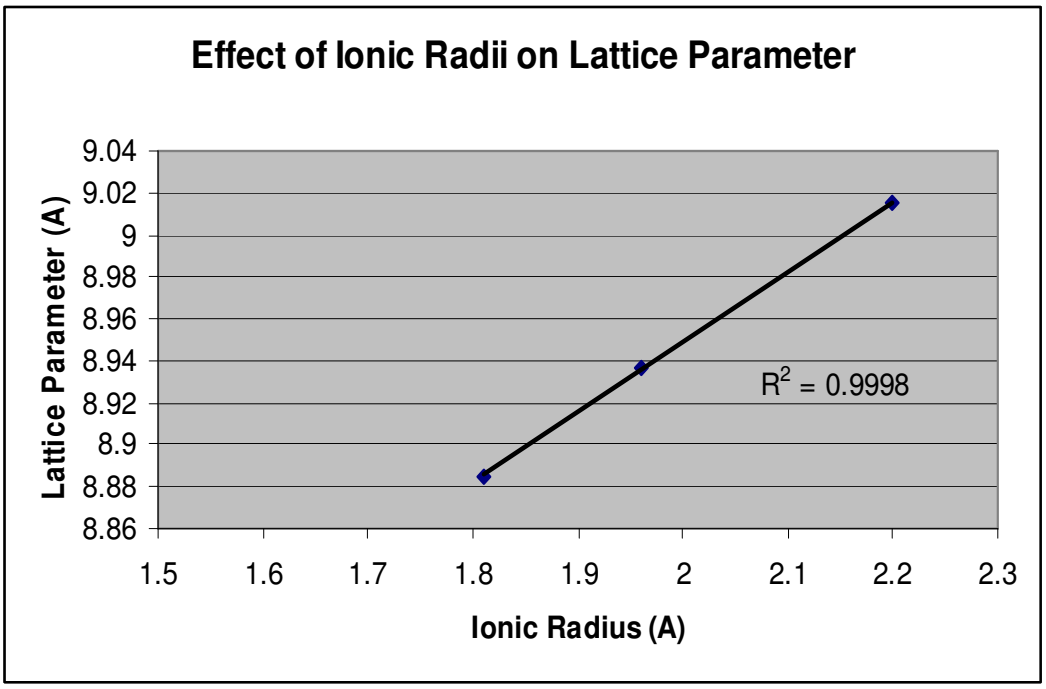

Fig 5.24 A graph showing the effect of ionic radius of included halogen on the lattice parameter of the sodalite system

The observed colouration upon tenebresence correlates to the difference in energy between the conduction band of the sample and the colour centres or f centres within the framework as shown in figure 5.2. It is possible that inclusion of larger halides such as bromine or iodine decreases the energy level of the colour centres leaving a larger energy difference between the conduction band and the colour centre.

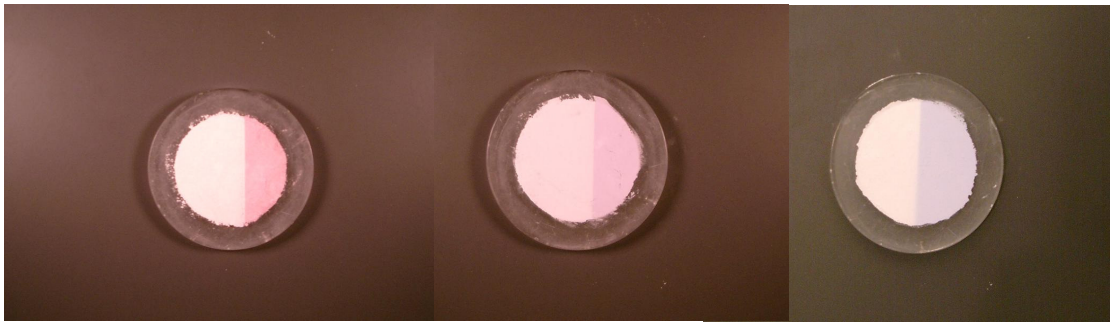

Fig 5.25 Photographs showing the various colour changes of sodalites upon exposure to 254nm UV radiation – From left to right containing chlorine, bromine and iodine

To this effect the colour of these synthetic hackmanites can be tailored by altering the energy difference between the colour centres and the conduction band. This allows access to colours of tenebrescence not displayed naturally by mineral samples of hackmanite, which are rich in chlorine.

5.14 Potassium Substitutions

With the results of the previous halide inclusion work above in mind, the inclusion of other non-framework cations was explored for the sodalite system. This would be achieved initially by using a different metal salt in the reduction stage of the synthesis to replace some of the non-framework sodium with potassium. It was hoped that the observed optical properties of the system could be further tailored in this way.

2g of zeolite A was ground and intimately mixed with varying amounts of potassium chloride (BDH 99.5%) and sodium sulphate (INC 99%) using a pestle and mortar. These reaction mixtures were then transferred into alumina crucibles, which were then placed inside a tube furnace. The furnace was then flushed with a mildly reducing gas mixture of 5% hydrogen in nitrogen for a period of 30 minutes. Next, the reaction was heated to 650 °C for 16 hours under flowing gas of 5% hydrogen in nitrogen. The product was then allowed to cool under the same gas mixture before being recovered, washed thoroughly with distilled water and dried in a drying oven.

Neutron diffraction data were collected for the potassium doped sodalite phases. Structural refinements of the sodalite compound library were performed using the Reitveld method. The sodalite phase was modeled in the space group P-43n using the GSAS program. Results of the Reitveld refinements are summarised below.

Table 5.8 Showing the variation in lattice parameter and average M-O bond distance of the sodalite system for varying amounts of sulphur and potassium chloride in the reaction mixture

Zeolite A (g)	**Sodium Sulphate (g)**	**Potassium Chloride (g)**	**Lattice Parameter (Å)**	**M-O distance (Å)**	**M-X distance (Å)**	**Salt/S molar ratio**
2.0	0.05	0.175	8.9193(5)	2.405(5)	2.744(11)	6.7
2.0	0.05	0.262	8.95234(25)	2.4001(24)	2.835(5)	10
2.0	0.05	0.350	8.9144(10)	2.417(10)	2.721(20)	13.3
2.0	0.05	0.437	8.9375(5)	2.375(4)	2.853(8)	16.7
2.0	0.0665	0.175	8.93291(29)	2.3926(32)	2.797(7)	5
2.0	0.0665	0.350	8.94793(21)	2.4018(22)	2.826(5)	10
2.0	0.0665	0.350	8.95536(20)	2.4067(22)	2.835(5)	10
2.0	0.083	0.175	8.9206(5)	2.409(6)	2.734(12)	4
2.0	0.083	0.262	8.95316(23)	2.4014(24)	2.834(5)	6
2.0	0.083	0.350	8.96017(23)	2.4026(23)	2.848(5)	8
2.0	0.083	0.437	8.94586(29)	2.3961(28)	2.833(6)	10
2.0	0.0999	0.437	8.94221(30)	2.3919(24)	2.830(6)	6.3
2.0	0.116	0.175	8.92639(34)	2.398(4)	2.767(8)	2.9
2.0	0.116	0.437	8.94685(31)	2.3882(28)	2.847(6)	7.2

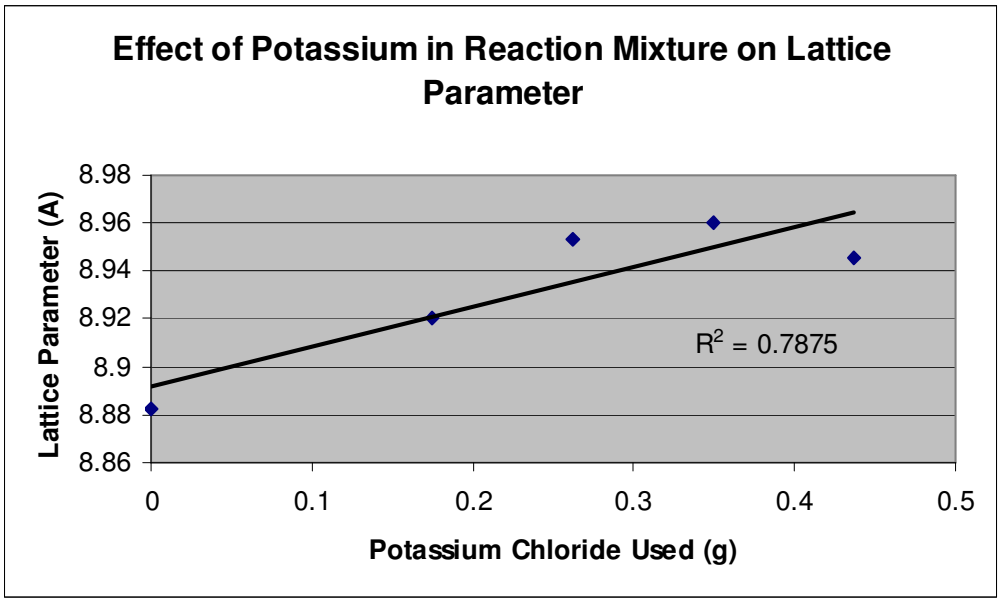

Fig 5.26 A graph showing the effect of the amount of potassium used in the reaction mixture on the lattice parameter of the sodalite system for a fixed weight of 0.083g of sodium sulphate in the reaction mixture

The first observation from the potassium doped phases is that the lattice parameters are generally larger than for the sodium chloride containing sodalite phases. This implies that some potassium has been successfully doped into the system and caused the beta cages in the framework to be slightly stretched by the inclusion of potassium. Secondly, as with the inclusion of the larger halides, there is a general increase in the lattice parameter from increased potassium doping into the sodalite.

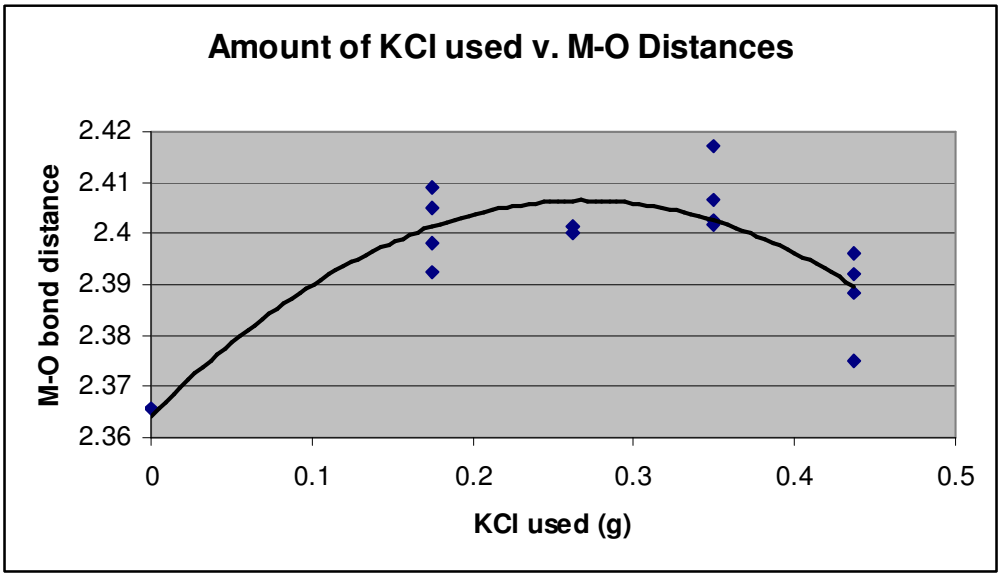

Fig 5.27 A graph showing the trend between amount of potassium used in the reaction mixture and the average M-O bond distance

Some points with anomalously large errors have been omitted from this graph due to large amounts of impurities in some of the samples.

In this example the increased use of potassium corresponds to the increased use of chloride at the anion site, because of the salt chosen (KCl). Fig. 5.26 shows that the trend of increased lattice parameter with increased potassium content does not continue for higher levels of potassium doping. It is apparent that the framework reaches a saturation point, after which no more potassium is substituted into the structure. This manifests as low level potassium impurities in the final sample, and hence no further increase in the lattice parameter.

The M-O bond distance can be seen to generally increase upon increased inclusion of potassium in the system in Fig 5.27. In this case we have the reverse of the bromide doped system, whereby the M-O interaction is reduced resulting in an increase in the corresponding bond distance. At around 0.35g of KCl used in the synthesis this trend is observed to reverse, which is probably due to increased impurities in the system as it corresponds to the point at which the lattice parameter stops increasing in Fig 5.26.

Fig 5.28 Photograph showing the colour of tenebrescence of a sodalite containing chloride and potassium replacing some sodium in the structure

The colour change upon tenebrescence of the potassium doped sodalite is very similar to that of the pure sodium chloride sodalites outlined earlier. Although there is a small change in lattice parameter, and hence possibly a change in the energy difference between the conduction band and the colour centre, it is not enough to dramatically alter the observed colour change of the samples.

Any trends between the amount of potassium chloride used in the reaction mixture an the M-X bond distances were also examined.

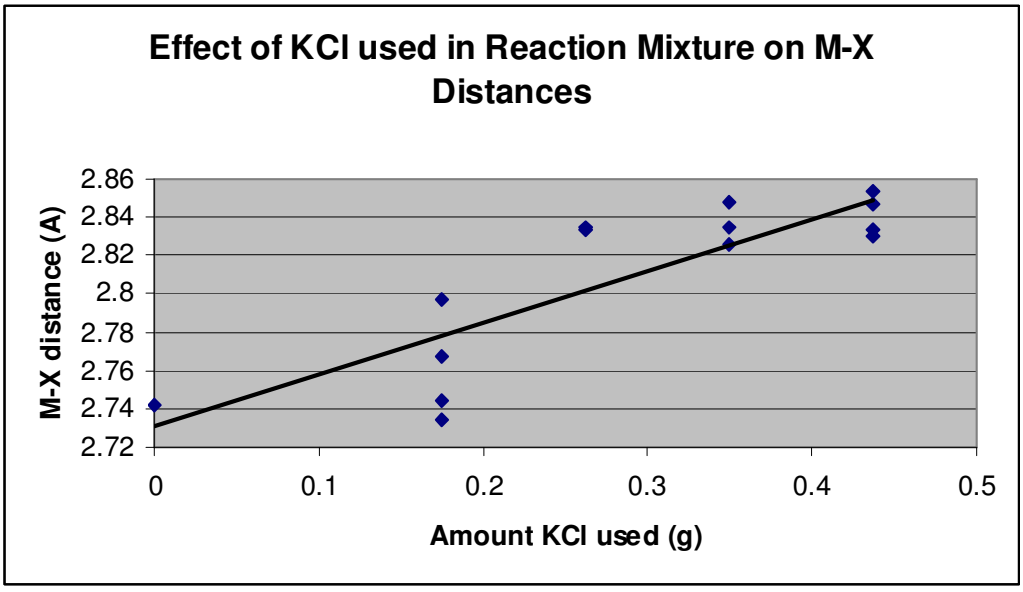

Fig 5.29 Showing the trend between the amount of potassium present in the reaction mixture and M-X bond distances

Fig 5.29 shows and increase in M-X bond distances upon increased use of KCl in the reaction mixture. The M-X distance is clearly seen to increase upon greater use of KCl in the mixture. The M-X distances for this data set are also greater than for the NaCl sodalites, showing that an increase in ionic radius on the cation site also has an effect on the M-X distance by a stretching of the beta cages. Any changes in bond length for potassium doping are not as pronounced as those for bromide doping, and the difference in colour of tenebresence is not altered as distinctly.

5.15 Potassium Bromide Substitutions

Experiments were undertaken to produce synthetic sodalites containing bromine and doped with a small amount of potassium. Again, it was hoped that changes in the structure could be used to tailor the effects of the optical property.

2g of zeolite A was ground and intimately mixed with varying amounts of potassium bromide (BDH 99.5%) and sodium sulphate (INC 99%) using a pestle and mortar. These reaction mixtures were then transferred into alumina crucibles, which were then placed inside a tube furnace. The furnace was then flushed with a mildly reducing gas mixture of 5% hydrogen in nitrogen for a period of 30 minutes. Next, the reaction was heated to 650 °C for 16 hours under flowing gas of 5% hydrogen in nitrogen. The product was then allowed to cool under the same gas mixture before being recovered, washed thoroughly with distilled water and dried in a drying oven.

Neutron diffraction data were collected for the potassium doped sodalite phases. Structural refinements of the sodalite compound library were performed using the Reitveld method. The sodalite phase was modeled in the space group P-43n using the GSAS program. Results of the Reitveld refinements are summarised below.

Table 5.9 Showing the variation in lattice parameter and average M-O bond distance of the sodalite system for varying amounts of sulphur and potassium bromide used in the reaction mixture

Zeolite A (g)	**Sodium Sulphate (g)**	**Potassium Bromide (g)**	**Lattice Parameter (Å)**	**M-O distance (Å)**	**M-X distance (Å)**	**Salt/S molar ratio**
2.0	0.0665	0.279	9.01677(16)	2.4111(13)	2.9752(27)	5
2.0	0.0665	0.419	9.00770(16)	2.4063(12)	2.9694(26)	7.5
2.0	0.0665	0.558	8.99453(24)	2.3929(19)	2.953(4)	10
2.0	0.0665	0.698	9.00453(20)	2.3972(15)	2.9739(30)	12.5
2.0	0.083	0.558	9.01155(18)	2.4069(15)	2.9772(30)	8
2.0	0.0999	0.419	9.01176(16)	2.4083(12)	2.9713(26)	5.1
2.0	0.0999	0.698	9.01016(16)	2.4047(13)	2.9777(27)	8.3
2.0	0.116	0.279	8.98432(27)	2.3872(24)	2.946(5)	2.9
2.0	0.116	0.279	9.01046(17)	2.4016(13)	2.9800(27)	2.9
2.0	0.116	0.419	8.99982(20)	2.3971(17)	2.9604(34)	4.3
2.0	0.116	0.558	9.01489(17)	2.4094(14)	2.9763(28)	5.7
2.0	0.116	0.698	9.00841(16)	2.4082(12)	2.9727(26)	7.2

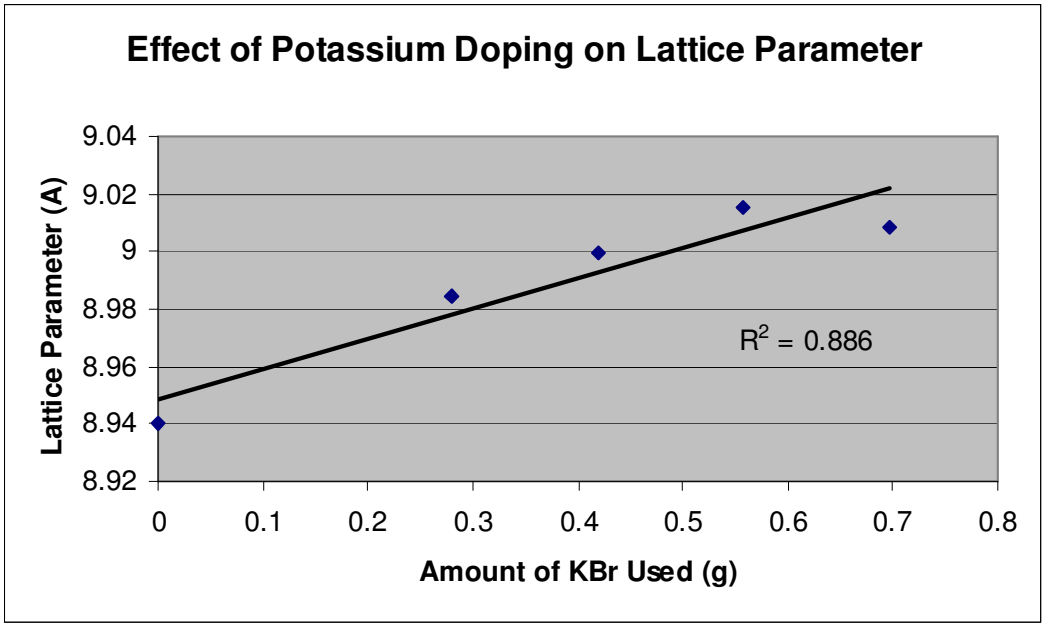

Fig 5.30 A graph showing the effect of potassium bromide content in the reaction mixture on the lattice parameter of the sodalite system

As with the chloride example the potassium bromide containing sodalites have significantly larger lattice parameters than their sodium bromide analogues. This translates to lattice parameters of roughly 9.00Å as compared to roughly 8.94Å for the sodium examples. This increase in lattice parameter implies a stretching of the overall framework and hence the successful inclusion of potassium in the framework. The lattice parameters of these potassium bromide containing sodalites is closer to that of the sodium iodide containing sodalites, which can be seen to be roughly 9.02Å. The colour change upon tenebrescence observed for these systems seems to lie at a wavelength in between that of the sodium bromide and the sodium iodide sodalites, which would suggest that the mechanism of tenebresence relies on the overall structure of the system as well as the specific anions and cations included in the framework.

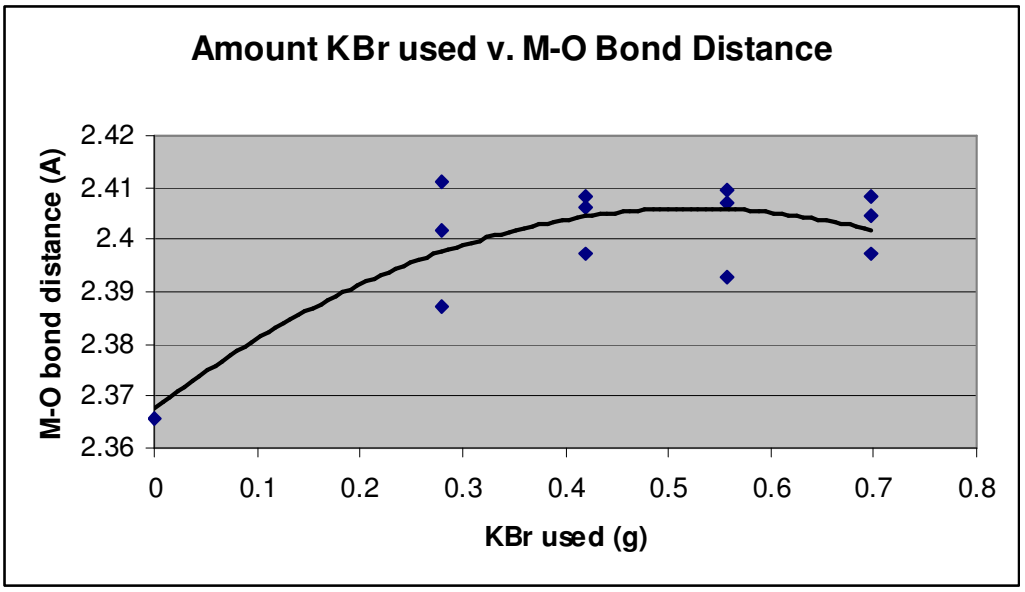

Fig 5.31 A graph showing the effect of KBr in the reaction mixture on M-O bond distances

One data set has been omitted from this plot, which possesses a very large error corresponding to large levels of impurity in the sample. This result set is unclear, although probably follows a similar trend as for the KCl system discussed above. The M-O bond distance is dramatically increased from a sodium and chloride containing sodalite, but after a small amount of potassium bromide doping the trend flattens and increases KBr content leads to no further increase in the M-O bond distance. This

could suggest that only a small amount of potassium bromide can be doped into the system before saturation. An alternative explanation for this trend is that both the metal-oxygen and the halide-oxygen interactions are reduced equally by the inclusion of KBr, resulting in no net movement of the oxygen position.

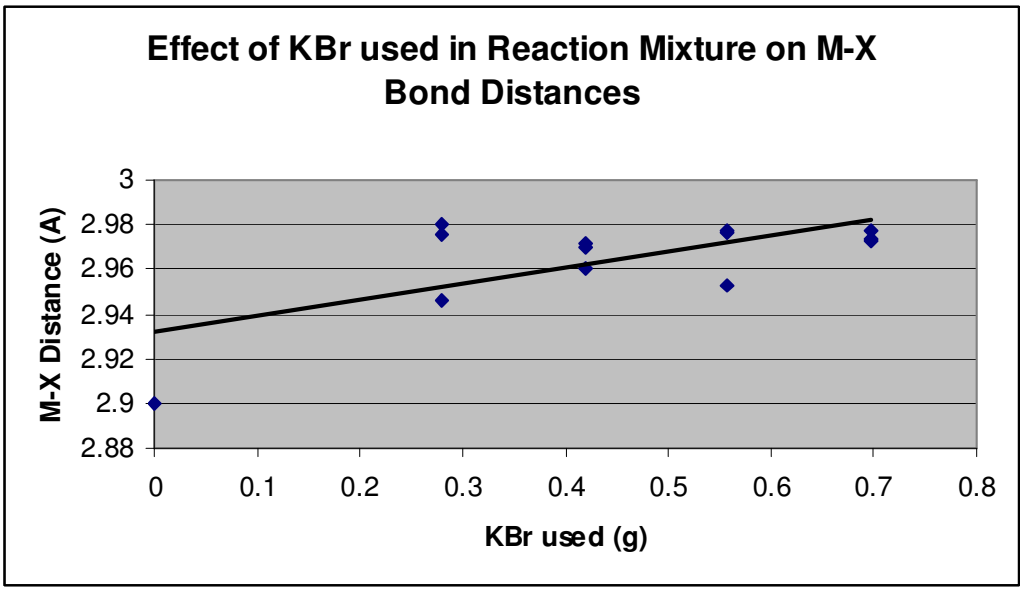

Fig 5.32 showing the effect of increasing the amount of KBr used in the reaction mixture on the M-X bond distance

As with all previous data sets an increased amount of KBr in the reaction mixture results in an increase in the M-X bond distance. The change to a larger cation seems to have a smaller effect on the bond distances than doping of a larger anion, and the bond distances for the KBr system are relatively close to those of the NaBr system. The colour of these systems upon tenebrescence is purple, whereas system with a much larger M-X distance, such as the NaI system exhibit a blue colour change.

5.16 Potassium Iodide Substitutions

Experiments were undertaken to produce synthetic sodalites containing iodine and doped with a small amount of potassium. Again, it was hoped that changes in the structure could be used to tailor the effects of the optical property.

2g of zeolite A was ground and intimately mixed with varying amounts of potassium iodide (Timstar 99%) and sodium sulphate (INC 99%) using a pestle and mortar. These reaction mixtures were then transferred into alumina crucibles, which were then placed inside a tube furnace. The furnace was then flushed with a mildly reducing gas mixture of 5% hydrogen in nitrogen for a period of 30 minutes. Next, the reaction was heated to 650 °C for 16 hours under flowing gas of 5% hydrogen in nitrogen. The product was then allowed to cool under the same gas mixture before being recovered, washed thoroughly with distilled water and dried in a drying oven.

Neutron diffraction data were collected for the potassium doped sodalite phases. Structural refinements of the sodalite compound library were performed using the Reitveld method[7,8]. The sodalite phase was modeled in the space group P-43n using the GSAS program[6]. Results of the Reitveld refinements are summarised below.

Table 5.10 Showing the variation in lattice parameter and average M-O bond distance of the sodalite system for varying amounts of sulphur and potassium iodide used in the reaction mixture

Zeolite A (g)	**Sodium Sulphate (g)**	**Potassium Iodide (g)**	**Lattice Parameter (Å)**	**M-O distance (Å)**	**M-X distance (Å)**	**Salt/S molar ratio**
2.0	0.05	0.399	9.0449(6)	2.427(6)	3.0073(34)	6.7
2.0	0.05	0.779	9.0556(5)	2.417(4)	2.9851(27)	13.3
2.0	0.0665	0.399	9.0260(12)	2.609(19)	3.127(10)	5.1
2.0	0.0665	0.584	9.0466(6)	2.409(4)	2.9896(28)	7.5
2.0	0.0665	0.779	9.0316(11)	2.603(19)	3.118(10)	10
2.0	0.0665	0.974	9.04627(35)	2.3964(21)	2.9683(18)	12.5
2.0	0.083	0.779	9.07384(15)	2.4237(11)	2.9459(9)	8
2.0	0.083	0.974	9.05697(31)	2.4077(19)	2.9628(16)	10
2.0	0.0999	0.399	9.0292(8)	2.533(18)	3.075(9)	3.3
2.0	0.0999	0.584	9.0435(7)	2.414(6)	3.002(4)	5
2.0	0.0999	0.779	9.0409(10)	2.587(19)	3.100(10)	6.3
2.0	0.116	0.399	9.0286(7)	2.455(13)	3.037(6)	2.9
2.0	0.116	0.584	9.03957(26)	2.3871(17)	2.9715(15)	4.3
2.0	0.116	0.779	9.04313(29)	2.3896(17)	2.9659(15)	5.7
2.0	0.116	0.974	9.06306(31)	2.4098(15)	2.9493(13)	7.2

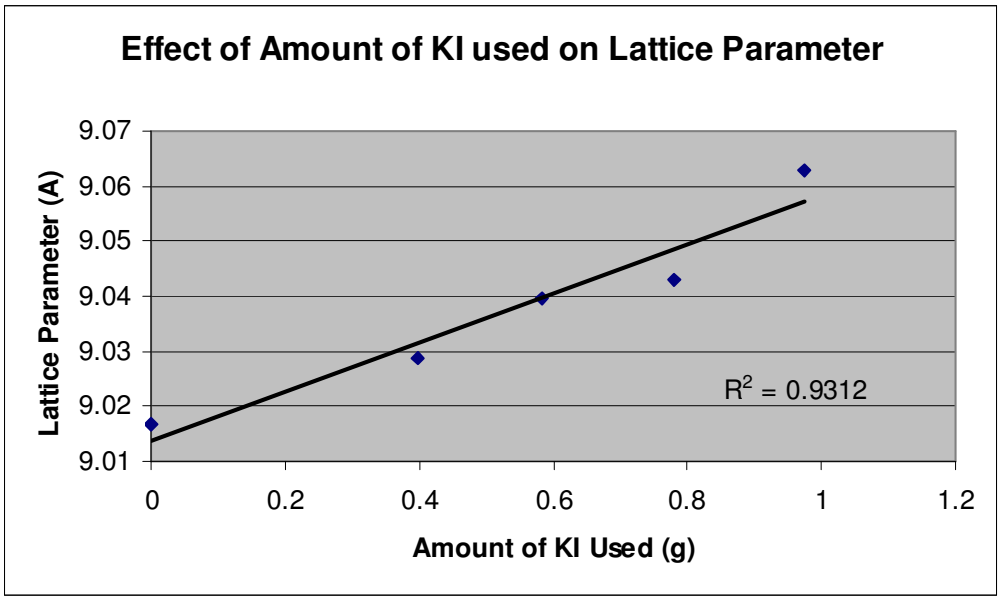

Fig 5.33 A graph showing the effect of the amount of potassium iodide in the reaction mixture on the lattice parameter of the sodalite system for a fixed weight of 0.116g sodium sulphate

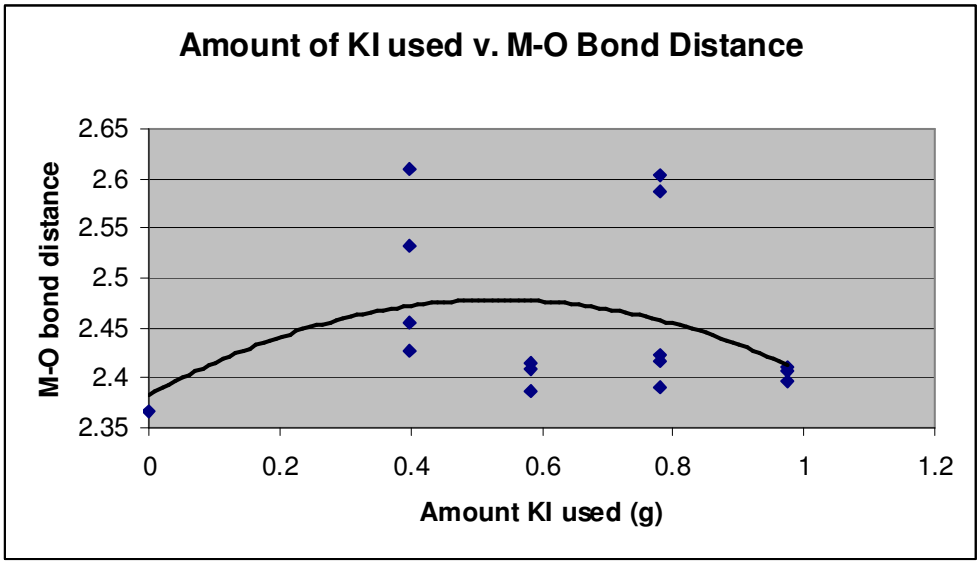

Fig 5.34 A graph showing the effect of KI in the reaction mixture on the average M-O bond distances

Data points with very large errors were omitted from this plot, as they probably contain large amounts of impurities. The inclusion of the larger anion results in a general increase in lattice parameter in this system. As with the other potassium systems there seems to be an increase in the M-O bond distances as the potassium halide is added, which then levels off, although the trend is less clear in this example. This is because the potassium iodide system has much larger errors than the other data sets corresponding to larger levels of impurities in the sample. It is clear from both Fig. 5.33 and Fig. 5.34 that some potassium iodide is successfully incorporated in the system, but the errors for this set make it unclear as to exactly how successful the substitution is.

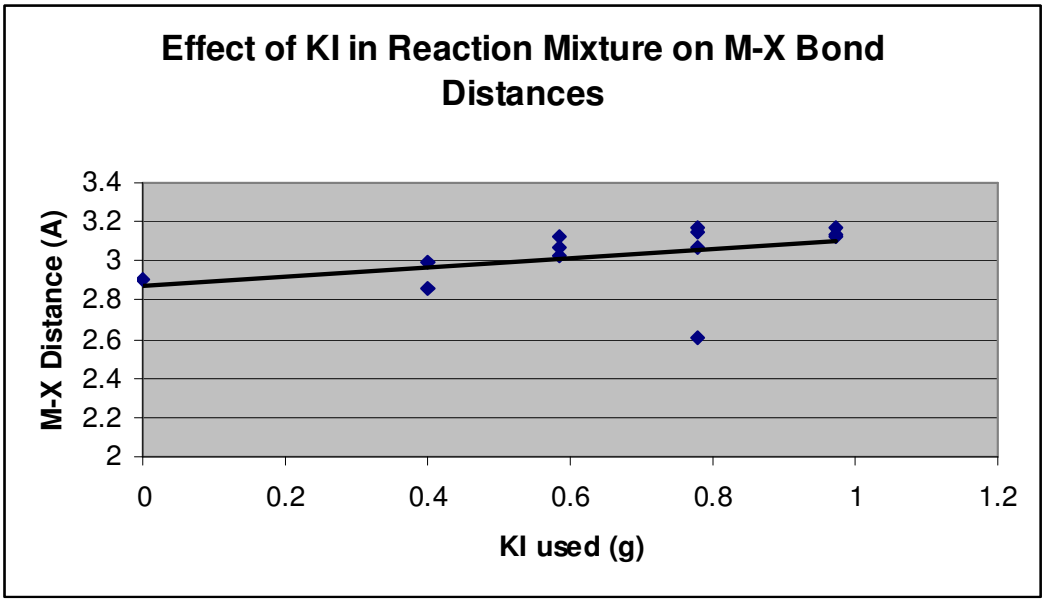

Fig 5.35 showing the effect of increasing the amount of KI used in the reaction mixture on the M-X bond distance

The relationship between M-X distance and amount of KI used in the reaction mixture was also examined, the results of which are shown above. Similar to previous examples a general increase in M-X bond distances is observed for greater masses of KI attributable to the beta cage expanding to accommodate the larger anion and cation, although the effect is less pronounced as in the previous series. These samples have the largest M-X bond distances of all the systems studied. The M-X bond distances of this system are most comparable to the NaI sodalite, with iodide inclusion

having the most pronounced effect on these distances. Both the NaI and KI sodalites exhibit a blue colour change upon tenebresence.

5.17 Other Non Framework Substitutions

It has been clearly seen from the work in this chapter that synthetic hackmanites derived from the sodalite framework can be successfully produced, and that these hackmanites display reversible photochromism, or tenebrescence upon exposure to UV radiation. It has also been observed that the observed colour of photochromism can be tailored by substitution of the non-framework ion in the structure, which also affects the structure and lattice parameter of the phase.

With these results in mind other syntheses were attempted using different metal salts to further tailor the optical property. Synthesis in this section are limited to the availability of a group I metal salt in the solid state, as the syntheses are high temperature solid state reactions.

5.17.1 Rubidium Chloride

2g of zeolite A was ground and intimately mixed with varying amounts of rubidium chloride (Aldrich 99.8%) and sodium sulphate (INC 99%) using a pestle and mortar. These reaction mixtures were then heated to 650 °C for 16 hours under flowing gas of 5% hydrogen in nitrogen. The product was then allowed to cool under the same gas mixture before being recovered, washed thoroughly with distilled water and dried in a drying oven.

Neutron diffraction data were collected for the rubidium doped sodalite phases. Structural refinements of the sodalite compound library were performed using the Reitveld method. The sodalite phase was modeled in the space group P-43n using the GSAS program. Results of the Reitveld refinements are summarised below.

Table 5.11 Showing the variation in lattice parameter and average M-O bond distance of the sodalite system for varying amounts of sulphur and rubidium chloride used in the reaction mixture

Zeolite A (g)	**Sodium Sulphate (g)**	**Rubidium Chloride (g)**	**Lattice Parameter (Å)**	**M-O distance (Å)**	**M-X distance (Å)**	**Salt/S molar ratio**
2.0	0.0665	0.333	8.884(4)	2.339(18)	2.770(35)	5.9
2.0	0.0665	0.666	8.8882(5)	2.336(5)	2.788(9)	11.8
2.0	0.0665	0.833	8.8852(7)	2.332(7)	2.783(13)	14.7
2.0	0.083	0.333	8.8966(4)	2.368(4)	2.758(8)	4.7
2.0	0.083	0.666	8.8903(5)	2.340(5)	2.782(9)	9.4
2.0	0.083	0.833	8.8875(7)	2.328(7)	2.788(13)	11.8
2.0	0.0999	0.666	8.8865(6)	2.336(5)	2.783(10)	7.8
2.0	0.116	0.5	8.9096(13)	2.354(9)	2.762(17)	5.1
2.0	0.116	0.666	8.9095(19)	2.350(14)	2.762(26)	6.7
2.0	0.116	0.833	8.9146(31)	2.315(15)	2.759(25)	8.4

The structures and lattice parameters are similar to the sodium chloride analogues and display the same colour upon tenebrescence. It is unclear as to whether any rubidium substitution has taken place for these syntheses and the optical property remains unaltered by the attempted substitution.

5.17.2 Caesium Bromide

2g of zeolite A was ground and intimately mixed with varying amounts of caesium bromide (Aldrich 99.5%) and sodium sulphate (INC 99%) using a pestle and mortar. These reaction mixtures were then heated to 650 °C for 16 hours under flowing gas of 5% hydrogen in nitrogen. The product was then allowed to cool under the same gas mixture before being recovered, washed thoroughly with distilled water and dried in a drying oven.

Neutron diffraction data were collected for the caesium bromide doped sodalite phases. Structural refinements of the sodalite compound library were performed using the Reitveld method. The sodalite phase was modeled in the space group P-43n using the GSAS program. Results of the Reitveld refinements are summarised below.

Table 5.12 Showing the variation in lattice parameter and average M-O bond distance of the sodalite system for varying amounts of sulphur and caesium bromide used in the reaction mixture

Zeolite A (g)	**Sodium Sulphate (g)**	**Caesium Bromide (g)**	**Lattice Parameter (Å)**	**M-O distance (Å)**	**M-X distance (Å)**	**Salt/S molar ratio**
2.0	0.05	0.749	8.9382(13)	2.401(8)	2.831(17)	10
2.0	0.05	1.250	8.9357(5)	2.367(5)	2.880(10)	16.7
2.0	0.0665	0.749	8.9397(5)	2.368(4)	2.811(9)	7.5
2.0	0.083	0.499	8.9413(5)	2.3372(5)	2.887(10)	4
2.0	0.0999	0.749	8.9380(9)	2.419(23)	2.77(5)	5
2.0	0.116	0.499	8.9481(5)	2.371(4)	2.886(9)	2.9
2.0	0.116	0.749	8.9475(5)	2.366(4)	2.889(9)	4.3
2.0	0.116	0.999	8.9412(6)	2.369(5)	2.883(10)	5.7

Again, the structures and lattice parameters are similar to the sodium bromide analogues. Upon tenebresence the caesium bromide containing sodalites exhibit a “bluer” colour change than their sodium bromide containing analogues. It would be expected that the beta cages would be further stretched and hence give a larger lattice parameter, but this is not apparent in this case.

5.18 Conclusions

A large compound library of reversibly photochromic sodalites has been successfully synthesized by collapsing zeolite A at high temperature in a mildly reductive atmosphere with sodium sulphate and various metal halide salts. It was found that the composition of the sodalite has a marked effect on the optical property, with various different colour changes being observed.

Mimicking natural samples containing sodium and chlorine, synthetic samples have been produced that display a stark white to pink colour change upon exposure to UV radiation. This was extended by introducing other halides and group 1 metals into the non-framework sites of the structure, which resulted in a dramatic change in the optical property. A purple colour change was observed when bromide was included in the framework, extending to a blue colour change upon iodide inclusion.

It was found that there was a correlation between the lattice parameters of the samples and the observed colour change, which could be tailored accordingly. Other tenebrescent hackmanites were successfully synthesised doping other metals into non-framework sites, namely potassium, rubidium and caesium.

5.19 References

[1] D. W. Breck, W. G. Eversole, R. M. Milton, T. B. Reed, T. L. Thomas, *J. Am. Chem. Soc.*, 1956, **78**, 5963

[2] O. I. Lee, *Am. Mineral.*, 1936 **21**, 764

[3] R. D. Kirk, *J. Electrochem. Soc.,* 1954, **101,** 461

[4] L. V. Bershov, V. O. Martirosya, A. N. Platon, A. N. Tarschan, *Neorganish. Mater.,* 1969, **5,** 1780

[5] W. D. Hodgson, J. S. Brinen, E. F. Williams, *J. Chem. Phys.,* 1967, **47,** 3719

[6] S. D. McLaughlan, D. J. Marshall, *Phys. Lett.,* 1970, **32A,** 343

[7] A. Hassib, O. Beckman, H. Annersten, *J. Phys. D.,* 1977, **10,** 771

[8] R. Allan, *Man. Mineral.,* 1834

[9] T. L. Walker, A. C. Parsons, *Univ. Toronto Studies, Geol. Series,* 1925, **20**, 5

[10] R. C. Peterson, *Can. Mineral.,* 1983, **21,** 549

[11] J. H. de Boer, *Rec. Trav. Chim. Pays-Bas*, 1937, **56**, 301

[12] D. B. Medved, *J. Chem. Phys.*, 1953, **21**, 1909

[13] R. D. Kirk, *J. Electrochem. Soc.,* 1954, **109**, 461

[14] A. C. Larson and R. B. Von Dreele, Generalized Structure Analysis System, MS-H805, Los Alamos, NM 87545, 1990

[15] H.M. Rietveld, *Acta Cryst*., 1967, **22**, 151

[16] H.M. Rietveld, *J. Appl. Cryst*., 1969, **2**, 65

Chapter 6
Framework Substitution of Sodalites: Gallium and Germanium

6.1 Introduction

The work in previous chapters has shown how structural variations can affect optical properties, such as colour, or more functional properties like the reversible photochromism seen in hackmanites. These optical properties can be tailored to some degree by altering the composition of the structure on non framework sites. This is clearly observed in the example of the hackmanite system where changing the non framework anions has a direct bearing on the wavelength of colour observed, ranging from pink for chloride, through purple for bromide, to blue for iodide inclusion.

The work in this chapter centred upon altering the framework atoms of the sodalites studied in previous chapters. Many zeolites, including sodalites, have known framework substitutions, in particular substitutions of aluminium for gallium[1] and silicon being replaced by germanium[2,3] are most prevalent. In these analogues the framework type is preserved. Most applications of such materials are as catalysts, an example of which being the use of gallium containing zeolites for the aromatization of propane[4,5].

Firstly, this work involved the attempted synthesis and characterisation of germanium and gallium analogues of sodalite. Secondly, attempts were made to produce a method of encapsulating sulphur chromophores into the beta cages of these sodalite analogues. It was hoped that reduction of these sulphur species would produce a new family of reversibly photochromic materials containing germanium and gallium on framework sites.

6.2 Synthesis of $Na_6[AlGeO_4]_6(H_2O)$

4.6g of sodium metagermanate (Aldrich 99%) was dissolved in 12.65g of deionised water in a polymethylpropylene beaker. This beaker was chosen over a normal glass beaker to assure that no silicon was introduced to the reaction via the reaction vessel. Next, 1.955g of hydrated alumina (Aldrich 99.9%) was added to the reaction mixture. The reaction was stirred and heated to 90 °C for a period of 5 days[6]. The white solid produced was recovered by filtration and washed thoroughly with deionised water

before being dried at 90 °C. Powder x-ray diffraction showed the product to be phase pure $Na_6[AlGeO_4]_6(H_2O)$, a hydrated sodalite framework type aluminogermanate with no silicon present.

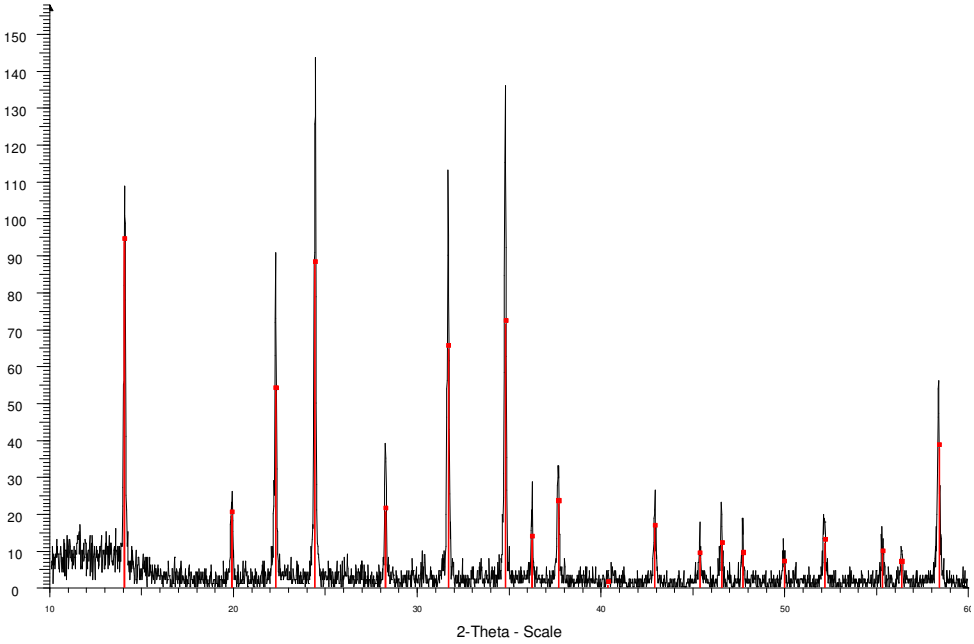

Fig 6.1 Diffraction pattern of the sodalite analogue $Na_6[AlGeO_4]_6(H_2O)$ with black lines showing the collected data and red lines showing the JCPDS pattern of $Na_6[AlGeO_4]_6(H_2O)$

6.3 Synthesis of $Na_6[GaSiO_4]_6(H_2O)$

1g of gallium oxide (Ga_2O_3) (Aldrich 99%) was added to 20ml of 6M sodium hydroxide (Fluka 97+%). To this was added 5.213 g of the sodium silicate $Na_2SiO_3.5H_2O$ (Fluka 97+%) and 6g of H_3BO_3 (Aldrich 99%)[7]. The reaction mixture was then loaded into a 45ml PTFE lined steel autoclave and placed in an oven. The reaction was heated to 90 °C for a period of 100 hours. After this time the white solid produced was recovered by filtration and washed thoroughly with deionised water before being dried at 90 °C. Powder x-ray diffraction showed the product to be phase pure $Na_6[GaSiO_4]_6(H_2O)$, an example of a gallosilicate of the sodalite framework type devoid of aluminium.

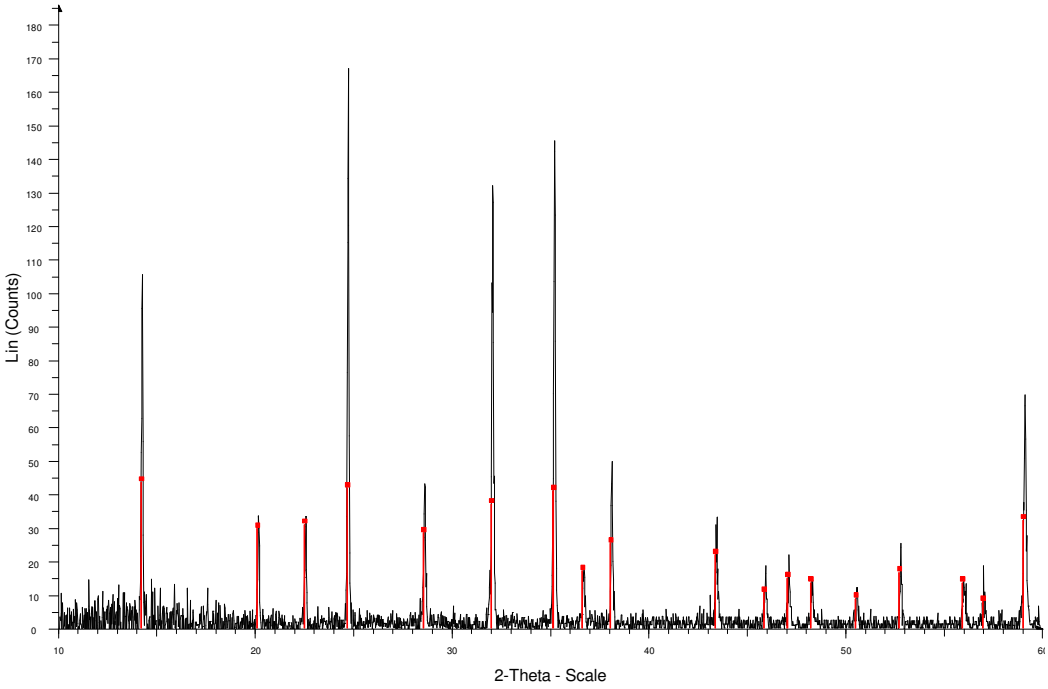

Fig 6.2 Diffraction pattern of the sodalite analogue $Na_6[GaSiO_4]_6(H_2O)$ with black lines showing the collected data and red lines showing the JCPDS pattern of $Na_6[GaSiO_4]_6(H_2O)$

6.4 Synthesis of $Na_6[GaGeO_4]_6(H_2O)$

$NaGaO_2$, Sodium gallate was first synthesised as a starting material. 0.849g of sodium carbonate (Aldrich 99%) was ground and intimately mixed with 1.503g of gallium oxide, Ga_2O_3 (Aldrich 99%) using a pestle and mortar. The reaction mixture was then heated to 800 °C for a period of 48 hours. The resultant white powder was characterised by powder x-ray diffraction and found to be phase pure $NaGaO_2$.

The germanium source used for the synthesis of $Na_6[GaGeO_4]_6(H_2O)$ was sodium metagermanate, Na_2GeO_3, which was also synthesised by a high temperature solid state reaction. 3.04g of sodium carbonate (Aldrich 99%) was ground and intimately mixed with 3.00g of gallium (IV) oxide (Aldrich 99%). The reaction mixture was then heated to 800 °C for a period of 24 hours. The resultant white powder was characterised by powder x-ray diffraction and found to be phase pure Na_2GeO_3.

The gallium germinate sodalite analogue $Na_6[GaGeO_4]_6(H_2O)$ was synthesised using a gel method[8]. 1.39g of the previously prepared sodium gallate and 1.85g of the sodium metagermanate were added to 5ml of deionised water. 15g of sodium sulphate (INC 99%) were added and the reaction mixture was stirred and gently warmed (<60 °C) to form a gel. The gel was then loaded into a 23ml capacity PTFE lined steel autoclave and heated to 180 °C for 48 hours. After this period a white solid was recovered by filtration, which was then washed with deionised water to remove the excess sodium sulphate. The powder was dried thoroughly at 90 °C before being characterised by powder x-ray diffraction and was found to be phase pure $Na_6[GaGeO_4]_6(H_2O)$.

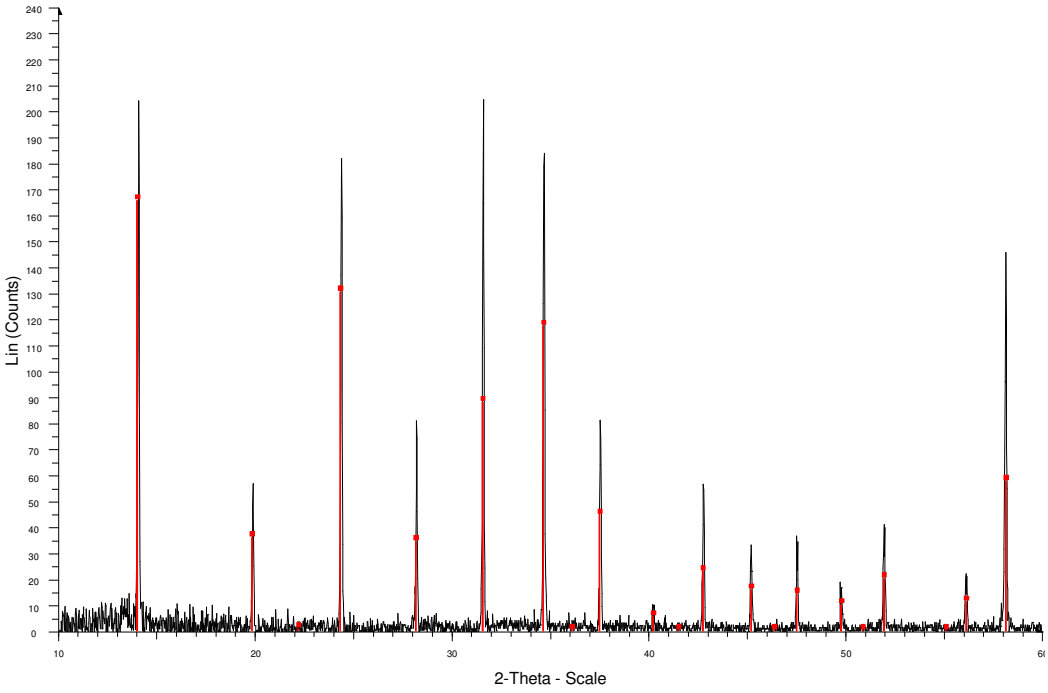

Fig 6.2 Diffraction pattern of the sodalite analogue $Na_6[GaGeO_4]_6(H_2O)$ with black lines showing the collected data and red lines showing the JCPDS pattern of $Na_6[GaGeO_4]_6(H_2O)$

6.5 Chromophore Inclusions

4.6g of sodium metagermanate was dissolved in 12.65g of deionised water in a polymethylpropylene beaker. 2.0g of sodium sulphate (INC 99%) was added to the reaction mixture. The reaction was then stirred and heated to 90 °C for a period of 5 days. The white solid produced was recovered by filtration and washed thoroughly with deionised water before being dried at 90 °C. Powder x-ray diffraction showed the product to be phase pure $Na_6[AlGeO_4]_6(H_2O)$, a hydrated sodalite framework type aluminogermanate with no silicon present. The product was then heated to 650 °C in a tube furnace under a flowing gas mixture of 5% hydrogen in nitrogen for a period of 18 hours. The resultant white solid showed no optical activity upon exposure to UV radiation and showed no sign of any sulphur inclusion by powder diffraction.

1g of gallium oxide (Ga_2O_3) was added to 20ml of 6M sodium hydroxide. To this was added 5.213 g of the sodium silicate $Na_2SiO_3.5H_2O$, 6g of H_3BO_3 and 2.0g of sodium sulphate (INC 99%). The reaction mixture was then loaded into a 45ml PTFE lined steel autoclave and placed in an oven. The reaction was heated to 90 °C for a period of 100 hours. After this time the white solid produced was recovered by filtration and washed thoroughly with deionised water before being dried at 90 °C. Powder x-ray diffraction showed the product to be $Na_6[GaSiO_4]_6(H_2O)$. The product was then heated to 650 °C in a tube furnace under a flowing gas mixture of 5% hydrogen in nitrogen for a period of 18 hours. The resultant white solid showed no optical activity upon exposure to UV radiation and showed no sign of any sulphur inclusion by powder diffraction.

Attempted synthesis of gallium and germanium analogues to the photochromic sodalites described in the previous chapter proved unsuccessful. It seems that the pore sizes in these analogues are unsuitable for supporting the slightly reduced sulphur chromophores responsible for reversible photochromism.

6.6 Other Sulphur Sources

Attempts were made to produce a tenebrescent sample containing gallium or germanium in the framework instead of aluminium and silicon. It was thought that interactions of the sulphur chromophores with these frameworks may have an effect on the optical property. A soluble sulphur source was used for the synthesis of such compounds, an example of which is outlined below.

4.6g of sodium metagermanate was dissolved in 12.65g of deionised water in a polymethylpropylene beaker and 1.955g of hydrated alumina was added to the reaction mixture. Next, 1g of elemental sulphur was dissolved in a solution of 20%wt ammonium sulphide in water. The two solutions were combined and the reaction was stirred and heated to 90 °C for a period of 5 days. A pale green powder was produced which was then recovered by filtration and washed thoroughly with deionised water before being dried at 90 °C. Powder x-ray diffraction showed the product to possess the same structure as $Na_6[AlGeO_4]_6(H_2O)$. The product displayed no tenebresence at either 254 or 365nm and there was no evidence of sulphur incorporation into the lattice.

Attempts were made to reduce any sulphur that may have been present within the product outlined above. The powder was heated to 650 °C in a tube furnace under a flowing gas mixture of 5% hydrogen in nitrogen for a period of 18 hours. The resultant white solid showed no optical activity upon exposure to UV radiation. Similar attempts were made to include sulphur species in other gallium and germanium containing frameworks, but no optical activity was observed in any example.

6.7 References

[1] K. Suzuki, *Zeolites,* 1985, **5**, 11

[2] M. S. Perlmutt, L. T. Todd, E. F. Ferrell, *Mat. Res. Bull.,* 1974, **9**, 65

[3] X. H. Bu, P. Y. Feng, T. E. Grier, *J. Am. Chem. Soc.,* 1998, **120**, 13389

[4] M. Guisnat, N. S. Gnep, F. Alario, *Appl. Catal. A.,* 1992, **89**

[5] B. S. Kwak, W. M. H. Sachtler, *J. Catal.,* 1994, **145**, 456

[6] G. M. Johnson, Y. Lee, A. Tripathi, J. B. Parise, *Microp. and Mesop. Mat.*, 1999, **31**, 195

[7] Th. M. Gesing, *Z. Kristallogr.*, 2000, **215**, 510

[8] G. M. Johnson, P. J. Mead, M. T. Weller, *Microp. and Mesop. Mat.*, 2000, **38**, 445

Chapter 7

Other Frameworks : Kalborsite Type Frameworks

7.1 Introduction

Framework materials have applications in the encapsulation of small molecules and species with interesting optical properties. In the preceding chapters we have seen the vast diversity of materials with useful applications that can arise simply by trapping different species in a framework. The small species are stabilised by the framework and thus are able to exhibit interesting optical properties. For example, the sodalite framework that has been studied in detail in this thesis can produce many different coloured ultramarine pigments such as the very well known blue colour and variations including green, pink, red and violet[1-5]. These are achieved by encapsulating different oxidation states of sulphur clusters in the β-cages. These types of pigments are of great commercial interest as the sodalite framework is both chemically and thermally stable and the colours very vivid.

By manipulating the sulphur species trapped in the beta cages we have also seen that the optical properties can be tailored. In the hackmanite synthesis covered in chapter 4b in this work the same sodalite framework with a slightly reduced oxidation state of the sulphur species to the ultramarine pigments produces a tenebrescent material[6]. These are colourless materials that reversibly change colour to pink or purple upon exposure to UV light sources, a starkly different optical property to the ultramarine pigments.

With such diversity of optical properties in the area of pigment synthesis, the quest for novel frameworks is ongoing. With different framework morphologies the properties of such pigments might be improved, such as higher chemical or thermal stability, or improved colour properties due to the incorporation of an increased concentration of coloured species. Frameworks with different sized pores or channels can be utilised to include a wider variety of coloured species.

The work in this chapter will centre on the development and synthesis of another framework material, potentially suitable for producing inclusion materials with interesting optical properties.

7.2 Preparatory Synthesis of Leucite

A synthetic route was identified for the synthesis of $K_2Al_2Si_3O_{10}(KCl)$[7], an anhydrous zeolite type framework with edingtonite topology. The framework is not technically a zeolite, as it contains no adsorbed water molecules, but the pore sizes are of appropriate dimensions for incorporation of small species, making it relevant to this work. The synthetic route uses leucite, $KAl_2Si_2O_6$, as a starting material, which can be produced by ion exchange of analcime, the sodium analogue. This work attempted to reproduce this synthesis of the zeolite type phase and then introduce other alkali metal halides into the structure with view to creating new frameworks suitable as hosts for optically active species.

For formation of analcime for ion exchange 0.225g of aluminium powder (Aldrich 99.9%) was dissolved in 25ml of 2M sodium hydroxide (Fisher 97+%) solution and 1.0g of silica (Aldrich 99.9%) was then added to the reaction mixture. The reaction mixture was subsequently loaded into a 45ml capacity PTFE lined steel autoclave before being heated to 200 °C for times of up to 18 hours. The reaction vessel was allowed to cool to room temperature before the product was recovered by filtration and washed thoroughly with deionised water. The resulting white powder was characterised by powder X-ray diffraction in reference with the JCPDS database. The product was found to be phase-pure analcime.

To form the potassium analogue, leucite, an ion exchange experiment was performed. 5.0g of potassium chloride (BDH 99.5%) was dissolved in 25ml of deionised water and loaded into a 45ml capacity PTFE lined steel autoclave. 1.0g of analcime was ground and added to the salt solution before the autoclave was sealed and warmed to 90 °C for 18 hours. The resulting white solid was recovered by filtration and washed thoroughly with warm deionised water before being dried and characterised by powder X-ray diffraction in reference with the JCPDS database.

The product was found to be a mixture of analcime and successfully ion exchanged leucite. This product was then returned to a solution of 5.0g of potassium chloride (BDH 99.5%) in 25ml of deionised water and heated for 18 hours at 200 °C in a 45ml capacity PTFE lined steel autoclave. After recovering the product by filtration and washing the product was found to be a mixture of analcime, leucite and sodalite by powder x-ray diffraction in reference with the JCPDS database. It seems that heating the analcime at this elevated temperature starts to force the analcime into an extended framework.

To produce phase pure leucite a low temperature for a longer time was required. Finally 5.0g of potassium chloride (BDH 99.5%) was dissolved in 25ml of deionised water and loaded into a 45ml capacity PTFE lined steel autoclave. 1.0g of analcime was ground and added to the salt solution before the autoclave was sealed and warmed to 90 °C for 18 hours. The product was recovered from this reaction and then the process repeated until all the analcime was successfully transformed by ion exchange into leucite, as observed by powder x-ray diffraction. This process needed to be repeated between 5 and 7 times before complete conversion was observed, and complete conversion was not seen when performing one experiment for 7 days. This is because ion exchange only occurs at very high potassium concentration, which needs to be continually replenished as the ion exchange proceeds.

7.3 Synthesis of $K_2Al_2Si_3O_{10}(KCl)$

Synthesis of $K_2Al_2Si_3O_{10}(KCl)$ was attempted using the synthetic leucite produced above as a starting material. Following the method by Ghose et. al.[7], 1.0g of reaction mixture was prepared by grinding and intimately mixing 0.34g of synthetic leucite and 0.66g of a mixture containing 34 wt% KCl (BDH 99.5%), 23 wt% KF (BDH 97%) and 43 wt% K_2CO_3 (Aldrich 99%) in a pestle and mortar. A small portion of this reaction mixture (about 200mg) was then sealed in a capsule made of gold tubing by welding, taking care not to heat the reaction at this stage. The gold tubing was pre-treated by cleaning in dilute acid, and then heated at 600°C for about 16 hours. This softened the gold to facilitate arc-welding into a sealed capsule around the reactants. No water was added to the reaction and the starting materials were thoroughly dried

before use, although a small amount of adsorbed water may have been present in the starting materials.

Fig 7.1 The welding tool and an example of a gold capsule before being welded shut

The capsule was then transferred to a bomb, followed by addition of a steel spacer rod, which reduces the amount of water in the system under high pressure and limits the risk of explosions. Finally, the remainder of the bomb was filled with distilled water.

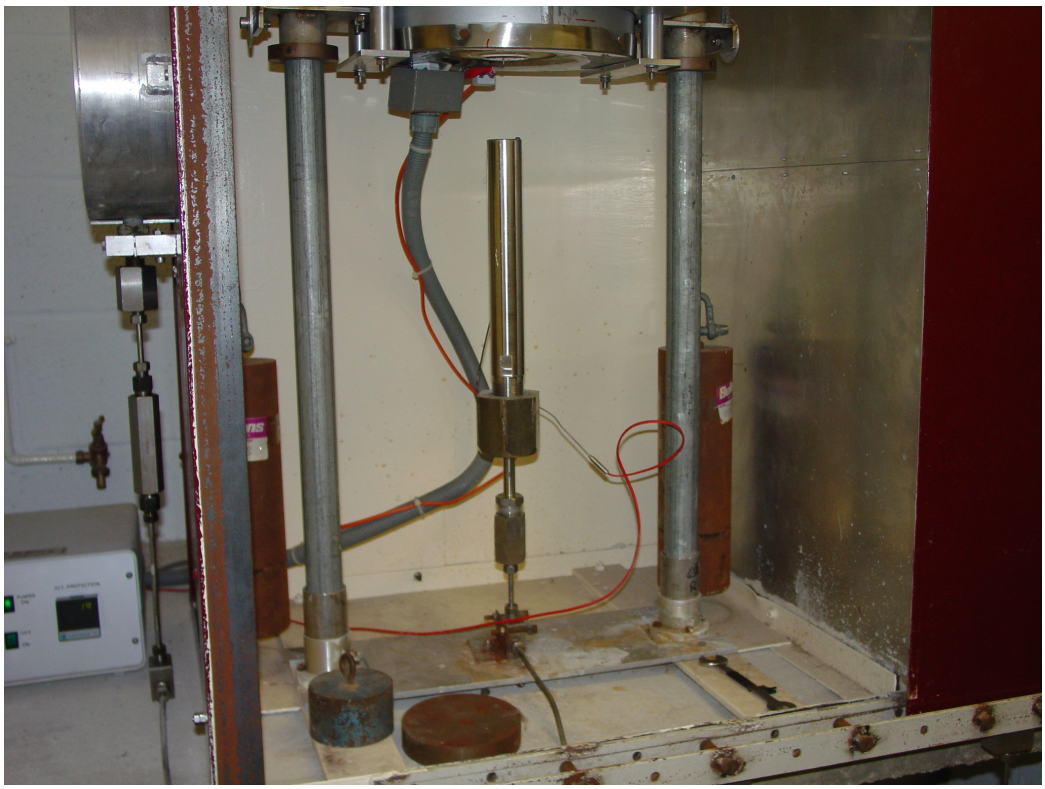

Fig. 7.2 Photograph of the hydrothermal rig showing the vertically mounted reaction vessel, reinforced furnace and steel safety cabinet

The assembled bomb was then mounted and secured onto the pump system, and sealed by pressurising a machined hardened steel cone onto the pressure line. A thermocouple was attached to the bomb and a vertically mounted tube furnace was pulled down over the reaction vessel. The extra thermocouple gives a more accurate reading of the temperature inside the reaction vessel than the furnace thermocouple. This assembly was housed in a steel cabinet with sliding door for safety reasons. The system was opened to a safety reservoir maintained at 1 kBar, whilst the reaction was heated to 570°C. The system was then isolated from the reservoir upon reaching the reaction temperature.

After this a hand pump was used to further pressurise the reaction chamber to 5000 psi, and the bomb was then isolated and left for 17 days for the reaction to proceed. After this period the reaction was then slowly cooled to room temperature over a period of 5 days. The reservoir was opened again while the apparatus cooled and the gold capsule was retrieved and opened.

The white solid was washed with deionised water and dried thoroughly before being identified by powder x-ray diffraction. The product was found not to be $K_2Al_2Si_3O_{10}(KCl)$, but a mixture of other potassium aluminosilicate phases, most prominently the mineral kalsilite, $KAlSiO_4$. It was speculated that the reaction conditions were of too low pressure and temperature to promote formation of the anhydrous framework $K_2Al_2Si_3O_{10}(KCl)$ and that a higher reaction temperature and corresponding pressure may force the formation of this structure.

With this in mind 0.2g of the leucite mixture used above was welded into another gold capsule. This was mounted in the reaction vessel in the same way described above. In this instance the reaction was heated to 670°C before the system was isolated from the reservoir. After this the hand pump was used to further pressurise the reaction chamber to 7000 psi, and the bomb was then isolated and left for 17 days for the reaction to proceed. After this period the reaction was then slowly cooled to room temperature over a period of 5 days. The product was the recovered from the gold capsule and washed thoroughly with deionised water.

Powder x-ray diffraction of the product showed a mixture of phases again. Predominantly, the desired phase $K_2Al_2Si_3O_{10}(KCl)$ had been formed although some impurity was present in the form of the $KAlSiO_4$ phase observed in the above experiment. Repetition of the experiment at more elevated temperatures and pressures produced this same mixture of phases. In the absence of a phase pure sample of $K_2Al_2Si_3O_{10}(KCl)$ it was decided to perform a 2-phase Rietveld refinement on the product using the GSAS program, modeling the impurity as well as the phase of interest. As only 50mg of product was acquired a low background sample holder was used. Data for the refinement was collected on a Siemens D5000 diffractometer between 5 and 110° for 48 hours.

7.4 Structural Refinement of $K_2Al_2Si_3O_{10}(KCl)$

Structural refinement of $K_2Al_2Si_3O_{10}(KCl)$ was carried out in the space group $P\text{-}42_1m$, using the structural model proposed by Ghose et. al[7]. The impurity phase kalsilite, $KAlSiO_4$ was modeled in the space group P31c. The refinement was carried out using the GSAS program. Initial stages of the refinement included all the instrument parameters (background, scale factor and peak shape parameters). The atomic parameters (atomic positions and temperature factors) of the predominant $K_2Al_2Si_3O_{10}(KCl)$ phase were then slowly introduced for all atoms. Next the atomic parameters (atomic positions and temperature factors) of the $KAlSiO_4$ phase were introduced to the refinement. The lattice parameters of the two phases were also introduced at this point, along with adding some additional background parameters. Finally, phase fractions of the two phases were allowed to vary.

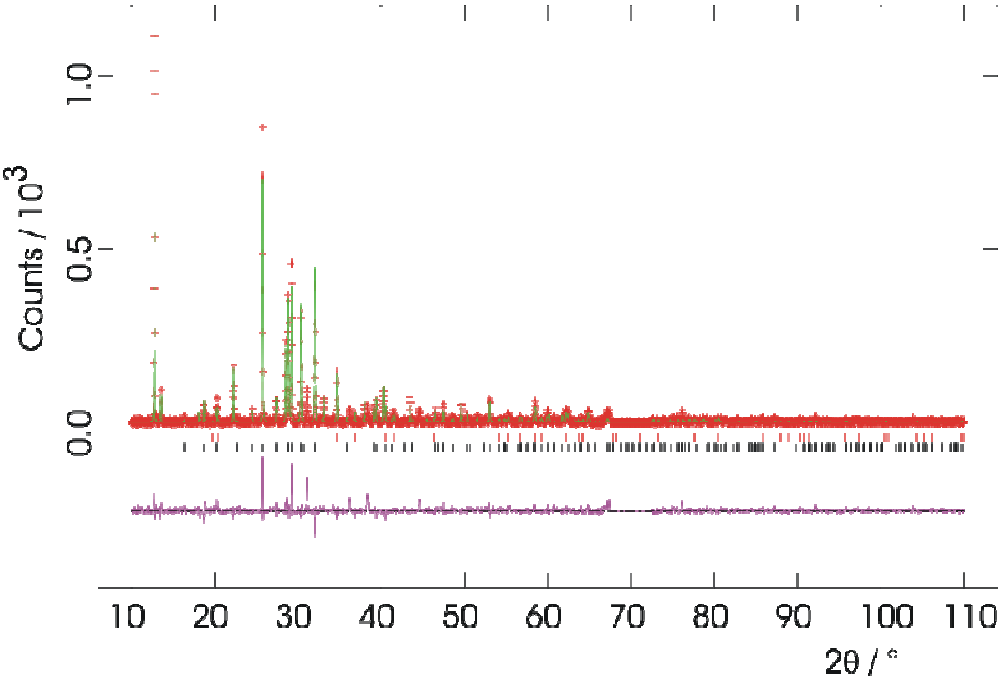

Fig 7.3 showing the 2 phase structural refinement of $K_2Al_2Si_3O_{10}(KCl)$ and $KAlSiO_4$, green line showing the data, red line showing the model and pink line showing the difference plot. Black tick marks $K_2Al_2Si_3O_{10}(KCl)$ and red tick marks $KAlSiO_4$

A portion of the data had to be omitted from the refinement, seen at around 70° 2θ, observed as a flat portion in both the data and the difference plot in figure 7.2. A plastic sample holder with appropriately low background at low angles was used for the data collection. This sample holder had a broad peak at around 70° 2θ, but was considered more useful for this experiment than one with a higher background at low angle. This is because of the volume of information present at low angles in zeolite type structures, which tend to have Bragg peaks below 20° 2θ because of the large repeating units found many zeolite and zeolite type frameworks. Details of the atomic positions, site occupancy and temperature factors for the $K_2Al_2Si_3O_{10}(KCl)$ phase are listed below.

Atom	**Site Occupancy**	**x**	**y**	**z**	**Uiso / Å^2**
T(1)	1	0	0	0	0.032
T(2)	1	0.1525(12)	0.1171(14)	0.6484(18)	0.050
Cl	1	1/2	0	0.091(5)	0.204
K(1)	1	1/2	0	0.5719(4)	0.181
K(2)	1	0.2534(11)	0.2466(11)	0.1257(19)	0.131
O(1)	1	0.2710(30)	0.2290(30)	0.575(5)	0.091
O(2)	1	0.0475(33)	0.1225(25)	0.461(5)	0.091
O(3)	1	0.0949(26)	0.1097(28)	0.8697(31)	0.091

Table 7.1 showing refined atomic coordinates and temperature factors for the anhydrous zeolite type phase $K_2Al_2Si_3O_{10}(KCl)$ T(1) = 20% AlO_4, 80% SiO_4, T(2) = 45% AlO_4, 55% SiO_4,

The tetragonal unit cell has lattice parameters a = 9.7488(41)Å and c = 6.4879(31)Å.

The atoms program was then used to produce a pictorial representation of the structure.

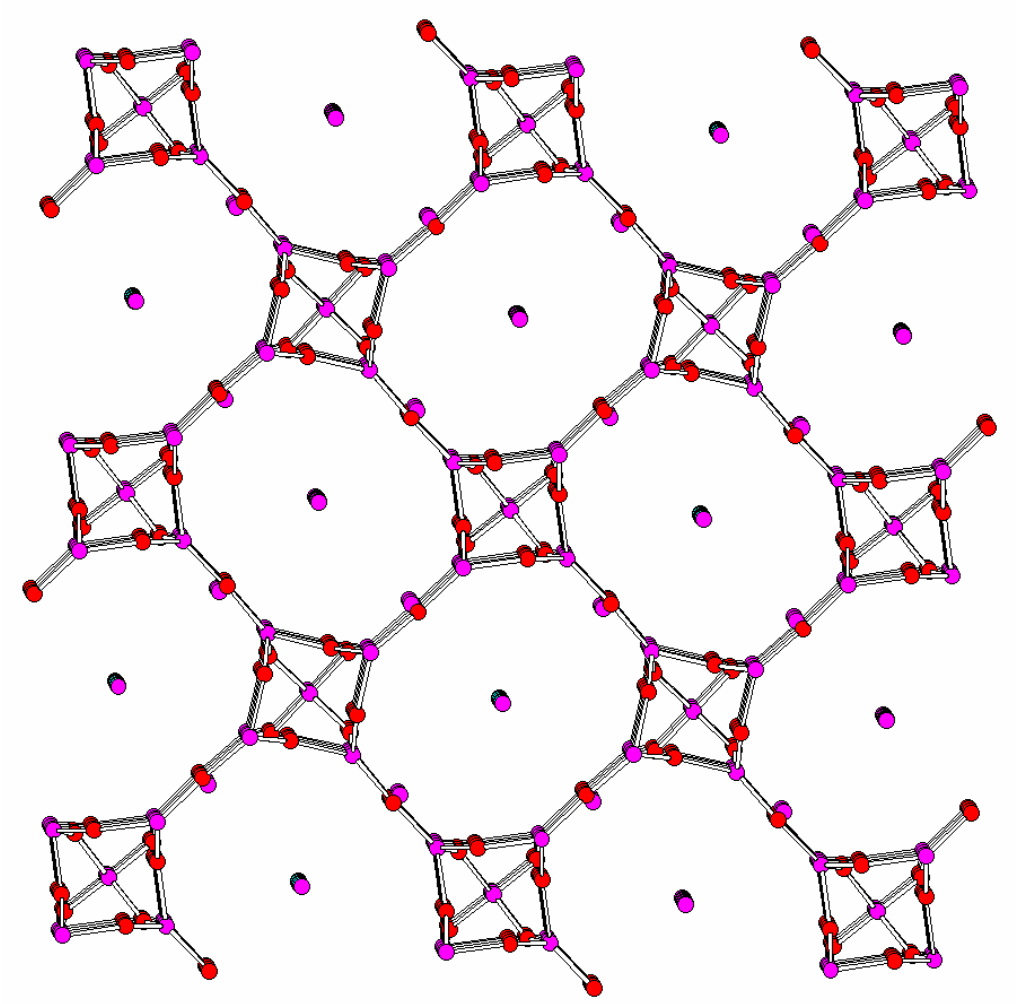

Fig 7.4 $K_2Al_2Si_3O_{10}(KCl)$ structure Al and Si atoms in pink, O atoms in red and K and Cl atoms in pink in the channels

7.5 Substitution of Other Salts into $K_2Al_2Si_3O_{10}(KCl)$

Substitution of other alkali metals and halides into the $K_2Al_2Si_3O_{10}(KCl)$ framework was investigated, working towards synthesising novel structures in the same edingtonite framework type. Phases of interest of which synthesis was to be attempted were $K_2Al_2Si_3O_{10}(KBr)$, $Rb_2Al_2Si_3O_{10}(RbCl)$ and $Rb_2Al_2Si_3O_{10}(RbBr)$. It was hoped that these phases could be synthesised using similar high temperature and pressure methods on the hydrothermal rig as yielded successful synthesis of the $K_2Al_2Si_3O_{10}(KCl)$ phase.

Firstly, as a precursor to forming the rubidium analogues of the $K_2Al_2Si_3O_{10}(KCl)$ phase, synthesis of the rubidium analogue of leucite, $RbAl_2Si_2O_6$ was performed. 5.0g of rubidium chloride was dissolved in 25ml of deionised water and loaded into a 45ml capacity PTFE lined steel autoclave. 1.0g of leucite was ground and added to the salt solution before the autoclave was sealed and warmed to 90 °C for 18 hours. The resulting white solid was recovered by filtration and washed thoroughly with warm deionised water. The solid was returned to a solution of 5.0g of rubidium chloride in 25ml of deionised water and the heating process was repeated several times. The product was again recovered and washed before being dried and characterised by powder x-ray diffraction in reference with the JCPDS database.

The product was found to be phase pure $RbAl_2Si_2O_6$ and thus the high pressure synthesis of $Rb_2Al_2Si_3O_{10}(RbCl)$ could be attempted using $RbAl_2Si_2O_6$ as a starting material. 0.2g of $RbAl_2Si_2O_6$ was ground and intimately mixed with 0.1g of RbCl, which was then welded into a heat softened gold capsule. The capsule was then transferred to a bomb, followed by addition of a steel spacer rod which was then filled with distilled water. The reaction was heated to 670°C before the system was isolated from the reservoir. After this the hand pump was used to further pressurise the reaction chamber to 7000 psi, and the bomb was then isolated and left for 17 days for the reaction to proceed. After this period the reaction was then slowly cooled to room temperature over a period of 5 days. The product was then recovered from the gold capsule and washed thoroughly with deionised water.

The product was found to be a mixture of phases, including the starting material, $RbAl_2Si_2O_6$ and a mixture of simple aluminosilicates. The reaction was repeated at various temperatures between 500°C and 750°C, with the resulting white products again found to be a mixture of $RbAl_2Si_2O_6$ and simple aluminosilicates. It is apparent that this edingtonite type framework is not flexible enough to encompass the larger rubidium ions over the smaller potassium ions. Potentially a higher pressure could be used to force this reaction to completion, but this is not available on the hydrothermal rig used here.

In a similar set of experiments synthesis of the bromide phase $K_2Al_2Si_3O_{10}$(KBr) was attempted on the high pressure hydrothermal rig. 1.0g of reaction mixture was prepared by grinding and intimately mixing 0.34g of synthetic leucite and 0.66g of a mixture containing 34 wt% KBr, 23 wt% KF and 43 wt% K_2CO_3 in a pestle and mortar. A small portion of this reaction mixture (about 200mg) was then sealed in a capsule made of heat treated softened gold tubing by welding. No water was added to the reaction and the starting materials were thoroughly dried before use, although a small amount of adsorbed water may have been present in the starting materials. The reaction was heated to 670°C before the system was isolated from the reservoir. After this the hand pump was used to further pressurise the reaction chamber to 7000 psi, and the bomb was then isolated and left for 17 days for the reaction to proceed. After this period the reaction was then slowly cooled to room temperature over a period of 5 days. The product was the recovered from the gold capsule and washed thoroughly with deionised water.

Again the reaction was unsuccessful, and was repeated at temperatures up to 750°C, with corresponding pressures of about 10000psi close to the limits of the instrument. The products were all found to be a mixture of leucite and other aluminosilicates, predominantly kalsilite, $KAlSiO_4$. Again it seems that the edingtonite framework is not flexible enough to accommodate these larger bromide ions at these pressures and further investigation at higher pressures is not achievable on this particular rig.

Consideration of the structure could explain why the inclusion of rubidium in the channels of the framework is not possible. The atoms program was used to produce a picture of the framework bond angles surrounding the potassium site in the $K_2Al_2Si_3O_{10}(KCl)$ structure.

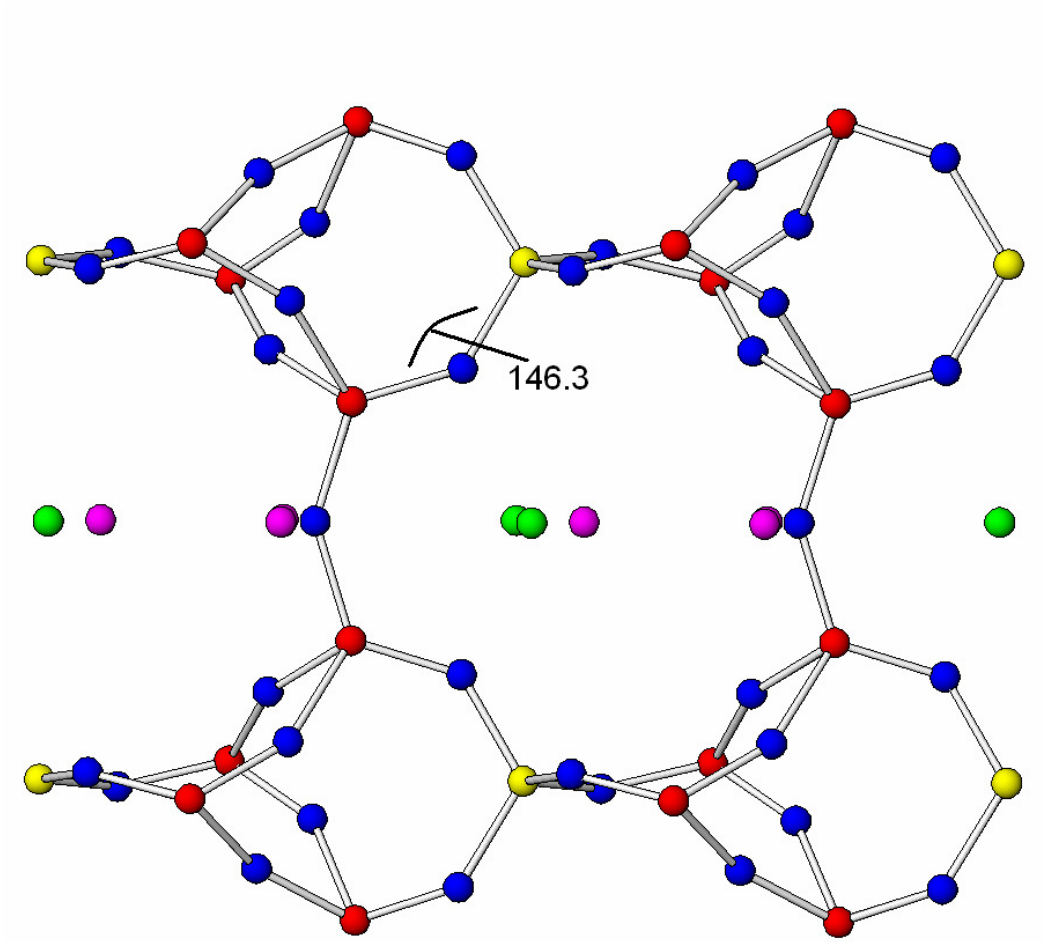

Fig 7.5 $K_2Al_2Si_3O_{10}(KCl)$ structure with Al and Si atoms in red and yellow, O atoms in blue and K and Cl atoms in pink and green in the channels

It can be seen from viewing the structure perpendicular to the axis of the long channels that the potassium site is contained within a buckled cavity with oxygen bridges of 146.3º pointing into the cavity. It is the presence of these oxygen atoms that hinder the inclusion of the larger rubidium ions in the framework. The aluminosilicate framework is not flexible enough to accommodate this larger ion, and thus the rubidium analogue of this system is not synthetically accessible.

7.6 Conclusions

Successful synthesis of the anhydrous zeolite type phase $K_2Al_2Si_3O_{10}(KCl)$ with edingtonite topology has been achieved using the high temperature, high pressure hydrothermal rig apparatus. The structure has been refined using the GSAS program in the space group $P\text{-}42_1m$ and the tetragonal unit cell was found to have refined lattice parameters of a = 9.7488 and c = 6.4879. The phase has been identified as a possible new framework type for use as a host for inclusion compounds. This could lead to formation of new pigments or photochromic compounds, by the inclusion of small optically active species in the framework.

Attempted synthesis of the analogous phases $Rb_2Al_2Si_3O_{10}(RbCl)$ and $K_2Al_2Si_3O_{10}(KBr)$ were found to be unsuccessful. It is thought that the larger rubidium and bromide ions are too large to fit in the relatively unflexible edingtonite framework. It is speculated that synthesis of these phases may be possible by using more forceful conditions at elevated pressures, but this is outside the specifications of the current instrumentation.

7.7 References

[1] R. J. H. Clark and M. L. Franks, *Chem. Phys. Lett*., 1971, **34(1)**, 69

[2] F. A. Cotton, J. B. Harmon and R. M. Hedges, *J. Am. Chem. Soc*., 1975, **98(6)**, 1417

[3] R .J. H. Clark and D. G. Cobbold, *Inorg. Chem.*, 1978, **17(11)**, 3169

[4] E. Podschus, U. Hofmann and K. Leschewski, *Z. Anorg. Allg. Chem.*, 1936 **228**, 305

[5] U. Hofmann, E. Herzensteil, E. Schoneman, K. H. Schwarz, *Z. Anorg. Allg. Chem*., 1969, **367**, 119

[6] O. I. Lee, *Am. Mineral.,* 1936*,* **21,** 764

[7] S. Ghose, H. X. Yang, J. R. Weidner, *Am. Mineral,* 1990, **75**, 947

Chapter 8
Investigation into Methods of Zeolite Film Deposition

8.1 Introduction

Zeolite films have many potential industrial applications, most of which centre around the porous nature of the zeolite framework[1-3]. Most simply the cavities and channels in these frameworks can be used to trap small molecules, for example water, leading to applications as molecular sieves. Zeolites can be used in this way to remove water from solvents to keep them dry. This principle can be extended further to zeolite films or membranes, which can be used to separate liquid or gas mixtures of very similar sizes[4]. With the vast array of known zeolite frameworks available a structure can be easily identified with the appropriate topology for the desired application. The zeolite will have internal dimensions favouring the passage of one gas over another, and thus allowing complete separation of the gas mixture.

The porosity of zeolite films and membranes makes them very versatile. As well as applications in separation, deposited films of zeolites are also used extensively in the gas sensor industry[5,6]. Again the application relies on small molecular species being adsorbed into the cavities and channels of the framework. The internal dimensions of the framework can be tailored to a specific gas to make the sensor device selective. The gases are then detected by the change in weight of the zeolite film with gas trapped inside. For this particular application a porous nanosized layer is preferable making for high sensitivity devices. Zeolites are also successfully employed in the catalyst industry[7].

The work in this chapter will investigate various methods of producing synthetic zeolite films with both mechanical and chemical deposition methods being explored. Potential routes will include depositing bulk zeolite samples onto substrates, or *in situ* synthesis of the zeolite on the substrate. These zeolite films will be characterised by SEM imaging and EDX and by powder x-ray diffraction. These films will be used for conversion into other zeolites, dye incorporation to form composites, or ultimately form the basis of a solid state array for high throughput type synthesis of zeolite compounds.

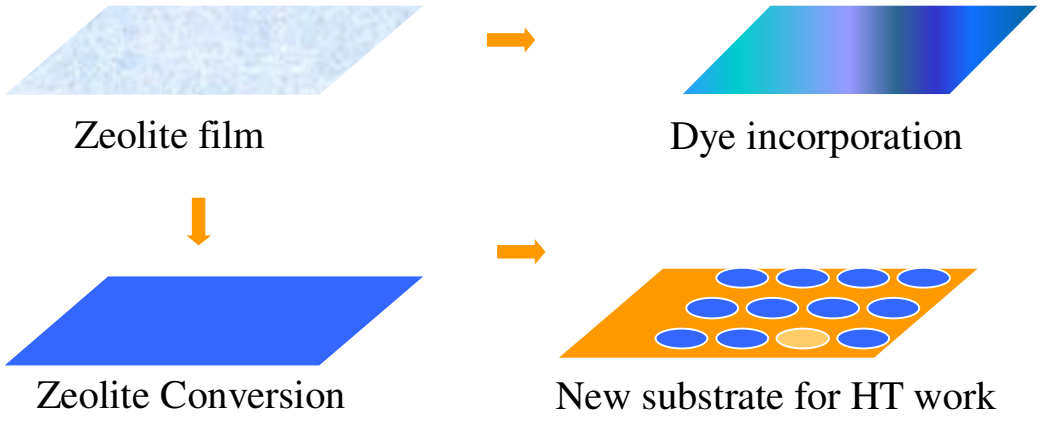

Fig 8.1 Showing some potential applications of zeolite films

The desired thickness of the zeolite film will be dependant on the application. For thermal conversions of the zeolite into a different framework a thick film will be most desirable. This will serve to preserve the integrity of the film upon heat treatment. A thick film will also allow a much easier characterisation of both the film and the thermally converted product by x-ray diffraction. This will be performed using the Bruker D8 Diffractometer with GADDS software (sec 2.5), ideal for dealing with substrates as it has a large flat sample platform and an area detector.

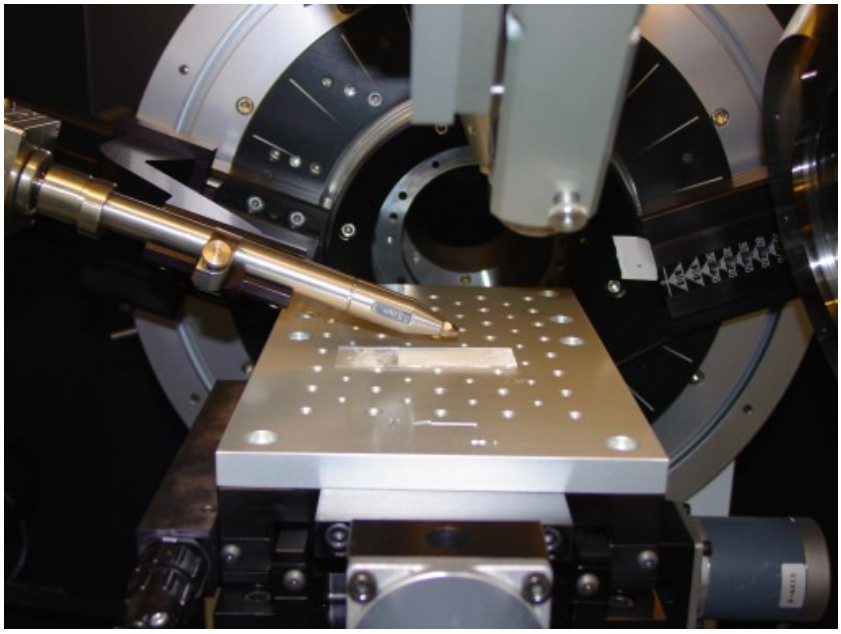

Fig 8.2 Photograph of the sample environment on the D8

Similarly, for a solid state high throughput type array a thick film will be most useful for ease of characterisation. An array could also be fully characterised by x-ray diffraction using the D8, as software can be used to program a set of coordinates for the robotic collimator to focus onto.

For other applications a thinner zeolite film would be required. An example would be the generation of interference effects to produce interesting optical properties by reflections from different layers of a composite. A composite of mica and various metal oxides can be used in this way to create lustre pigments. In these composites reflections from different layers of mica interfere with each other to produce the lustrous effect, and the colour is controlled by the deposited metal oxide, for example mica coated with iron oxide creates a red lustre pigment. This optical property relies on the fact that the distance between the layers is similar to that of the wavelength of visible light. Thinner films will be much harder to characterise by x-ray diffraction, as they will inherently contain less material. Again, the D8 with GADDS will be very useful, as the area detector will increase sensitivity by collecting a much larger amount of data than a point detector.

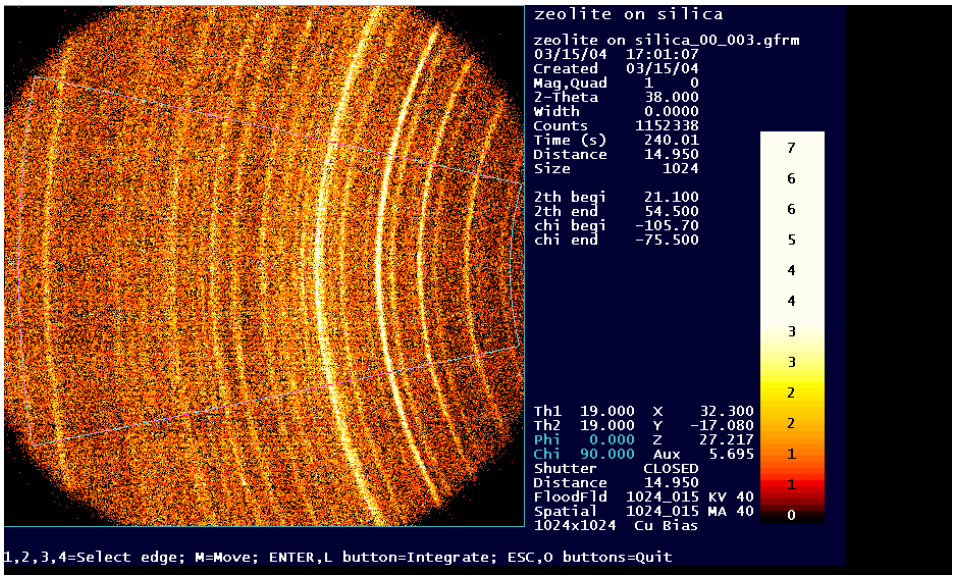

Fig 8.3 Picture of the GADDS software showing slices from cones of diffraction

8.2 Synthesis of Zeolite Films by Direct Crystallisation

This method of film formation involves the inclusion of a substrate in the reaction mixture, upon which the desired zeolite will crystallise as it forms, with the substrate acting as a nucleation site. This method of film synthesis is known as "direct growth" [8-11] as the zeolite is formed directly onto the substrate. Zeolite membranes have been successfully grown on many different substrates, including silver, steel and glass[12-14]. Zeolite films can even display 2-dimensional ordering of the crystals within the film[15], which can arise from the morphology of the substrate or be controlled using templating agents[16]. Films produced by this method will tend to possess a fairly rough topology and will be reasonably thick, of the order of a few hundred microns. The thickness of the film should be to some extent controllable by the reaction conditions employed. Other methods of film production involve attaching the zeolite crystallites to the substrate after synthesis, namely "postsynthetic crystal attachment" and will be discussed later.

8.2.1 Experimental – Direct Crystallisation

Synthesis of a film of zeolite a on a glass substrate was attempted. The reaction mixture was prepared using 3.375g of sodium aluminate (Aldrich 99%) and 3.55g of sodium metasilicate (Fluka 97+%) . This was added to a solution of 6.25g of sodium hydroxide (Fisher 97+%) in 75ml of deionised water. This mixture was loaded into a 125ml capacity PTFE lined steel autoclave. A glass microscope slide was then placed in the reaction vessel, which is an appropriate substrate working at low temperatures, before the autoclave was sealed. The autoclave was then placed in an oven horizontally, and gently agitated to make sure the substrate was lying horizontally within the vessel. The reaction was then heated to 90 °C for 16 hours before being allowed to cool to room temperature.

The coated substrate was then recovered from the autoclave using a pair of tweezers, taking care not to damage the zeolite coating. The substrate was washed thoroughly with deionised water before being dried and at 90 °C in a drying oven. The D8 diffractometer with flat sample stage allowed the film to be characterised by powder x-ray diffraction

without damaging the substrate, and integration of the raw data from the area detector gave a more conventional plot of intensity against 2θ. This resulting diffraction pattern was then referenced with the JCPDS database for phase identification and was found to be zeolite A with small quantities of impurities present.

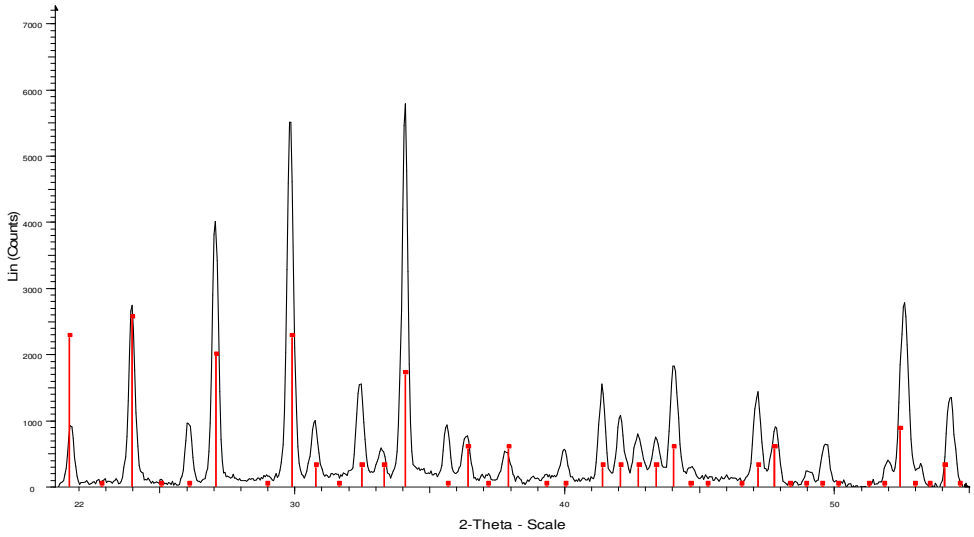

Fig 8.4 Diffraction pattern of the zeolite A showing JCPDS data in red

SEM imaging and EDX were performed on the zeolite film using a Phillips XL30 ESEM instrument. Prior to imaging the highly charged zeolite framework was sputtered with gold and mounted onto aluminium stubs using double sided carbon tape. Firstly EDX was performed and showed the zeolite coating to possess roughly a 1 : 1 aluminium to silicon ratio. This is concurrent with a zeolite A deposition and corroborates the x-ray diffraction data. Next, SEM imaging was used to study the morphology of the surface of the film.

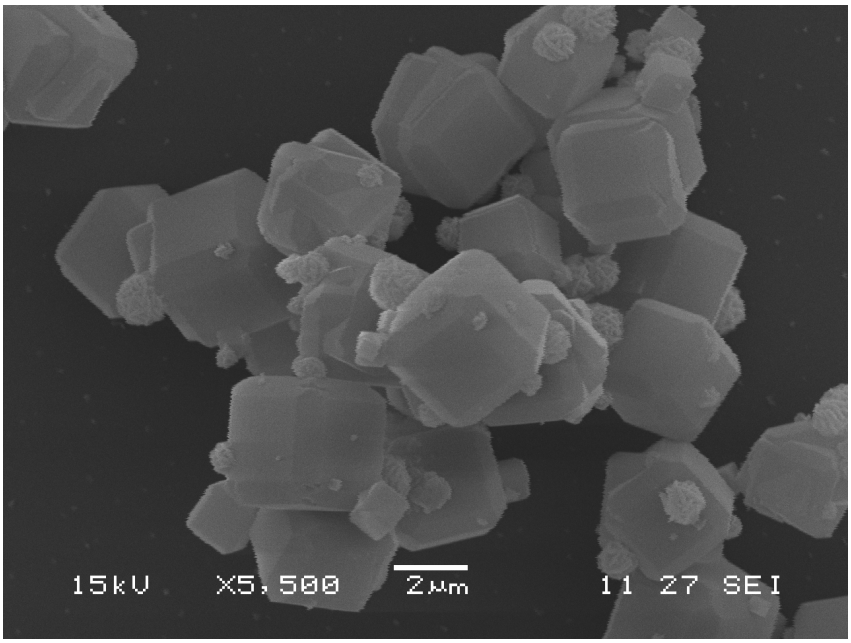

Fig 8.5 Cubic zeolite A particles present in the film formed by direct crystallisation

These pictures displayed a rough surface comprised of clusters of cubic zeolite A crystallites, mostly about 5 microns across

The Phillips XL30 ESEM instrument allows for the sample stage to be tilted perpendicular to the incident electron beam. This facilitates the viewing of a cross section of film, although the stage is not free to move through a full 90°. This means that the thickness of film can be estimated from end on SEM images.

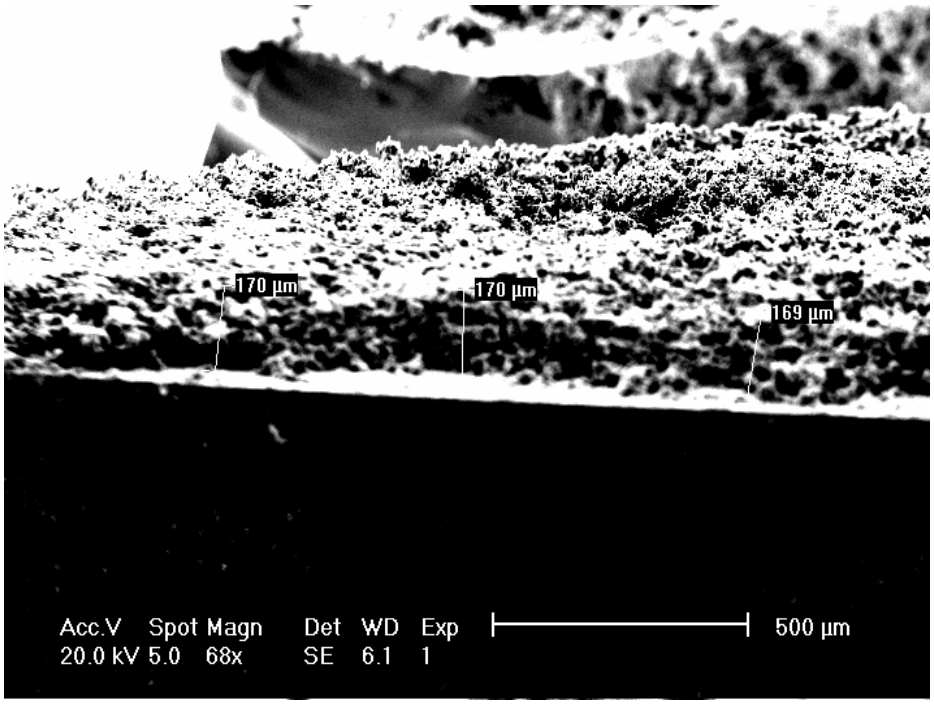

Fig 8.6 SEM image of the edge of the zeolite film produced from direct crystallisation

From these images it was estimated that the thickness of the films formed by direct crystallisation were between 150 and 200 microns.

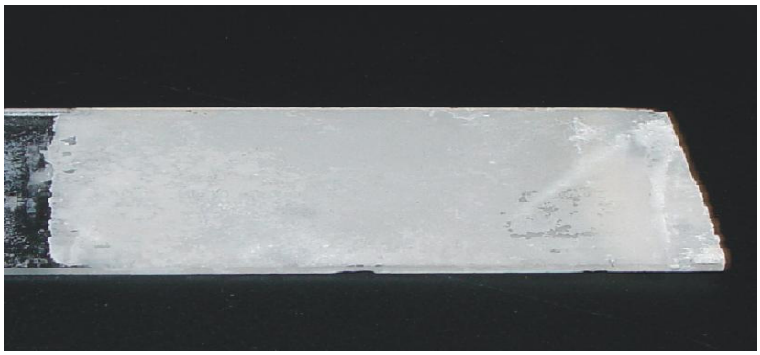

Fig 8.7 Photograph of glass slide coated with zeolite A by direct crystallization

8.3 Synthesis of Zeolite Films by Chemical Deposition

Another method of depositing zeolites onto glass substrates is using long chain organic molecules as a chemical link between the zeolite and the substrate[17,18]. This method provides the substrate with a monolayer of zeolite crystallites, and can lead to two dimensional ordering of the crystallites on the substrate. A number of different chemical linkers can be used for this purpose, most of which rely on the reaction of different species bound to the zeolite and glass substrate through silanol bridges. One particular example utilises a ring opening of an epoxide bound to the glass by a primary amine bound to the zeolite phase.

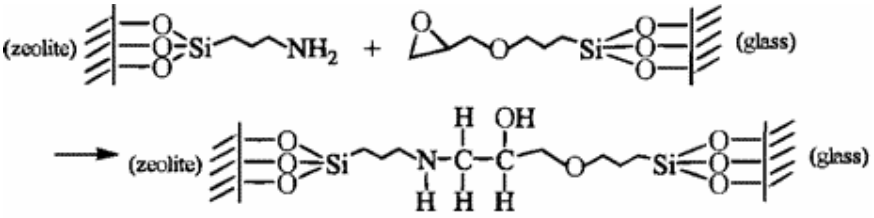

Fig 8.8 Schematic of chemical deposition of zeolite onto glass using amines and epoxides as chemical linkers

8.3.1 Experimental – Chemical Deposition

To conduct the synthesis of a zeolite film Zeolite A was prepared in bulk using solution based laboratory methods. 25g of sodium hydroxide (Fisher 97+%) was dissolved in 300ml of deionised water and 13.5g of sodium aluminate (Aldrich 99%) was added to the solution. Simultaneously 14.2g of sodium metasilicate (Fluka 97+%) was dissolved in 200ml of deionised water. Both solutions were heated to 90°C before the sodium aluminate/hydroxide solution was added slowly to the sodium metasilicate solution whilst hot. The reaction was then stirred for 4 hours at 90°C before the product was recovered by filtration and washed thoroughly with deionised water.

The film deposition was then conducted as a three stage process using the zeolite A and a glass substrate as starting materials. The reaction is performed in stages to eliminate chemical links between zeolite crystallites by binding the amine to the

zeolite and the epoxide to the substrate in separate reactions. These can then be combined to complete the chemical linkage by epoxide ring opening.

0.8 g of the dried zeolite A was suspended in 40ml of the amine 3-amino-propyltriethoxysilane (Aldrich 99%) and refluxed at 110°C under nitrogen for 1 hour. In parallel a piece of silica (76mm x 26mm) was submerged in 50ml of toluene and refluxed at 110°C under nitrogen for 1 hour with 20ml of 3-Glicidoxy-propyltrimethoxysilane (Aldrich 99%), added via a needle and syringe to the nitrogen purged system. After this the linker treated silica was submerged in toluene and the amine treated zeolite was added under nitrogen. The two were refluxed at 110°C for a further 2 hours under nitrogen. Post reaction the silica plate was sonicated in toluene for a few minutes to remove any physically bound zeolite on the surface.

Because of the air and moisture sensitivity of the organic linker molecules and the size of substrate required a slightly complex apparatus set up was needed. A broad neck flask was used to accommodate the substrate with enough inlets for a condenser, suba-seal and nitrogen inlet.

Fig 8.9 Photograph of the wide neck reflux apparatus

The substrate was then characterised by powder x-ray diffraction using the Bruker D8 Discover with GADDS, and by SEM imaging. From these it was shown that the substrate had only limited coverage by the zeolite. This is due to the fact that the 3 member epoxide ring on the 3-Glicidoxy-propyltrimethoxysilane is very moisture sensitive, and any small amount of residual water in the system will cause an epoxide ring opening. The coverage was estimated to be around 30% of the total substrate surface area and no 2 dimensional ordering was observed.

8.4 Self Assembly using Surfactants

Thin films of zeolites are readily formed using a solution of long chain surfactant molecules such as hexanoic acid and colloidal zeolite particles[19]. The surfactant molecules possess a polar head group which has an affinity for the highly charge zeolite surface and a long hydrocarbon chain which is hydrophobic. During self assembly the hydrophilic head group is adsorbed to both the suspended zeolite particles and the substrate, which has been pretreated with sodium hydroxide solution to create a charged surface. The hydrophobic aliphatic chains of the surfactant then pack together to minimise any interactions with the water, zeolite and substrate. If the surfactant concentration is chosen correctly this manifests as a bilayer at the silicon water interface. The aggregation of the colloidal zeolite particles at this bilayer forms the thin film of zeolite on the substrate. Care must be taken to manipulate the pH to assure that the head group remains protonated.

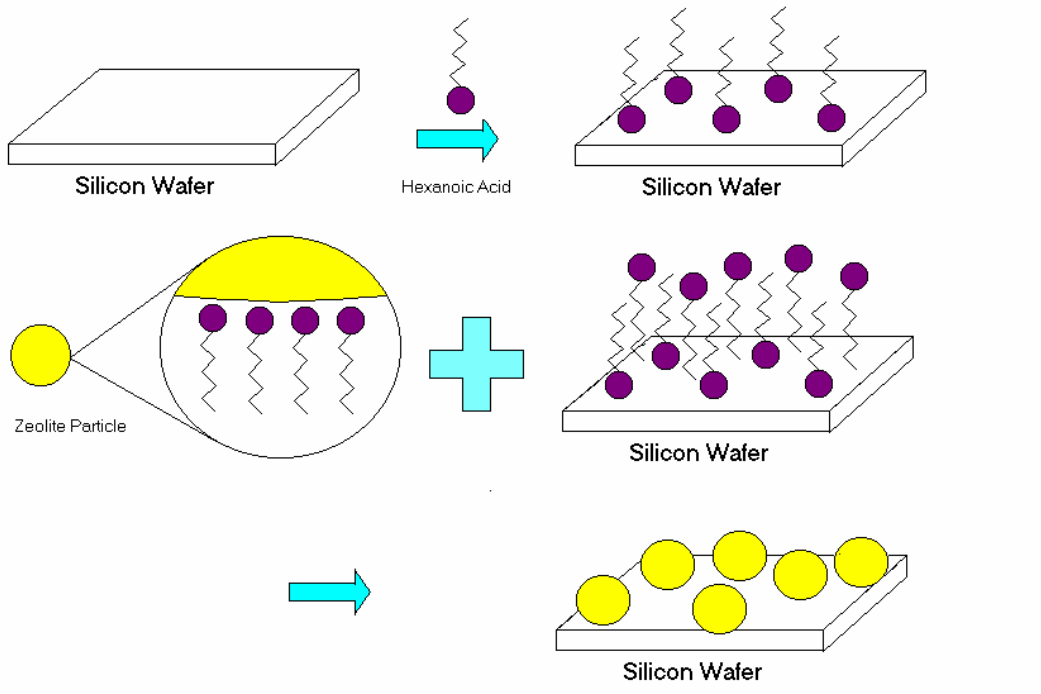

Fig 8.10 The mechanism of film deposition of zeolites by self assembly using hexanoic acid to aggregate the zeolite particles at the substrate surface

8.4.1 Experimental – Self Assembly

Bulk zeolite A was prepared using solution based laboratory methods. 25g of sodium hydroxide (Fisher 97+%) was dissolved in 300ml of deionised water and 13.5g of sodium aluminate (Aldrich 99%) was added to the solution. Simultaneously 14.2g of sodium metasilicate (Fluka 97+%) was dissolved in 200ml of deionised water. Both solutions were heated to 90°C before the sodium aluminate/hydroxide solution was added slowly to the sodium metasilicate solution whilst hot. The reaction was then stirred for 4 hours at 90°C before the product was recovered by filtration and washed thoroughly with deionised water.

To conduct the self assembly into a zeolite film a glass microscope slide was treated with 4M sodium hydroxide solution to ensure a clean, deprotonated surface for the zeolite particles to aggregate at. A 20mM solution of hexanoic acid (Aldrich 99.5%) (0.25g of hexanoic acid in 100ml of dionised water) was prepared and placed in a large dish. 0.2g of zeolite A was milled using a mechanical ball mill to ensure a uniform particle size and suspended in the hexanoic acid solution. A small wire table was constructed and placed in the dish below the water level, upon which was placed the treated glass substrate. This allowed the suspension to be stirred without interfering with the substrate.

The reaction was then adjusted to pH 3 by adding concentrated hydrochloric acid to the suspension dropwise using a pipette. This ensured that the polar head groups on the hexanoic acid molecules remained protonated for the aggregation. The suspension was then warmed to 50°C and stirred gently for 10 hours. After this period a white film could clearly be seen on the surface of the substrate. The substrate was then recovered from the suspension and gently washed with ethanol to remove all traces of the organic surfactant from the surface.

The zeolite film was then characterised by powder x-ray diffraction using the Bruker D8 Discover with GADDS, and by SEM imaging.

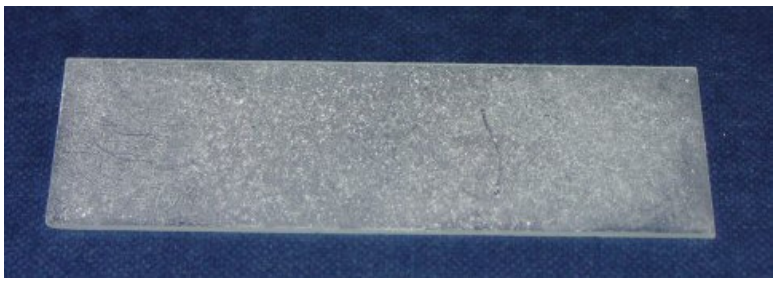

Fig 8.11 Photograph of a zeolite A film formed by self assembly using hexanoic acid on a glass microscope slide

The zeolite film was found to be single phase zeolite A by powder x-ray diffraction, showing that the aggregation and self assembly process did not alter the structure of the framework. SEM imaging showed complete coverage of the substrate by zeolite particles with a uniform size of about 3 microns.

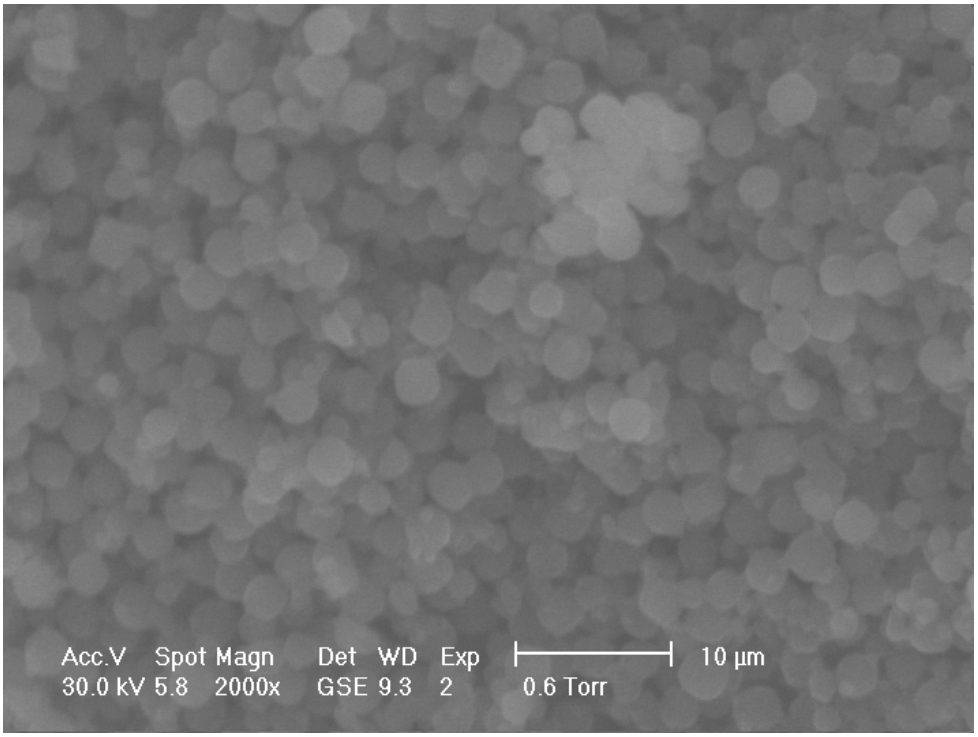

Fig 8.12 SEM image of a zeolite A film formed by self assembly using hexanoic acid to aggregate the particles at the substrate surface

8.5 Dip Coating and Evaporation to Zeolite Films

Mechanical film deposition of zeolites can be achieved by evaporation of a suspension of zeolite particles on a substrate. Two such methods have been employed in this work. The first being dip coating in a suspension of zeolite before evaporation, and the second being drop addition of a suspension onto the substrate prior to evaporation.

To dip coat the substrate 0.2g of zeolite A was milled thoroughly using a mechanical ball mill to give a uniformly small particle size and was then suspended in 100ml of deionised water. The substrate was treated with concentrated sodium hydroxide solution to clean it and provide a smooth surface, and was then manually dipped into the zeolite A suspension.

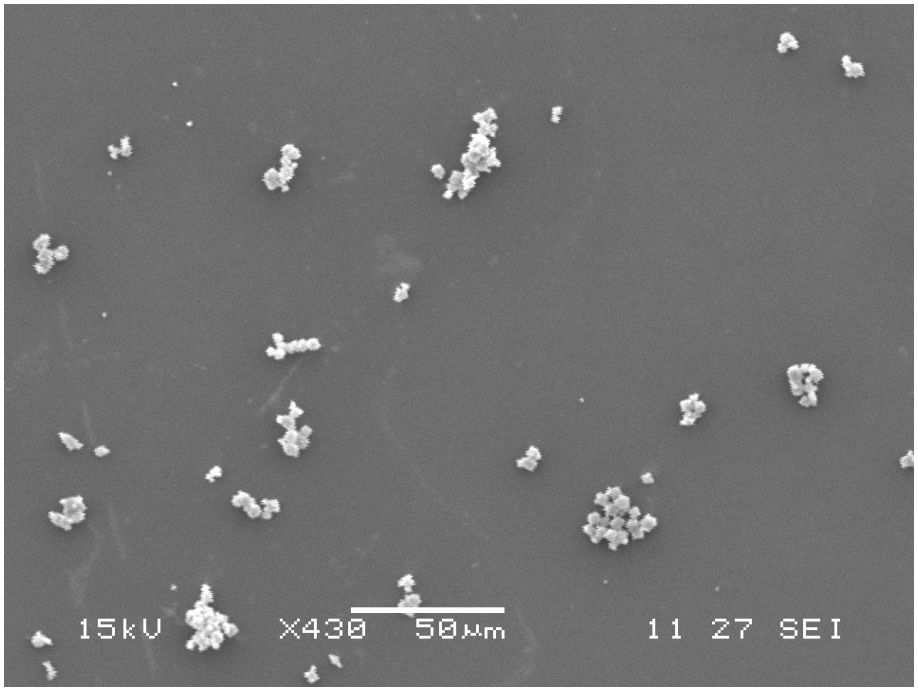

Fig. 8.13 SEM image of zeolite particles deposited by dipping the substrate in a suspension of zeolite

The substrate was then dried fully at 90°C and characterised by powder x-ray diffraction, which showed that zeolite A had been deposited onto the glass slide. SEM

imaging (Fig. 8.13) showed the deposited zeolite crystallites were clustered on the surface, and that coverage of the substrate was minimal.

8.6 Drop Coating and Evaporation to Zeolite Films

To drop coat the substrate 0.2g of zeolite A was milled thoroughly using a mechanical ball mill to give a uniformly small particle size and was then suspended in 100ml of deionised water. The substrate was treated with concentrated sodium hydroxide solution to clean it and provide a smooth surface. 3 drops of the zeolite suspension were then placed manually onto the substrate using a dropping pipette, which was then allowed to evaporate to leave a white film which was then dried at 90°C.

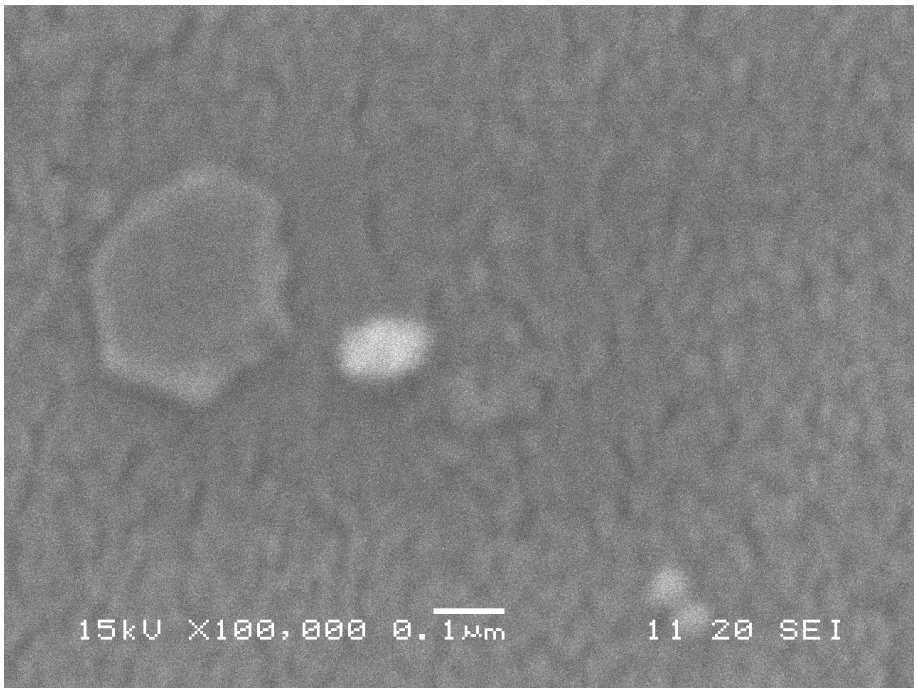

Fig. 8.14 Close up of background texture of ball milled zeolite A deposited by drop coating a suspension onto a glass substrate

X-ray diffraction again showed that zeolite A had been successfully adsorbed to the glass substrate by the drop coating method. SEM imaging (Fig8.14) at very high magnification showed that the substrate was completely coated by the zeolite.

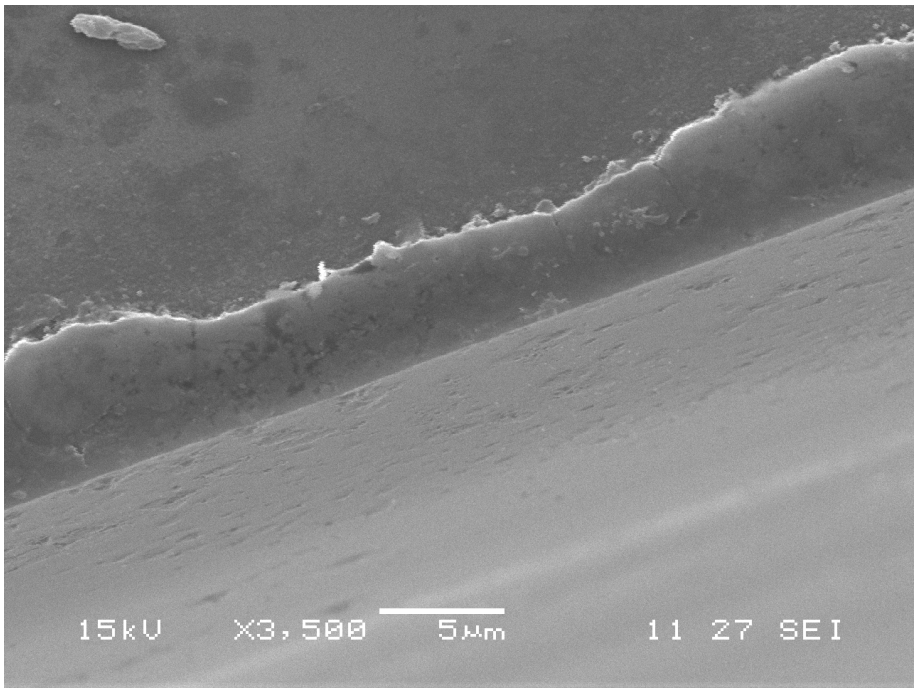

Fig 8.15 SEM image of the edge of the substrate showing a film deposited by drop coating of a zeolite suspension onto glass

To study the integrity of the film, the edge of the substrate was viewed by tilting the sample stage through 30° and collecting images (Fig 8.15). This would also make it easier to distinguish between the deposited zeolite texture and the glass underneath. It is clearly observed that there is a complete and uniform coverage of the substrate, which is broken about 5 microns from the edge of the substrate. This is probably due to shrinkage of the film when it is dried prior to imaging.

From these sets of evaporation coating experiments it is clear that electrostatic interactions between the substrate and the zeolite are not alone enough to create a uniform zeolite coating, as shown by the dip coating experiments. Drop coating provides a much more reliable method of producing uniform thin films of zeolite coatings on glass substrates.

8.7 Thermal Conversion of Zeolite Films

Thermal processing of zeolite films bound to substrates provides a synthetic route to thin films of other materials, for example the thermal conversion of zeolite A into sodalite talked discussed in this thesis. This can lead to thin films of optically active materials, such as the ultramarine family of pigments or other interesting optical properties like the reversible photochromism displayed by hackmanites. Zeolite films also have potential uses as a high throughput type solid state array used for a combinatorial style approach for synthesis in the solid state. In this section the feasibility of using zeolites bound to substrates for this type of high pressure synthesis will be investigated.

To start a zeolite film was synthesised on a substrate suitable for high temperature conversion. A quartz glass substrate was chosen for this purpose, which will remain solid up to about 700°C. For ease of characterisation and viewing a thick film was desirable, and the direct crystallisation method of deposition was chosen to produce this. The reaction mixture was prepared using 3.375g of sodium aluminate (Aldrich 99%) and 3.55g of sodium metasilicate (Fluka 97+%). This was added to a solution of 6.25g of sodium hydroxide (Fisher 97+%) in 75ml of deionised water. This mixture was loaded into a 125ml capacity PTFE lined steel autoclave. The quartz substrate was then placed in the reaction vessel, before the autoclave was sealed. The autoclave was then placed in an oven horizontally, and gently agitated to make sure the substrate was lying horizontally within the vessel. The reaction was then heated to 90 °C for 16 hours before being allowed to cool to room temperature.

The coated piece of quartz was then recovered and washed thoroughly with deionised water before being dried at 90 °C. Powder x-ray diffraction using the Bruker D8 discover with GADDS software suitable for characterising films showed that the quartz substrate was coated with zeolite A. SEM imaging of the sample was not attempted at this stage, as the substrate would have to be broken to fit on the sample stage of the imaging instrument.

Fig 8.16 Zeolite A film produced by direct crystallisation on a high temperature quartz substrate suitable for high temperature work

Next, thermal conversion of the zeolite film into a tenebrescent hackmanite was attempted. First a solution of sodium chloride and sodium sulphate in water was prepared. 0.1g of sodium chloride (Aldrich 99%) and 0.2g of sodium sulphate (INC 99%) were dissolved in 5 ml of deionised water. The solution was then added dropwise evenly over the zeolite film using a dropping pipette. The substrate was then transferred to a tube furnace for the thermal conversion.

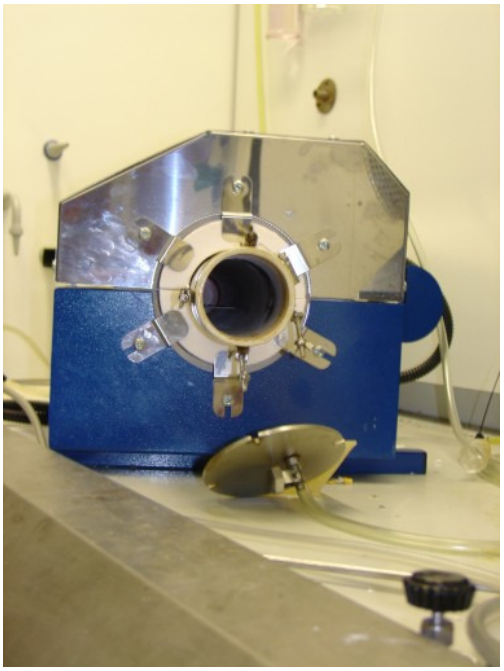

The substrate with adsorbed zeolite film was much larger than a normal reaction vessel, thus special apparatus was used to house the experiment. The requirement of a reducing gas mixture meant that a wide bore tube furnace had to be used in this instance.

Fig 8.17 Photograph showing the wide bore tube furnace used for the thermal conversion of the zeolite film into hackmanite

The tube furnace was flushed for 30 minutes with a reducing gas mixture of 5% hydrogen in nitrogen. The reaction was then heated to 650 °C by ramping the temperature at 1 °C every one minute. This ramp rate was set to avoid the film being damaged by too great a rate of heating. If the zeolite collapsed into the sodalite framework too quickly the film could break up on the substrate. The reaction was then maintained at 650 °C for a further 18 hours under a continuous flow of the hydrogen / nitrogen gas mixture.

After this time the reaction was allowed to cool to room temperature and the substrate was recovered. The product was then washed gently with deionised water before being dried at 90 °C in an oven. The resultant white film was characterised by x-ray diffraction using the Bruker D8 Discover with GADDS, which showed a complete thermal conversion of the zeolite A film into a hackmanite film. The substrate was then exposed to 254nm UV radiation using a bench top UV lamp to assess the optical activity of the sample.

Fig 8.17 A photochromic sodalite film produced by thermal conversion of a zeolite A film under reducing conditions shown in the coloured state

The sample was found to display reversible photochromism, turning pink on exposure to 254nm UV radiation and slowly bleaching back to a white state in the presence of white light or natural sunlight. The response time of the film to change fully to the excited state was roughly 30 seconds, with a bleaching time of between 15 minutes and 2 hours, depending on the light source. Quicker bleaching times were observed when the sample was exposed to direct sunlight, whereas slower bleaching times were observed from exposure to an artificial white light source.

8.8 Conclusions

Several different methods for the formation of zeolite films on substrates have been investigated, and the properties of these films compared with view to thermal processing of the films into new framework types, or forming the basis of a high throughput solid state array. These methods include direct crystallisation onto the substrate, chemical deposition using amines and epoxides, self assembly at the surface using surfactants and physical deposition using drop or dip coating methods.

The different methods of film formation lead to films of different thickness and coverage of the substrate, making them suitable for a variety of applications. Direct crystallisation gave rough films of fairly uniform thickness of between around 150 and 200 microns. Chemical deposition provided a very limited coverage of the substrate due to the moisture sensitivity of the reactants, and did not produce films suitable for thermal processing. Self assembly using surfactants produced films of the order of 50 microns. Physical deposition methods produced mixed results. Dip coating provided a very limited coverage of the substrate, and was not investigated further. Drop coating and evaporation gave a uniform coverage of the substrate and produced thin films less than 1 micron in thickness.

Thermal processing of the zeolite films was performed to collapse the zeolite into a sodalite film with reversible photochromic properties. A film produced by direct crystallisation was considered most suitable for this purpose, as this type of film was particularly robust. The thickness of the films produced via this method means they are less vulnerable to breaking up during the heating process and are much easier to characterise by powder x-ray diffraction. In this manner a film of optically active hackmanite was successfully produced by thermal processing of a zeolite A film.

8.9 References

[1] D. W. Breck, *Zeolite molecular Sieves,* 1974, Wiley, New York

[2] R. M. Barrer, *Zeolites and Clay Minerals as Sorbents and Molecular Sieves,* 1979, Academic, London

[3] W. M. Meier, D. H. Olsen, *Atlas of Zeolite Structure Types,* 1988, Butterworths, London.

[4] Z. Lai et. al., *Science*, 2003, **300**, 456

[5] D. R. Rollison, *Chem. Rev.* 1990, **90**, 867

[6] Y. Yan, T. Bein, *J. Phys. Chem.*, 1992, **96**, 9387

[7] M. E. Davis*, Ind. Eng. Chem.,* 1991, **30**, 1675

[8] S. Feng, T. Bein, *Nature*, 1994, **368**, 1839

[9] A. Gouzinis, M. Tsapatsis, *Chem. Mater.*, 1998, **10**, 2497

[10] T. Munoz, Jr.*,* K. J. Balkus, Jr., *Chem. Mater.,* 1998, **10**, 4114

[11] G. Clet, J. C. Jansen, H. van Bekkum, *Chem. Mater.*, 1999, **11**, 1696

[12] W. O. Haag, J. G. Tsikoyiannis, *U.S. Patent No. 5019263,* 1991

[13] W. O. Haag, J. G. Tsikoyiannis, *U.S. Patent No. 5110478A,* 1991

[14] R. M. Dessau, R. K. Grasselli, R. M. Lago, J. G. Tsikoyiannis, *U.S. Patent No. 5316661,* 1994

[15] J. C. Jansen, H. van Rosmalen, *J. Cryst. Gr.,* 1993, **128**, 1150

[16] V. Tricloli, J. Sefcik, A. V. McCormick, *Langmuir*, 1997, **13,** 4193

[17] Y. Yan, T. Bein, *J. Am. Chem. Soc.*, 1995, **117**, 9990

[18] Z. Li, C. Lai*,* T. E. Mallouk, *Inorg. Chem.,* 1989, **28**, 178

[19] G. Cho, J. Lee, D. T. Glatzhofer, B. M. Fung, W. L. Yuan, E. A. O'Rear, *Adv. Mater.,* 1999, **11**, 497

Chapter 9:
Conclusions

9.1 Conclusions

During the course of this work various aluminosilicate framework systems have been explored with view to developing smart pigments that react to an external medium. Both solid state and solution based hydrothermal synthetic routes towards various zeolite precursor systems have been investigated, in particular zeolite A, faujasite and sodalite. These syntheses have been tailored to provide maximum yield and phase purity. The precursors have then been successfully thermally converted into optically active pigments.

The thermal conversion of zeolites into sodalite has been investigated in detail using variable temperature neutron diffraction to monitor any phases present during this transition. These thermodiffraction experiments showed that there are no intermediate phases formed during this transformation.

A library of reversibly photochromic sodalites has been successfully synthesized by collapsing zeolite A at high temperature in a mildly reductive atmosphere with sodium sulphate and various metal halide salts. It was found that the composition and structure of the sodalite has a marked effect on the optical property, with various different colour changes being observed.

The anhydrous zeolite type phase $K_2Al_2Si_3O_{10}(KCl)$ has been identified as a possible framework capable of incorporation of sulphur chromophores and a potential new family of reversibly photochromic materials. Currently only small amounts of the phase have been successfully synthesized using a high pressure hydrothermal rig. The structure has been refined using the GSAS program in the space group $P\text{-}42_1m$ and the tetragonal unit cell was found to have refined lattice parameters of a = 9.7488 and c = 6.4879. The phase has been identified as a possible new framework type for use as a host for inclusion compounds.

Various methods have been employed for the synthesis and characterization of thin films of zeolites on substrates including glass and mica. Methods investigated include direct hydrothermal crystallization, evaporation coating using a suspension of the

zeolite, self assembly using a dilute solution of surfactants and chemical linkages using an amine for an epoxide ring opening. These films were characterised by SEM and powder x-ray diffraction using a D8 advance with a flat sample stage. Of these methods it was found that the physical deposition methods provided a more uniform and robust film for the purpose of a thermal conversion into an optically active film. A reversibly photochromic sodalite film was produced by thermal conversion of a film of zeolite A deposited on a high temperature glass substrate.